RADIOCHEMICAL TRANSFORMATION OF HIGH PRESSURE METHANE UNDER GAMMA, ELECTRON, AND NEUTRON IRRADIATION

A Thesis

by

JEFFREY TYLER CLEMENS

Submitted to the Office of Graduate and Professional Studies of
Texas A&M University
in partial fulfillment of the requirements for the degree of

MASTER OF SCIENCE

Chair of Committee,	Sean M. McDeavitt
Committee Members,	Lin Shao
	Emile Schweikert
Head of Department,	Yassin Hassan

May 2014

Major Subject: Nuclear Engineering

ABSTRACT

The chemical effects of irradiation on high pressure methane and noble gas mixtures were investigated using gamma, electron beam, and neutron irradiation sources. The gamma source used was the La-140 source from the Nuclear Science Center (NSC) at an activity of 400 Ci. The electron source was a 10 MeV, 15 kW, linear accelerator at the National Center for Electron Beam Research. The neutron source was the NSC reactor running at 1 MWth. The in-core positions were used for the neutron irradiations had neutron fluxes ranging from 5×10^{12} to 1×10^{13} n/cm^2/s. The gases used for the study included research grade methane, argon, and helium. The compressed gases were irradiated in a several separate irradiation vessels made with minimal nonmetal parts to reduce contamination. The majority of the vessels were pressurized to 2.07 MPa (300 psi) for the irradiation. The vessels were irradiated by one of the three irradiation sources for a maximum dose. The methane was mixed with the noble gases helium and argon, these gases were added to dilute the methane concentration, and study charge transfer effects on radiation chemical yields.

The reaction products were measured using a gas chromatography mass spectrometer (GCMS). In addition to the GCMS, a lab made mass spectrometer system was used to measure the hydrogen and ethane concentrations within the gas post irradiation. The NSC Reactor irradiations show a measurable increase in the concentration of ethane and hydrogen, the La-140 and electron beam irradiations do not show measurable increases in hydrogen and ethane concentrations.

The primary accomplishment of this research was the design of systems that are capable of performing high pressure gas irradiations. The irradiation experiments developed three separate irradiation vessels during the course of the experiments. The analysis system was a mass spectrometer system that is capable of trace molecule detection. The experiments that had shown measurable change in the hydrogen and ethane concentrations had the G-values of the individual reaction products calculated for the NSC reaction irradiations. The G-values for were calculated to be 2.61±0.62 and 1.16±0.34 for hydrogen and ethane production, respectively. The effects of different types of radiation were examined during this thesis, and a future experimental work is proposed..

DEDICATION

I would like to dedicate this work to my grandfather, Harley Clemens, who first taught me the love of all things technical.

ACKNOWLEDGEMENTS

I would like to thank Dr. McDeavitt for his continuing guidance, support, and encouragement throughout my research. I would like to thank Dr. Simon North for guidance on detection methods. I would like to thank Adam Parkison for his continuing guidance, support, and encouragement throughout my research. I would like to thank all of the undergraduate students for their help in the construction of the instruments used for hydrogen measurements. I would like to thank Jerry Newhouse and all of the staff at the NSC for their help with reactor irradiations. I would like to thank the National Center for Electron Beam Research for letting me use there irradiation facilities, especially Mickey Speakmon and Dr. Suresh Pilla for their guidance and patience.

NOMENCLATURE

NSC	Nuclear Science center
NSCR	Nuclear Science Center Reactor
MCNP	Monte Carlo N-Particle Transport
RGA	Residual Gas Analyzer
GTL	Gas-to-Liquids
LET	Linear Energy Transfer
PDF	Probability Distribution Function
AMU	Atomic Mass Units
ECU	Electronics Control Unit
MM	Molecular Mass
GCMS	Gas Chromatography Mass Spectroscopy
IVR	Intramolecular Vibrational Redistribution

TABLE OF CONTENTS

Page

LIST OF FIGURES

Page

LIST OF TABLES

Page

1 INTRODUCTION

The objective of this research was to characterize the chemical changes of methane gas (CH4) that may be induced by interaction with gamma, beta, and neutron radiation. Methane has been shown to be polymerized into heavier hydrocarbons through radiation interactions, but the utility of using this route has not been explored with much interest. This is being investigated to evaluate radiation as a potential catalyst for the production of motor-grade hydrocarbon fuels to compete with other chemical production methods like Fischer-Tropsch[1] or Mobile[2] processes. The primary advantage of this radiation-induced polymerization process compared to the current chemical methods is that the polymerization reaction happens in a single step[3]. Also, this process generates a great deal of hydrogen gas that can be used in other area of petrochemical processing (coal gasification, reforming, etc.). This process can be used to produce liquid fuels from the large natural gas reserves in the United States. These radiation induced addition reactions tend to have energy efficiencies that are far below commercial chemical processes that are mentioned.

The focus of this project is to develop and test a process to quantify polymerization of hydrocarbon species under varying dose, particle type, methane concentration, and various noble gases. Systems and experiments were designed that are capable of quantifying conversion rates of hydrocarbons for three types of gas irradiations. These are gamma irradiation of high pressure gas from a La-140 source at the Texas A&M University Nuclear Science Center (NSC). The second method involves electron beam

irradiation of high pressure gas at the National Electron Beam Facility at Texas A&M University. The third method is direct neutron irradiation of high pressure gas in the NSCR. The first two methods involve irradiation from only gamma and electron irradiation, in which the particle tracks have low linear energy transfer (LET). The last method involves neutron and proton irradiation, which are high LET methods. The neutron irradiation method also generates dose from gamma rays, electron, neutrons, and protons from knock-on collisions.

The experiments were performed using methane gas in steel and aluminum vessels pressurized up to 300 psig (2.07 MPa), as described in Chapter 3. The methane gas was blended in varying concentrations of the noble gases helium and argon. The temperature was near ambient for all irradiations.

The product gases were initially analyzed by mainly by Gas Chromatography Mass Spectroscopy (GCMS) in the mass spectroscopy laboratory at Texas A&M University and later in a qaudrupole mass analyzer system created for this project. The GCMS measurements were used to confirm the existence of chemical change due to gas irradiation in the initial experiments. The gas components were separated by boiling points, and then analyzed by a mass spectrometer. These sets of experiments found that there was significant chemical change from the irradiation of methane and noble gas mixtures in the NSCR, but the conversion was not observed for methane alone. The electron beam and La-140 gamma irradiations produced very low hydrocarbon formation. The GCMS measurement method suffered one severe flaw in that it was unable to quantify hydrogen

concentrations in the gases, which is crucial for showing chemical change. This system was not able to measure hydrogen concentrations since the carrier gas of this system was helium (4 amu), making a specialized mass spectrometer system necessary for the measurement of hydrogen standards.

Therefore, a residual gas analyzer (RGA 200) was used to measure the hydrogen concentration in the later experiments systems. This system was designed to be mobile and contained all necessary systems to ensure the operation of the mass spectrometer. It was used to measure the hydrogen concentrations from electron beam irradiations of the methane-noble gas mixtures under high pressure.

As a means of comprehending the internal radiation interactions within the various process vessels, the Monte Carlo transport tool MCNPX was used to simulate the dose applied in the various experimental vessels for the various conditions tested. The doses for the electron and gamma irradiations were calculated using an f6 tally for each of the experimental runs. The f6 tally on MCNPX calculates the total amount of energy deposited in a volume per particle, which can then be correlated to total dose by multiplying the tally by the particle fluence. The LET card, which calculates the energy loss per particles per unit path length, was used to measure the average LET for the electron tracks in the high pressure gas. The reactor irradiations in the NSCR were also simulated using MCNPX with an f6 tally to measure the combined heating from electrons, gammas, protons, and neutrons. A separate dose calculation was done only for the gamma

and electrons contributions. An LET card was used with an f4 tally, which calculates particle flux, to calculate the LET from the neutron knock-on collisions.

The reaction yields for the radiolysis experiments are given in terms of G-values, which define chemical change with respect to energy deposition. Many of the G-values for the experiments performed in this thesis range from 0.016 to 2.61. The G values of hydrogen were calculated for all experiments with the dose calculations from MCNPX. The hydrogen generation was also compared to the LET of the different radiation conditions.

The following chapters present detailed descriptions of the context, methods, results, and interpretation of the results for the methane/noble gas irradiations. Chapter 2 describes the experimental and theoretical background information regarding radiation interaction mechanisms, radiation-chemical change, chemical kinetics of molecular radicals and ions, dissociation dynamics and kinetic gas theory. Chapter 3 describes the experimental systems and procedures that were used to for the gas irradiations, as well as the mass spectrometer systems for the gas analysis. Chapter 4 describes the results of the irradiations. Chapter 5 discusses the significance and meaning of the results. Finally, Chapter 6 describes a brief summary of the primary results and suggestions for future research on this topic.

2 BACKGROUND AND THEORY

A gas-to-liquids (GTL) process is being investigated that is capable of transforming light (CH_4, C_2H_6, etc.) hydrocarbons into heavier hydrocarbons ($>C_3$) through radiation-induced polymerization. This process, if successful, would enable single step conversion of light hydrocarbons into liquid hydrocarbons and hydrogen. This may have numerous advantages over conventional GTL plants in that it will require fewer processing steps and smaller reducing plant sizes. Research in GTL technologies is becoming more commonplace as economically accessible domestic natural gas has become more accessible and is now a major portion of the American energy mix with electricity production at 29.8% of total generation in 2013.[4-6]

These processes all take natural gas as a feedstock and strive to chemically convert it into a liquid form. The majority of the GTL processes do this by turning the natural gas feedstock into long chain hydrocarbons using a series of chemical interactions. The end result of these processes, bypassing all of the intermediate steps, is shown in the equation below.

$$nCH_4 \rightarrow C_nH_{2n} + (n-1)H_2 \qquad 1$$

2.1 Current Chemical Processes

Current GTL industrial processes transform the methane in a number of chemical steps. All of the common processes start by turning the hydrocarbons into syngas, which is a mixture of CO and H_2. The ratio of the CO and H_2 is dependent upon the processing conditions. The two most common processes are steam reforming and autothermal re-

forming. Autothermal reforming is accomplished by adding methane to mixtures of oxygen and carbon dioxide. In contrast, steam reforming uses a mixture of water and methane in order to make the syngas. Both processes are normally carried out at temperatures between 1100 and 1400K and at pressures as high as 10 MPa.[7]

After the syngas is produced, it is inserted into a reactor where long chain hydrocarbons are synthesized. The names for the most common two methods for gas-to-liquids technologies are the Fischer-Tropsch (FT) process and the Methanol-to-Gasoline (MTG) process.[4, 8] In the FT process, the syngas is sent to a chemical reactor in which many hydrogenation reactions occur on the surface of a metal catalyst. The CO molecules stick to the metal catalyst, forming metal carbonyls. The hydrogen in the syngas then reacts with the CO, cleaving the C-O bond, replacing it with CH_2, and allowing C-C bonds to form. This process continues until long chain hydrocarbons are formed off the metal catalyst.[1] This process is normally accomplished between 473K and 573K and between 1 and 6 MPa.[1] The other common process, the MTG process, the syngas is converted into methanol, dehydrated to dimethyl ether, and further dehydrated into heavier hydrocarbon fuels over a zeolite catalyst.[8]

2.2 Radiation Induced Polymerization

Experiments have been performed to investigate the reactions of methane and light hydrocarbon polymerization under gamma, electron, and proton, irradiation.[3, 9] The experiments show low conversions of light hydrocarbons to heavy hydrocarbons. All of the investigations have found similar trends, namely, during the irradiation higher

molecular weight hydrocarbons are formed from the combination of lighter hydrocarbons. The irradiation of polymers is often used to alter the material's physical properties through the breaking and crosslinking of polymer chains. The cross linking of chains in polymerization in polyethylene makes them stronger, and gives them excellent tensile and impact properties.[10]

2.2.1 Select Methane Experiments

The experimental procedures for the experiments carried out in this thesis were meant to complement irradiation studies of previous authors. Three experiments in particular were examined, the proton irradiations by Sack[11], the flow experiments done Ponomarev[3], and the static irradiations of liquid methane and liquid argon by Sheridan-Libby[12]. These experiments were chosen because they encompass three types of methane irradiation experiments. The three experiments will be compared by the average LET of the irradiations calculated by MCNPX. These calculated vales is compared to selected

First, the Sack experiment used a high LET proton irradiation of methane at atmospheric pressures. The radiolysis produced high levels of ethane, ethylene, as well as heavier hydrocarbon with concentration decreasing as molecular mass increases.

The Ponomarev experiments used a high energy electron beam to irradiate light hydrocarbons at atmospheric pressures. This system flowed petroleum gas through an irradiation cell where it was irradiated by a 40 kW, 500 keV electron beam. The concentration of ions and radicals produced by this experiment was extremely high due to the

power density within the gas stream. This allowed for the radicals and ions to be created in large amounts, and in close proximity to one another, which allowed from more efficient combination of radical and ion species to form heavy hydrocarbons. This high power density, and lower pressure, allowed for high conversion of light gaseous alkanes into heavier, motor-grade liquid fuels.

The Sheridan-Libby experiments used a high intensity gamma source for the irradiation of solid methane. This experiment was very different from the others in that it used a gamma source (30 kCi Co-60) for the irradiation of mixture of solid methane and argon. These products of these irradiations were high molecular weight hydrocarbon waxes. The average molecular weight of the hydrocarbon wax is independent to dose between 0.001 to 1 MGy. This is an odd result since the density of the methane in a liquid form is much higher than in the experiments done in this thesis.

2.3 Radiation-Chemical Interactions

There are many mechanisms through which radiation interacts with matter. In general, every time a high energy particle interacts with matter, some of the particles energy is lost. This energy transfer causes the matter to absorb energy in one of three general methods, excitation, ionization, and disassociation, as described below.

2.3.1 Excitation

Excitation is a mechanism wherein the overall energy of a molecule is raised. This is accomplished either through (1) the promotion of an electron to a higher molecular orbital, (2) an increase in the vibrational energy of the molecule, (3) an increase in the

rotational energy of the molecule, or (4) a combination of the three. This excitation process can be caused by collisions of high energy particles, thermal agitation, photons, chemical activation, and charge transfer. The primary types of excitations that are relevant in radiation chemistry arise from interactions of photons or high energy particles and excitation through charge transfer. [13]

2.3.2 Ionization

If the magnitude of the energy transfer from the radiation source to the material is greater than the ionization potential of the component atoms within an irradiated system, then it is possible for affected atoms to eject an electron and become ions. In hydrocarbon gases, this normally happens from the loss of an electron or a proton. The loss of a proton occurs from a knock on collision from a neutron, a proton, or a heavy ion. The loss of an electron comes from the electronic stopping of a charged particle or the absorption of a photon with energy greater than the ionization potential.[13]

An ion pair will be created from an ionization event. The pair will undergo recombination if the kinetic energy of the ejected electron is too low to escape, or a solvated electron is attracted to the cation.[14] The recombination will add energy to the molecule, making fragmentation more likely.

2.3.3 Dissociation

Dissociation is a process wherein a molecule has absorbed sufficient energy to overcome the energy difference between the molecule and the separated components. The tendency of the molecule to dissociate is dependent upon the energy required for the

molecule to reach a dissociative state. This will often be induced by an increase in vibrational energy until dissociation occurs. This is illustrated in Figure 2-1.

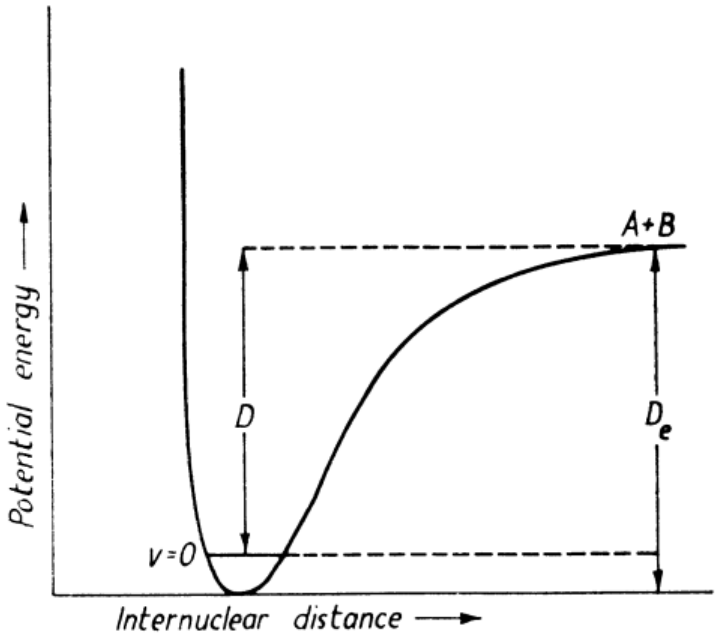

Figure 2-1: Dissociation energy for a molecule[15]

In the diagram above, the dissociation energy is given by D, which is the difference in energy between the ground vibrational state (v=0) and De, which is the total potential energy. This process results in two molecular fragments, shown as A+B above.

Figure 2-1 shows dissociation for a ground electron state, but dissociation can often occur in electronically excited molecules. The vibrational energy curve is shown for the first electronic excited state is shifted toward higher interatomic distances and the potential wells are normally shallower. Electronic excitation is often much faster than the molecular vibrational frequency, resulting in nearly no change in interatomic distance during the excitation. This will place the molecule in an excited vibrational state due to the vertical transition. This jump into a higher vibrational energy with an electronic excitation is known as the Frank-Condon principle.

The excited molecule can also enter a predissociative state, in which the molecule has transitioned into a state where less energy is required for dissociation in the ground electronic state, but is able to dissociate due to intersystem crossing. Both of these processes are shown in Figure 2-2.

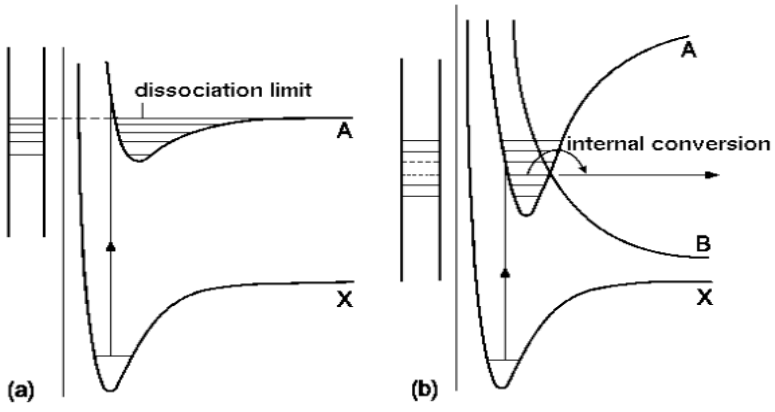

Figure 2-2: A) Dissociation in the electronic excited state B) Predissociation[16]

In radiation chemistry, high energy particles deposit a great deal of energy during interactions. This will often cause excitation into higher electronic states, which may lead to dissociation.[13]

2.4 Radiation Interaction Mechanisms

There are four common radiations particles seen in radiation chemistry; they are gamma rays (and high energy x-rays), electrons, neutrons, and light ions[17, 18]. Each of these radiation types have characteristic interactions within the medium they pass through. The charged particles, electrons and light ions, slow down by interactions with electrons and nuclei in the bulk material .[13] The slowing down of these charged particles is nearly continuous across their passage as the slowing down is primarily due to interaction with electrons and nuclei in the material. The energy that the particle deposits over its track length is used to calculate its stopping power. This Linear Energy Transfer (LET) is dependent upon the particles energy, and will change as the particle losses energy.

Neutrons and gamma rays are neutral forms of radiation. They are able to interact with matter through the production of secondary charged particles, predominately light nuclei and electrons. These charged particles then slow down through electronic and nuclear stopping [17, 18].

2.4.1 Gamma Interactions

Gamma rays deposit energy primarily through the creation of secondary electrons which stream through the medium.[19] Electrons are commonly generated in one of

three processes: Compton scattering, the photoelectric effect, and pair production. The type of interaction is dependent upon the energy range of the photon, and the material it is interacting with. The photoelectric effect is dominant at lower energies, Compton scattering dominates intermediate energies, and pair production is dominate at high energies.[20] The three processes are described below in greater detail.

In Compton Scattering, a gamma ray interacts with a bound electron of an atom. An electron and a scattered photon are then emitted over a continuous energy range and emission angle. This process is shown in Figure 2-3 below.

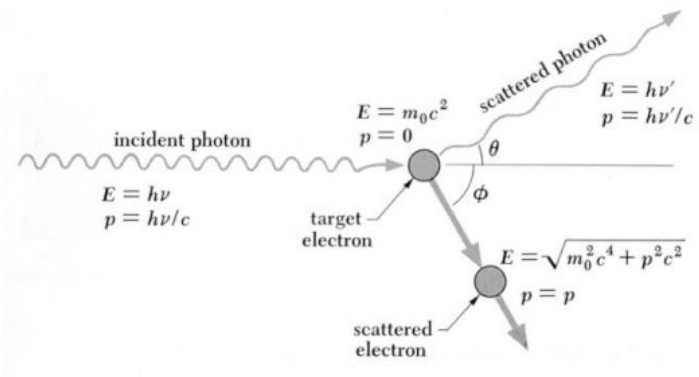

Figure 2-3: Compton Scattering[21]

Pair production is the dominant photon interaction mechanism at high energies (i.e., greater than 1.022 MeV). In pair production, a photon interacts with a nucleus and

produces a positron and an electron. The kinetic energy of the two particles is proportional to the energy of the incident photon. The positron and electron deposit their energy through interactions with charged particles. The positron will annihilate with another electron after it has lost all of its kinetic energy, releasing two photons with energy equal to the rest mass of the electrons (i.e., 0.511 MeV).[20]

The photoelectric effect is the dominate photon interaction mechanism at low energies. In this process, the photon interacts with a bound electron, ejecting it from the nucleus with an energy that is equal to the photon energy minus the binding energy of the electron. [20]

2.4.2 Neutrons

Neutrons interact through the generation of charged particles from the collisions with nuclei. The majority of the interaction will result from scattering events in which the neutron imparts kinetic energy upon light nuclei which travel through the medium depositing energy as the slowdown. The generation of high energy charged particles from collisions results in neutrons having higher LET than electron and gamma rays.[20]

Protons are generated from the collisions of high energy neutron and hydrogen. All of the neutrons energy can be imparted to the proton from head on collisions, but generally only half of the neutrons kinetic energy is transferred.[22] The collision will transfer energy that dependent upon the nuclides mass which it collides with. This is given in the equation below.

$$\frac{E}{E'} = \frac{1-\alpha}{2} \qquad 2$$

Where E is the energy of a neutron after a collision, E' is the initial kinetic energy and α is a scattering parameter given by the equation below.

$$\alpha = \left(\frac{A-1}{A+1}\right)^2 \qquad 3$$

Where A is the atomic mass of the nuclide the neutron collides with. The protons deposit energy in the gaseous medium through electronic stopping. The greater the charge of the particle that moves through, the greater their LET will be. These light nuclei will move through a medium, creating a trail of ionizations in their wake.

Light ions interact in much the same way as the protons do. They are generated from the collisions of high energy neutrons with light nuclei. The LET of these particles is greater than that of the protons due to their higher charge, so they create a greater number of ion-pairs per path length of the traveling particle.[19]

2.4.3 Interaction Cross Sections

The probability of neutron interaction for nuclei of interest in hydrocarbon gas irradiation is shown in Figure 2-4 for many energy ranges.

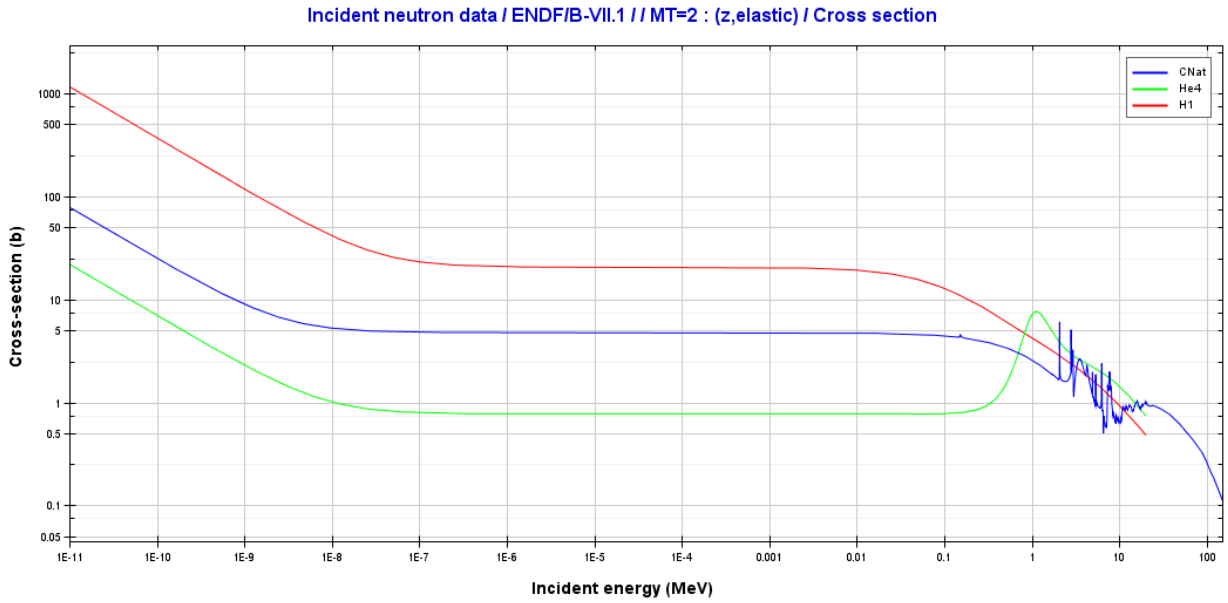

Figure 2-4: Neutron interaction probabilities for natural carbon, hydrogen, and helium over a spectrum of neutron energies (Generated using Janis 4.0)

The probability for neutron interaction with hydrogen is greater than that of helium and carbon for lower energy ranges. Helium and carbon interactions begin to dominate at the higher energy ranges above 800 keV. The plot above show the probability of neutron interaction with some of the constituents of hydrocarbon gases and noble gas, the greater the interaction cross section of the nuclei with a neutron, the more secondary ions will be created.

2.5 Radiation Chemical Reactions

The chemical reactions that occur due to radiation interaction are unlike other, more conventional, chemical reactions. Radiation chemistry reaction principles are quite

similar to the principles of photochemistry, in which molecular excitation is the dominate method for chemical conversion. The reaction mechanisms are predominately from ion-molecule and radical reactions. These reactions are dependent upon the type of radiation, the type of molecules, and the state of the system. The effects of different forms of irradiation will be explained in the following sections.

2.5.1 Linear Energy Transfer Effects

Each form of radiation has a characteristic LET depending upon the material medium and the radiations energy. The loss of energy of a particle moving through a medium is commonly described by stopping power as defined by Bethe formula for electrons is shown in the equation below. [23]

$$-\frac{dE}{dx} = \frac{4\pi}{m_e c^2} * \frac{nz^2}{\beta^2} * \left(\frac{e^2}{4\pi\epsilon_0}\right)^2 * \ln\left[\left(\frac{2m_e c^2 \beta^2}{I(1-\beta^2)}\right) - \beta^2\right] \qquad 4$$

Where $m_e c^2$ is the mass-energy of the electron, z^2 is the charge of the particle, *n* is the electron density within the medium, ϵ_0 is the vacuum permittivity, *I* is the mean ionization potential of the medium, β is the fraction of the speed of light.

In general, the lower the energy of the particle the greater it's stopping power. This is evident in the stopping powers listed in Figure 2-5 for a variety of particles, as computed using the stopping power equation for electron and proton stopping.

Radiation quality	LET (eV/Å)
^{60}Co-γ (500-KeV electron)	~0.02
10-KeV δ-ray	0.3
Tritium β (6 KeV average)	0.5
1-MeV proton	3
Po-α (5.3 MeV)	9
Stripped carbon nucleus (10 MeV/amu)	17
Fission fragments[a]	100–1000

[a]LET of a fission fragment starts at a very high value but is quickly reduced because of electron capture, resulting in an average of ~200–300 eV/Å.

Figure 2-5: LET for common radiation particles[18]

The stopping mechanism for the particles as they move through a gas is dependent upon their energy. The greater the energy of the particles the lower the stopping power of the medium. As the particles begin to slow, there electronic stopping increases as the bare nuclei is able to attract electrons from the surrounding medium. At the lower ion velocities, the dominant stopping power mechanism shifts away from electronic stopping, in which the particle interacts with bound electron. As the particles energy further decreases nuclear stopping begins to dominate. Nuclear stopping is due to direct collisions with the particles and the nuclei of the material which it is passing through.

The energy of the particles and the LET of the radiation lead to different interaction methods with matter. The greater the LET of the radiation, the more interactions it

will have across its path of travel. The radiation interaction on a more macroscopic scale is in the form of blobs, spurs, short tracks and continuous ionization.

The blobs and spurs are a result of an interaction event in which an electron is ejected from an atom and the secondary electron has enough energy to induce further ionizations. This process will continue until enough energy is spent such that it is no longer possible to induce further ionization. This process creates interaction volumes known as spurs and blobs, the spurs are caused by glancing collisions from electrons, in which around 100 eV of energy is deposited per collision.[19] The blob is caused by the energy deposition of around 500 eV, the greater energy deposition allows for larger amounts of electrons to be created.[19] This is shown in Figure 2-6 below.

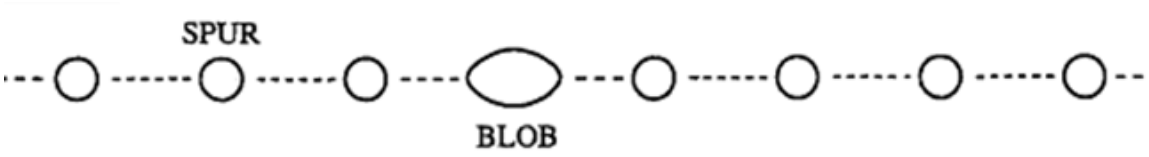

Figure 2-6: Blob and spur formation within gas medium [19]

Blobs and spurs primarily occur in lower LET conditions, such as gamma and electron interactions. The interaction sites are generally independent from one another, and the density of the ions and excited state molecules formed along the track is low

compared to higher LET radiations from light charged particle tracks like protons and alphas.

Continuous ionization occurs where high LET conditions create charge tracks that contain a much higher concentration of ions and excited molecules in their wake. The excitation and ionization of the medium may be continuous along the main particle's track, forming a region of highly reactive molecules. Reactions are prevalent in these tracks since these excited molecules and ions are in close proximity to one another. Though this region is highly reactive, the diameter of this continuous ionization region is on the order of a few nanometers in diameter. Secondary electrons that are emitted from the primary tracks generate another lower LET outside of the main particle tracks. This primary track and the secondary electron paths are shown in Figure 2-7.

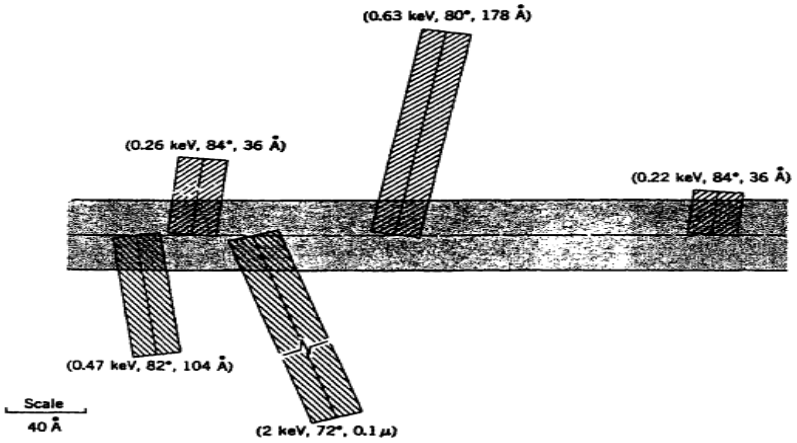

Figure 2-7: Secondary tracks formed from high LET particles [19]

The secondary electrons form a region outside of the main particle track from the secondary particles outside of the main track. A schematic of the regions created by the primary particle track and the secondary track are shown in Figure 2-8.

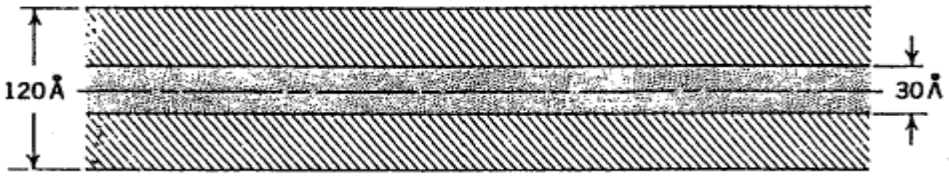

Figure 2-8: Primary Ionization and secondary core formed from high LET particles [19]

2.5.2 Clustering

Another primary interaction mechanism is the formation of clusters around ions and free electrons. Clustering is caused by Wan Der Waals forces induced by the charged particle or ion and has the effect of bringing ions and molecules into close proximity to one another.[24] This contact ,may cause de-excitation though quenching reactions in which the molecule transfers energy to surrounding molecules through the quenching of excited states with nearby molecules. Generally, vibrational excitations in molecules overlap in energy with other with vibrational states in the molecules of the surrounding medium. Therefore, vibrationally exited molecules will quickly lose their energy through quenching.[25] The quenching rate of excited state molecules is dependent upon the

pressure and the temperature of the bulk gas. The density of the molecules increases in the gas as the gas pressure increases. This causes the collisional frequency of the molecules to increase, which will increase the energy lost from excited state molecules through quenching.[25, 26]

2.5.3 The G-value

The G-value is a metric used for determining chemical changes induced through radiation interaction. It is defined as the number of molecules that undergo a specific change with respect to energy deposition from radiation and the standard energy deposition used is 100 eV. Therefore the unit for the G-value is "molecules per 100 eV." Each molecule that is formed as a result of radiolysis has its own characteristic G-value. The G-Value calculation is given in the equation below.

$$G(H_2) = \frac{\text{No. Molecules Changed}}{100\ \text{eV}} \qquad 5$$

2.5.4 Polymerization

Radiation induced polymerization occurs due to the interaction of radicals and ions with one another in a manner that leads to the formation of larger molecules. Due to the high energy nature of the radiation, and the large number of fragments that can be generated from the radiolysis, the polymerization of methane in this present study does not fall into one general category. The polymerization reactions generally proceed through two processes: cationic or radical polymerization.

Cationic polymerization occurs when a positively charged initiator ion is able to react with a neutral monomer, the charge from the initiator transfers to the neutral molecule which then becomes reactive. The polymerization process will continue as long as there is enough energy to for the charged initiator to react with another neutral molecule. In radiation chemistry, some of the cationic fragments that are formed as a result of irradiation are energetic enough to initiate cationic polymerization. Common ion-molecule reactions are shown in the equations below.

$$CH_4^+ + CH_4 \rightarrow CH_5^+ + CH_3 \qquad 6$$

$$CH_2^+ + CH_4 \rightarrow C_2H_4^+ + H_2 \qquad 7$$

$$CH_2^+ + CH_4 \rightarrow C_2H_5^+ + H \qquad 8$$

These reactions represent just a few of the possible cationic reactions that may occur during radiation polymerization. These reactions are driven by the energy of the cationic fragment and the ionization potential of the neutral monomer. The reaction process will continue until the energy from the collision of the ion and the fragments no longer have the ability to overcome the kinetic barrier of the propagation reaction.

The addition of rare earth gases into the hydrocarbon mix can also foster the formation of heavier hydrocarbons though the charge transfer processes. This process occurs due to the higher ionization potential of the rare earth gases compared to the hydrocarbons species.

$$M^+ + CH_4 \rightarrow CH_4^+ + M \qquad 9$$

The addition of rare earth gases in gas mixture under irradiation has two effects. Fist, charge transfer processes increase the hydrocarbon cation population during irradiation. This will allow for a greater number of reactions to occur. Second, the noble gas molecules act a non-reacting body with which the cation can collide. The excited state molecules do not transfer their vibrational energy when colliding with a noble gas. The presence of the noble gas will reduce the frequency of quenching reactions, allowing longer lived excited states, and ultimately greater molecule dissociation.

Paraffinic hydrocarbons with high molecular weight have lower ionization potential than those with lower molecular weight. The lower ionization potential allows for their reaction with lower energy cationic fragments.[3, 11]

$$CH_3^+ + C_2H_6 \rightarrow C_3H_7^+ + H_2 \qquad 10$$

Much of the polymerization in radiation chemistry is due to radical mechanisms. The radicals are formed by the dissociation of excited state molecules. The excited state molecules are generally formed in two ways; (1) the recombination of an electron and a cation or (2) bond cleavage from molecular excitation due to direct radiation interaction. The formation mechanisms for radicals through charge pair recombination and dissociation through direct radiation interaction are shown on the following page.

$$CH_4^+ + e^- \rightarrow CH_3^* + H \quad (11)$$

$$CH_4 + hv \rightarrow CH_3^* + H \quad (12)$$

Regardless of the formation mechanism, reactive radicals are formed. The radicals are very reactive and are able to polymerize methane through the interactions with one another, or with neutral molecules.

One of the primary mechanisms for the formation of hydrocarbon chains from radical processes of saturated hydrocarbons is through radical recombination, as shown in the figure below.

$$C_nH_m^* + C_kH_l^* \rightarrow C_{(k+n)}H_{(l+m)} \quad (13)$$

There are few direct propagation steps for paraffinic hydrocarbons under many other radical polymerization schemes. Only the higher energy radicals, such as those formed during irradiation, are capable of initiating these reactions. The radical species that are formed after the initiation steps do not have enough energy to react with saturated hydrocarbons; there will be no propagation steps in these cases, only initiation and termination steps.

2.5.5 Gas Phase Kinetics

The reactions rates within a gas are dependent upon collision rates of the molecules, and the energy at which they collide. In radiation chemistry, the effect of excited state lifetimes in molecules must also be taken into account. The collision rate of the

molecules is dependent upon the density of the molecules, and their speed. The density of the molecules is directly related to the pressure and temperature of the gas, which is approximated through the ideal gas law.

$$\frac{n}{V} = \frac{P}{RT} \qquad 14$$

Where $\frac{n}{V}$ is the mole concentration, P is the pressure, R the ideal gas constant, T is the absolute pressure. This approximation is valid for light, highly symmetric, molecules at low and intermediate pressures. The velocity of the molecules is dependent upon the bulk temperature of the gas and tends to follow a Maxwell distribution in which an entire range of velocities is possible at a given temperature.[27] This probability distribution function is shown in Figure 2-9.

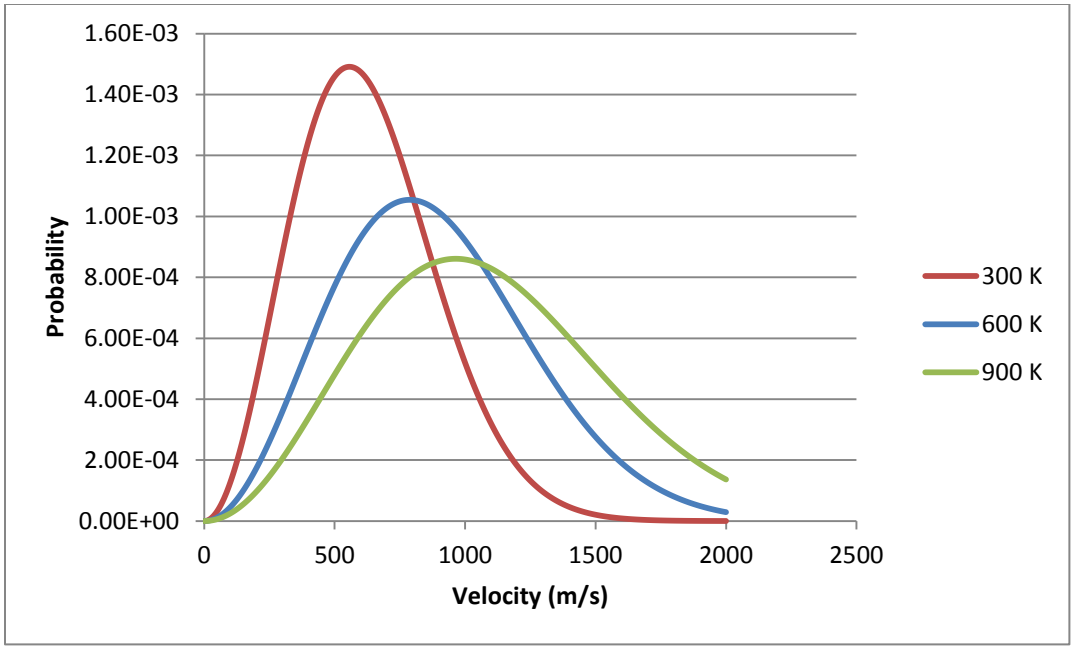

Figure 2-9: Maxwell distribution of gas velocities.

The most probable velocity of the molecule is pushed toward the right as the bulk temperature of the gas increases. There is also an increase in the mean speed of the gas, which is given in the equation below.[28]

$$v = \sqrt{\frac{8RT}{\pi M}} \quad 15$$

Where R is the gas constant, T is the temperature, and M is the molecular mass. The concept of mean speed of the molecules in a gas mixture can be used to determine the average collision rate of the molecules, as well as the collision rate density. This calculation is given in the equation below.

$$z_{12} = \rho_2 \pi d_{12}^2 \sqrt{\frac{8kT}{\pi\mu}} \quad 16$$

Where, ρ_2 is the density of molecules, d_{12} is the average distance between two molecules, and μ is the reduced mass of the two colliding bodies. This model uses the mean relative speed between the molecules to calculate the collision rates. The model also assumes that the colliding bodies are hard spheres which are approximately valid for small, high symmetry molecules.

2.5.6 Dissociation Dynamics

The rate and the manner of molecular dissociation are dependent upon the molecules properties, the gas temperature, and the LET of the radiation. In general, fragmentation is more likely when molecules have large amounts of energy injected into them. The larger amounts of energy allow for molecules to be moved into higher-energy, less-stable, short-lived states. These molecules will de-excite or fragment by processes described in the dissociation section.

In gas phase dynamics, the de-excitation of molecules is dependent upon the collision frequency and temperature. The higher the collision frequency corresponds to greater energy transfer from excited state molecules. In addition, when gas is in a higher temperature state, there is an increase in collisional frequencies arising from the increasing mean speed of the molecules. Higher temperatures increase populations of higher excited states of the bulk gas molecules, allowing for greater energy overlap with molecules excited by radiation interaction.

2.5.7 Radiation Interaction Time Scales

Each of the processes described in the previous sections have their own characteristic time scales, the time scales for each process determines the overall kinetics and the products of the radiolysis. The time scales for the reactions are generally parsed into three stages: (1) the physical stage, (2) the physiochemical stage, and (2) the chemical stage. These stages, and their timescales, are shown in Figure 2-10 below.

$-\log_{10} t$ (sec) $\equiv pt$	Event	Stage
18	Fast electron traverses molecule.	Physical
17	MeV proton traverses molecule. Energy loss to fast secondary electrons.	
16	Energy loss to electronic states (vertical excitation).	
14	Fast ion–molecule reaction (H-atom transfer). Molecular vibration.	
13	Solvated electron formed in water. Longitudinal dielectric relaxation in water. Fast dissociation.	
12	Electron thermalized in nonpolar media. Spur formed. Self-diffusion time scales in simple liquids.	
11	Transverse dielectric relaxation time in water.	Physiochemical
9	Spur reactions continued.	
8	Charge neutralization in media of low viscosity. Secondary reactions including intertrack reactions.	
6	Electron escape time in low-viscosity media.	
0	Radiative lifetime of triplets.	Chemical
−3	Neutralization time for media at very high viscosity.	

Figure 2-10: Approximate time scales for events in radiation chemistry[13]

The time scales for these reactions are specific to each system under irradiation. The table is not to be taken literally for each system and each of the stages shown may span many orders of magnitude. It is only meant to show that each time scale has relatively few processes competing within each time scale. The products at the end of one timescale serve as the input for the next timescale.

The energy absorbed within a molecular system is quickly redistributed between many modes.[13] The energy distribution is shown in Figure 2-11 for a generic system. The initial energy absorbed is in the form of electronic excitation with a transition time that is much shorter than the order of molecular vibrations. This allows the transition into both an electronically and vibrationally excited state through the Frank-Condon principle. The vibrational energy state can be high enough to exceed the dissociation energy, thus causing molecular dissociation. Predissociation is also possible, but generally occurs on longer timescales. The remaining energy will be lost through quenching. These time scales are only approximate and many of the precise details are unknown.

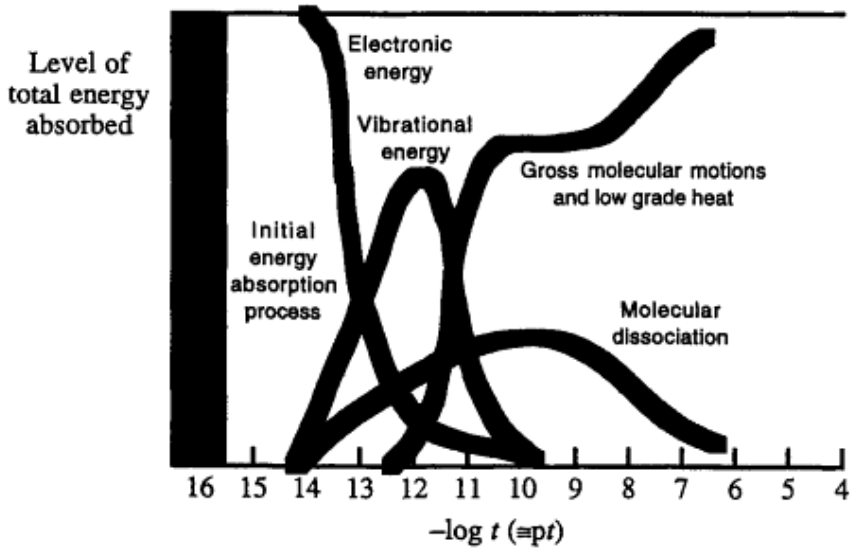

Figure 2-11: Energy distribution with respect to time after energy absorption[13]

3 EXPERIMENTAL DESIGN AND PROCEDURES

The several experimental systems that were tested throughout the experimental portion of this research are described in this Chapter. The first irradiation experiment of this type was actually conducted using carbon dioxide-hydrogen mixtures at the NSCR. The outcome was negligible, but the system is described here as it led to the methods developed for the methane irradiations. The CO2 experiments were intended to build upon the previous radiation chemistry experiments of Beattie in which methane and heavy hydrocarbons were formed from the mixture of ^{3}H and CO_2 gas.[29] This system was not pursued further after one initial test due to the extraordinary dose requirement (above 1×10^{8} Gy) for the chemical conversion to take place and the dangers associated with handling near kCi amounts of tritium gas mixtures at high pressures.

The methane irradiations focused on a variety of gas mixtures gas in test vessels and irradiation sources that evolved over the course of the experimentation. The testing proceeded in the following sequence:

1. Neutron irradiation in the NSCR. The methane was charged under high pressure (2.07 MPa) to emulate conditions that may be found inside of industrial gas processing systems.

2. Electron beam irradiations using a manifold with eight smaller stainless steel vessels to hold methane and methane-noble gas mixtures for irradiation. These irradiations were done using a conveyor belt at the facility and stationary under the electron beam.

3. The manifold of steel vessels was also used for hi intensity gamma irradiation using a La-140 isotopic source at the NSC. Each of these experiments is described in more detail below.

4. A last irradiation at the NSCR was performed using the same irradiation vessel as in the first experimental series (1). The system was pressurized with a mix of helium and methane gas at high pressure (2.07 MPa).

3.1 Initial NSCR Gamma Irradiation of CO_2

The irradiation carried out at the NSC for carbon dioxide was performed to emulate an experiment by Beattie, et al.[29] and the gas mixture mimicked the highest yield tests from that study with 0.0759 MPa hydrogen and 0.0027 MPa CO_2. A large steel vessel was placed alongside the NSCR core immediately after shutdown. The experiment can be seen in Figure 3-1 and Figure 3-2 in which images of the vessel being tied up for the irradiation and the other of the vessel next to the NSCR. The vessel was lowered into the reactor core by suspending it using a simple set of nylon and a crane. The vessel had a steel plate lying on the bottom of the vessel to make sure that it was not buoyant. The reactor was scrammed as the vessel was brought into proximity of the core. At the point of shutdown, an initial gamma dose rate of 2.26×10^3 Gy/hr of gamma radiation was incident upon the steel vessel. The dose rate rapidly declined within minutes of reactor shutdown. The vessel was left against the reactor core for approximately 7 hours.

Figure 3-1: The steel vessel with all of the ropes attached.

Figure 3-2: Stainless steel vessel sitting against the reactor core.

3.1.1 Gas Extraction with CO_2 Systems

The post-irradiation gas product was extracted by condensing the gas in a small pressure vessel. The condensing vessel was submerged in liquid nitrogen in order to liquefy any methane that may have been formed as a result of the irradiation. After the gas transfer, the small pressure vessel was allowed to warm up to ambient temperatures. A pressure gauge fitted the system showed an increase in pressure as the vessel warmed, indicating gas was extracted. The pressure vessel was cooled, and kept cold until the product gas was ready for analysis in the GCMS. Prior to analysis, the gas was allowed to warm to room temperature.

3.2 Neutron Irradiation Systems

Gas samples were irradiated in the NSCR in an all-aluminum pressure vessel pressurized up to 300 psig with methane/noble gasses, and held approximately 380-mL of gas, with a diameter of 5.08 cm. The samples were placed in one of three positions in the NSCR for neutron irradiation. The neutron fluxes in these positions are measured and varied between 5E12 to 1E13 $n/cm^2/s$. A schematic of the NSCR with irradiation locations are shown in Figure 3-3.

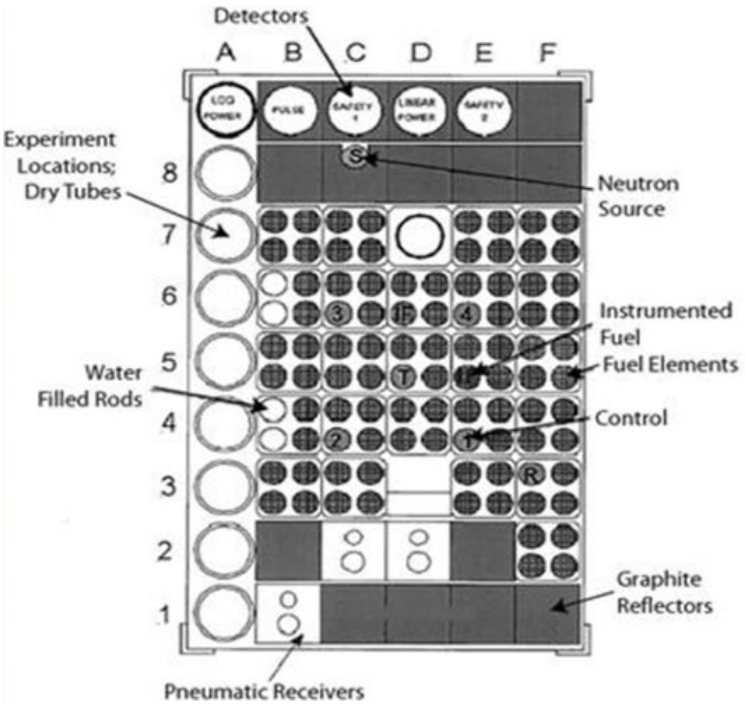

Figure 3-3: Schematic of NSCR Core

Figure 3-4 shows the small welded aluminum pressure vessel used in the subsequent NSCR irradiations; The inlet was a closed Swagelok™ quick-connect capable of working at pressures up to 4.14 MPa. This vessel is placed inside of a CO_2 filled, aluminum dry tube that is placed next to the reactor for irradiation. The small pressure vessel is shown in Figure 3-4.

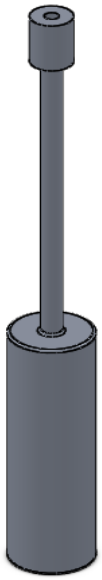

Figure 3-4: 5.04 cm diameter, 380-ml, aluminum pressure vessel used for first reactor irradiations

The gas was extracted using and existing gas transfer system at the NSC. This system was originally developed to transfer argon gas from the reactor vessel shown above to another tank that could then be taken out of the NSC. A schematic of the operational logic for this transfer system is shown in Figure 3-5.

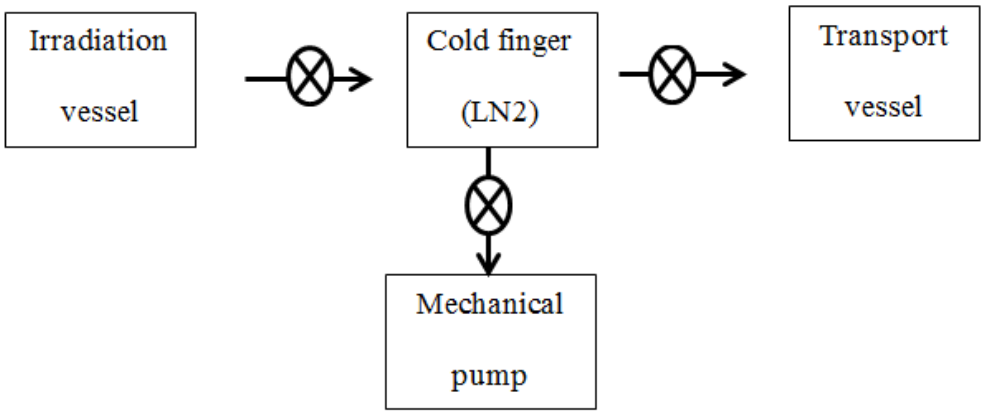

Figure 3-5: Schematic of gas transfer system.

The gas is transfer system was evacuated to remove air and residual volatile contaminants. Then, the valve between the irradiation vessel and the cold finger was opened and the gas pressure was allowed to equilibrate. The cold finger was then submerged in liquid nitrogen, causing the gas within to liquefy. The valve between the irradiation vessel and the cold finger was then closed and the valve between the cold finger and the transport vessel was opened. The cold finger was then removed from the liquid nitrogen, causing the pressure to increase; the pressure is allowed to equilibrate between the cold finger and the transport vessel. This process is repeated several times until no further gas was able to be withdrawn from the irradiation vessel.

The gas was analyzed through the use a GCMS in the mass spectroscopy laboratory in the chemistry department of Texas A&M University. The gas tank is brought to

the mass spectroscopy laboratory along with a regulator with a hose and a needle to enable gas injection directly from the gas tank into the GCMS.

3.2.1 Methane

The methane gas was high purity gas obtained by AOC in Bryan, Texas, and was brought to the NSC in a small pressurized cylinder. The gas was transferred to the small cylinder with three backfills from the high purity methane tank to reduce contamination. The gas was transferred through the use of high pressure regulators and hoses to the aluminum pressure vessel. The vessel shown in Figure 3-4 was then filled to approximately 2.07 MPa (300 psig) with methane gas. The vessel was placed in the reactor core for approximately 8 hours in position D3 with the reactor operating at 1 MWth. The gas tanks were then taken to the GCMS in the mass spectroscopy lab in the chemistry department for analysis. Gas collection and analysis was carried out in the GCMS using the same method described above.

3.2.2 Methane/Argon Irradiation

The irradiation vessel shown in Figure 3-4 was filled to 2.07 MPa (300 psig) with a 50:50 mixture of methane and argon gas. The gas was placed on core in the A3 position and irradiated for approximately 6 hours. After the irradiation the gas is extracted using the gas transfer system, the radioactive argon that was generated through neutron capture was allowed to decay overnight. The gas was then taken to the mass spectroscopy laboratory to be analyzed by GCMS using the method described above.

3.2.2 Methane/Helium Irradiations

The irradiation vessel shown in Figure 3-4 was filled to 0.9653 MPa of helium and methane gas at 0.3447 MPa and 0.6206 MPa, respectively. The reason for this difference in pressure was operator error on operation of the regulators. The gas was placed in the D3 position for an irradiation that lasted approximately 6 hours. The gas was removed by the argon transfer system as described above. There was difficulty in the gas extraction since helium does not condense at liquid nitrogen temperatures; this made gas recovery more difficult. The gas was then taken to the mass spectroscopy laboratory to be analyzed by GCMS using the method described above.

A second methane helium run was done using the same system as the first irradiation. The irradiation vessel shown in Figure 3-4 was filled to 300 psig of helium and methane gas with 164.7 psi methane and 150 psi helium. This vessel was placed into the reactor in the A3 position. The power was run at approximately 1 MW for 6 hours, and was then removed from the core. The gas was analyzed using the MS system described below in Section 5.3.4.

3.3 Electron Beam Experiments

An irradiation vessel manifold was constructed that utilized eight stainless steel pressure tanks capable of holding hydrocarbon gas at high pressures and temperatures. This system is shown in Figure 3-6. This system was used to irradiate methane gas at the National Electron Beam Facility at Texas A&M University. This facility houses two 10 MeV 15 kW electron beams that are capable of delivering very high doses. The pressure vessel system was placed on a conveyer belt to be irradiated by one of the two linac ac-

celerators. The accelerators scan their electron beams back and forth at high frequencies such that the electron beam approximates linear geometry.

Figure 3-6: Pressure system used for gamma and electron beam irradiations (shown without shields)

Figure 3-7: The pressure vessels moving to the irradiation zone

The system is shown entering the electron beam irradiator in Figure 3-7 with steel shields placed over the valves. The electron beam from the linac emits a line source of electrons that evenly irradiates the items that pass underneath. This is done through the use of a rapidly oscillating magnetic field which changes the beam into a line source.

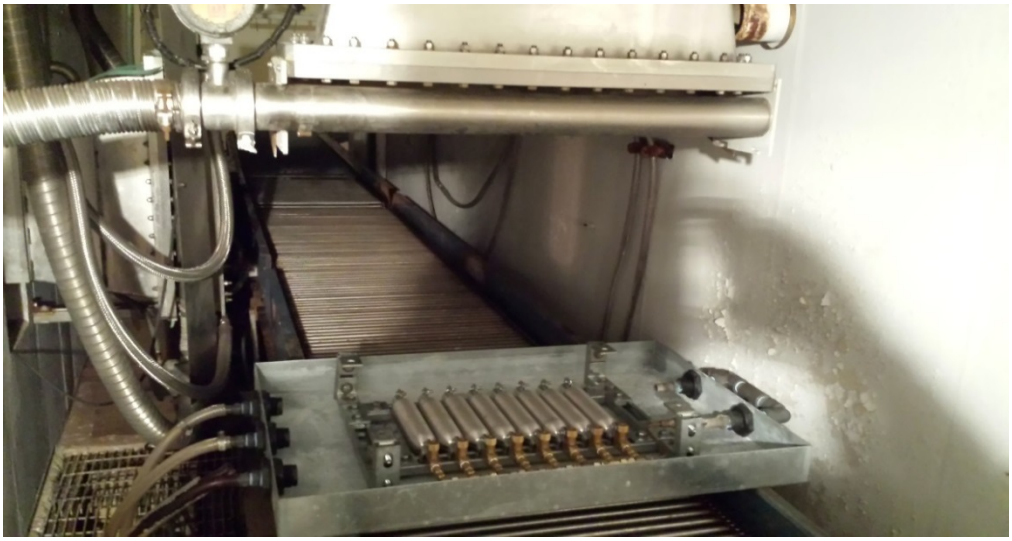

Figure 3-8: Irradiation cell of the electron beam facility

Figure 3-8 shows the vessel fixed directly under the electron beam window in a secondary tray designed to enable much higher doses. When the vessel position is fixed underneath the accelerator, it is contained within the aluminum tray with cooling water flowing through it. The cooling water ensured that the vessels underneath of the beam did not overheat. This water filled tray is shown in Figure 3-9.

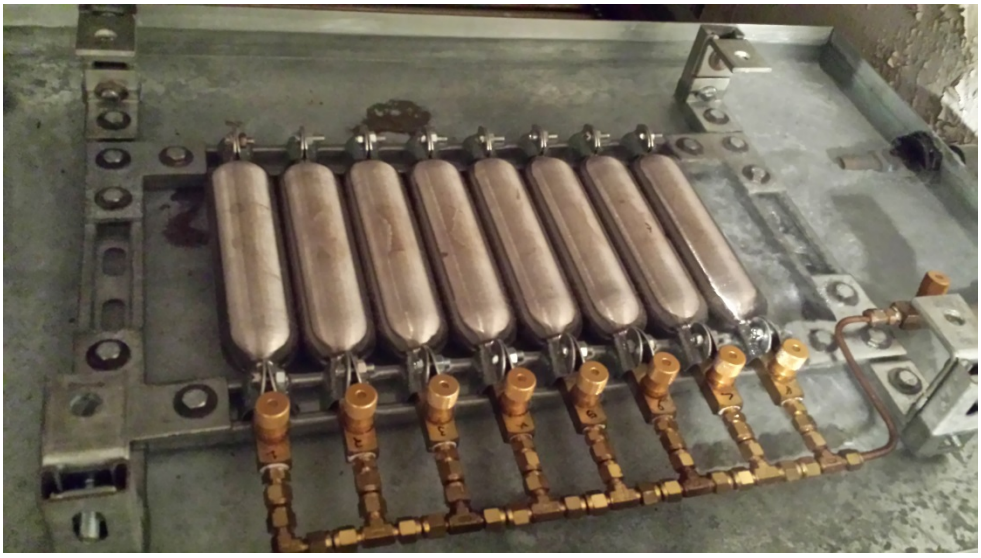

Figure 3-9: The pressure vessel submerged in water post irradiation

3.4 La140 Irradiations

An isotopic La-140 source at the NSC was used to irradiate methane gas at high pressures with high intensity gamma irradiation. This La140 source is comprised of an array of La_2O_3 rods in an aluminum block shown in Figure 3-10. The block is activated by neutron irradiation from the NSCR until the desired La-140 activity is reached, at which point the source array is moved away from the reactor to enable samples with electron and gamma irradiations. The same vessel manifold from the electron beam irradiations, shown in Figure 3-11, was placed underwater against the activated La-140 source overnight for gamma irradiations. The system was maneuvered in front of the La-140 source with the use of ropes. The shields used to protect the valves from the electron beam were removed to reduce weight, allowing the vessel to be lowered and raised out

of the water with ease. For the exposures in this work, the La-140 source activated to 400 Ci.

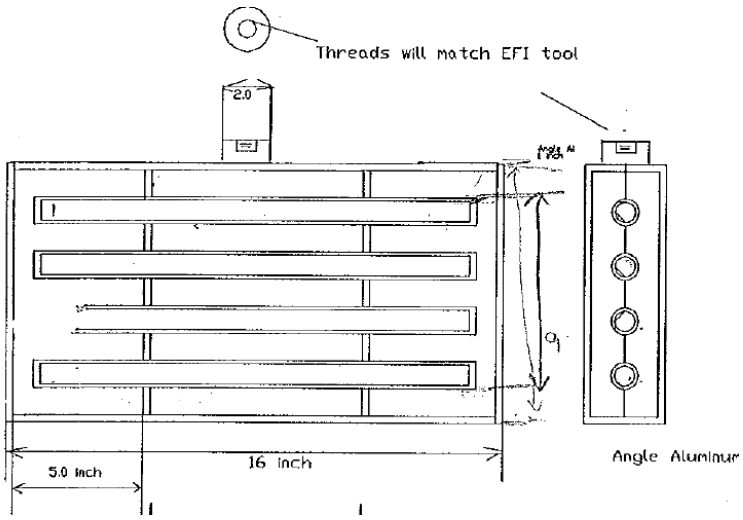

Figure 3-10: La-140 source used for gamma irradiations

The activation scheme for the production of La-140 is given in the figure below.

$$La^{139} + n \rightarrow La^{140} + \gamma \qquad 17$$

The La-140 will then decay to Ce-140 through beta decay, releasing an electron, and several gamma rays.[30]

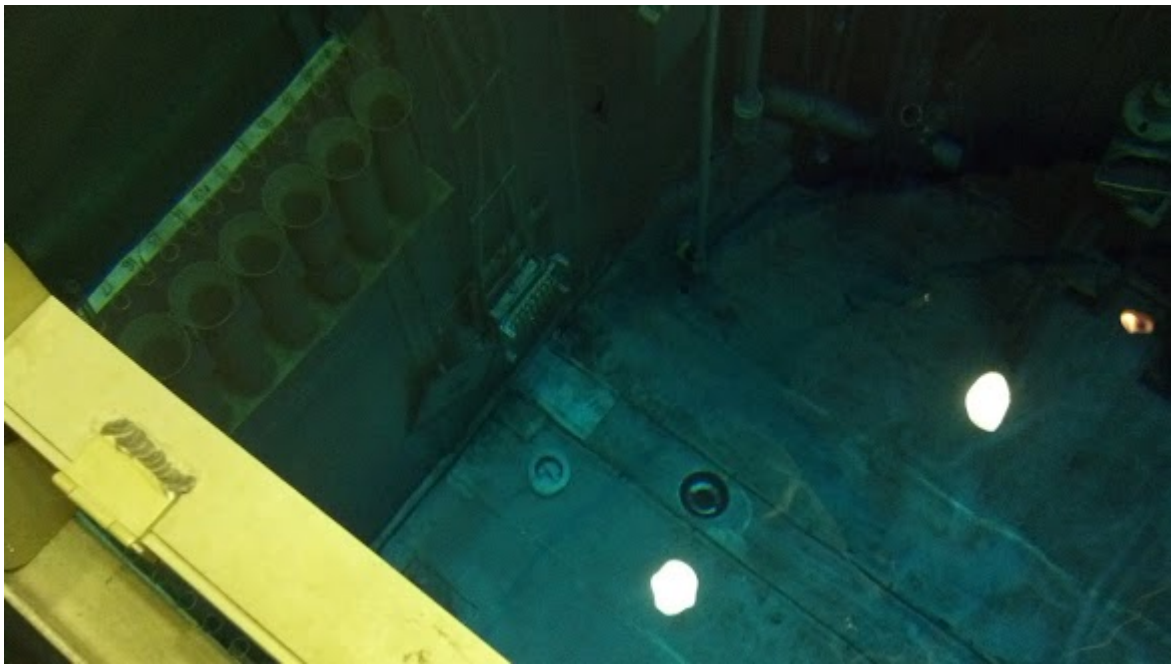

Figure 3-11: Steel vessel sitting next to the radioactive La-140 source

This source was used in two experiments for the gamma irradiations of high pressure helium and methane mixtures. After irradiation, the vessel was brought back to the laboratory. The gas tank was fitted with a needle that allowed for direct injection into the GCMS at the mass spectroscopy laboratory.

3.5 Mass Spectroscopy

The principle detection method for hydrocarbons was mass spectroscopy. This was employed as an efficient detection method for the detection of heavy hydrocarbon species, as well as the presence of excess hydrogen. The presence of excess hydrogen

was used as an indicator for the polymerization of light hydrocarbons to heavier hydrocarbons.

3.5.1 GCMS

The Gas Chromatography Mass Spectroscopy (GCMS) system uses a gas chromatograph with one end connected to a mass spectrometer. The gas chromatograph portion is used to separate hydrocarbons by their intramolecular attractions to the surface of a capillary column. The capillary column has a non-polar surface which attracts non-polar molecules. This will cause molecules with greater non-polar intramolecular interactions to have a greater affinity to the column. Since all of the molecules that enter the column have different affinities, they will all desorb at different temperatures. This allows the molecules in a gas sample to be separated by manipulating the temperature of the column; the molecules are effectively separated by their boiling points. A schematic of a GCMS unit is shown in Figure 3-12.

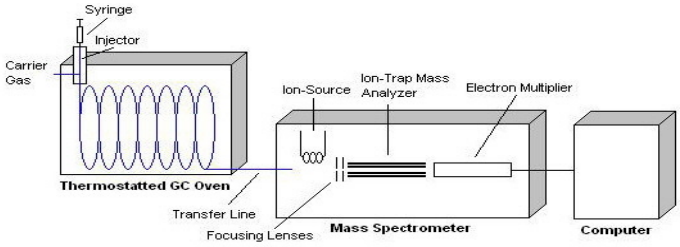

Figure 9. Schematic of the GC/MS system.

Figure 3-12: GCMS schematic[31, 32]

The degree of separation is dependent upon the characteristics of the column, the carrier gas flow rates, and the column temperature. In order for the concentration of each of the components to be analyzed, each of the molecules must be separated from one another. The area under each of the peaks may then be compared to standards to determine the concentrations of each component in the mixture. This is done by computing a response factor for each of the molecules of interest in the sample, which is given in the equation below:

$$R = \frac{A_c * m_s}{m_c * A_s} \qquad 18$$

Where A_c is the area under the peak of the sample, m_s is the mass of the molecule in the standard, A_s is the area of the peak in the standard, and m_c is the mass of the molecule in the sample.[31]

Response factors are challenging to compute if there is insufficient separation between the components of the mixture. The degree of separation is given by the column resolution, which can be used to estimate the purity of each peak in the GC spectrum. This is given by the equation below:

$$R_s = \frac{2 * \Delta Z}{W_A + W_B} \qquad 19$$

Where ΔZ is the difference in the retention times between two peaks in the spectrum, and W_A and W_B are the widths of adjacent peaks from sample A and B. The greater the resolution factor, the greater the purity of each peak.[31]

After the gases are separated in the chromatograph, they travel to a mass spectrometer for analysis. The mass spectrometer produces and m/z spectrum for the components contained within each of the peaks. Also, the total ion count, which is the total amount of ions that are incident upon the detector, is also recorded.

3.5.2 Quadrupole Mass Spectroscopy

The second type of mass spectroscopy used in this study was a qaudrupole mass spectrometer. This spectrometer is able to separate molecular fragments by their mass-to-charge ratio (m/z). A schematic illustrating the principles of operation for the qaudrupole mass analyzer is given in Figure 3-13.

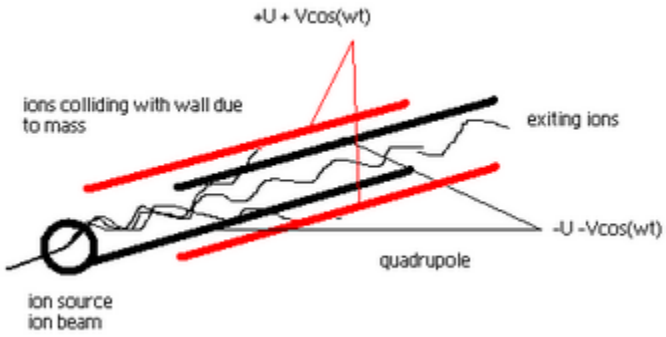

Figure 3-13: Quadrupole mass analyzer[33]

This type of spectrometer uses electron impact to turn the molecules into molecular ions.[34] These ions are then sent into a region that contains four parallel metal rods.

Each of the opposing pair of rods is connected together electrically, and a radiofrequency (RF) voltage is applied between the two pairs of rods. A direct current (DC) voltage is then superimposed onto the RF voltage. The ions are sent down the quadrupoles with the varying AC and DC voltages. The each pair of opposing rods has either a DC or AC voltage between them. The electric fields caused from RF and DC voltages cause the ions to oscillate between the quadrupoles as they travel down the spectrometer tube. The ions are collected by either a faraday cup or an electron multiplier where they are counted for analysis. The ions that do not have the right m/z ratios will collide with the quadrupoles before they make it to the detector.

The molecular ions are generated by molecular impact from 70 eV electrons between the filament and the cathode.[31] This is a hard ionization source that causes the molecules to fragment upon impact, which makes the mass spectrum contains many molecular fragments and fewer molecular ions. These spectrums make it easier to determine the structure of the molecules since the fragments identity can be easily identified.

3.5.3 Hydrocarbon Fragmentation

Hydrocarbons have characteristic fragmentation patterns inside of mass spectrometers. The fragmentation products are dependent upon of the ionization method used and the molecular structure. The ionization source used inside of many mass spectrometers is electron ionization, which is a hard ionization source. This causes a great deal of fragmentation of molecules as they are accelerated down the tube. This will create a dis-

tribution of ion fragments in the mass spectrum which is characteristic of each molecule.[31]

The distribution of the cationic fragments once they reach the detector is dependent upon it relative stability. The more stable the fragment, the greater the number that will be formed. As a general rule, the most stable fragments will be able to delocalize the positive charge of the ion through electron donation or resonance.

The spectrometer directly measures the current from the ions for each m/z ratio, it is not directly able to measure the partial pressure of each of the components in the gas mixture. In order to convert the current from the component to pressure, the current must be multiplied by a sensitivity factor given in below.

$$S_f = \frac{(H - H_0)}{(P - P_0)} \qquad 20$$

Where $H - H_0$ is the change in the principle mass peak height corresponding to $P - P_0$, the change of the partial pressure of the component. In order for careful quantitative analysis to be performed, the sensitivity factors must be calculated for each of the components of the gas mixture prior to making the measurements. These factors will change depending on the age and history of the detector head, the ionization energy, emission current, mass filter setting, type of detector, etc.

3.5.4 Mobile Mass Spectrometer System

In order to carry out the final (and potential future) gas irradiation experiments at the NSC, a portable mass spectrometer system was built that is capable of measuring hy-

drogen, methane, and volatile hydrocarbons (from 1 to 200 m/z (amu to charge)). This mass spectrometer system uses a Stanford Research Systems Residual Gas Analyzer. This translates directly to molecular mass of fragments in most cases since most of the ions in the mass spectrometer are singly charged (z=1). This spectrometer utilizes an electron impact ionizer that operates at 70 eV; this hard ionization source will cause a great deal of fragmentation of the parent molecular ion, causing the spectrum to contain a greater number of fragment peaks. Attached to the RGA is the electronics control unit (ECU) which is a self-contained unit that is able to provide control of scan parameters for the mass spectrometer. The RGA is pumped down with a Varian V-81A turbo pump and a Varian SH-110 dry scroll pump that is capable of bringing the pressure within the RGA below 1 x 10^{-8} torr. This system has a high precision needle valve that is capable of controlling flow from a high pressure environment (>0.1 MPa) to the high vacuum environment of the RGA (<10^{-6} torr). During measurements, the flow through the valve is regulated such that the pressure within the spectrometer is ~10^{-6} torr. A simplified schematic of the mass spectrometer system is shown in Figure 3-14.

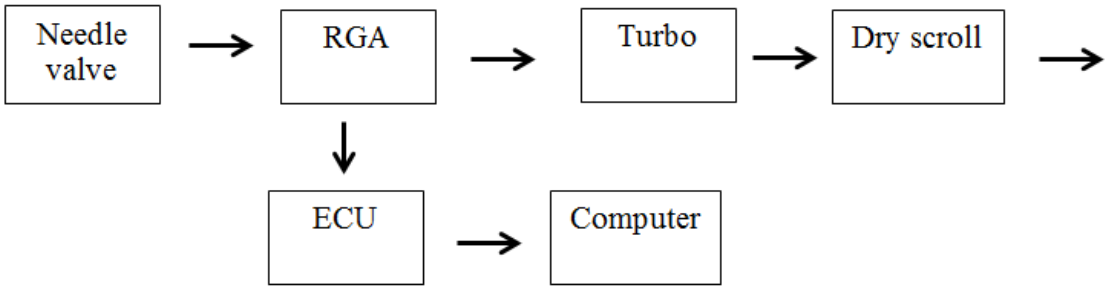

Figure 3-14: Simplified schematic of the mass spectrometer system

The mass spectrometer and all of the supporting pumps, controllers, and gauges are shown in Figure 3-15. This system is used to measure the hydrogen, methane, and light hydrocarbon contents of irradiation vessels.

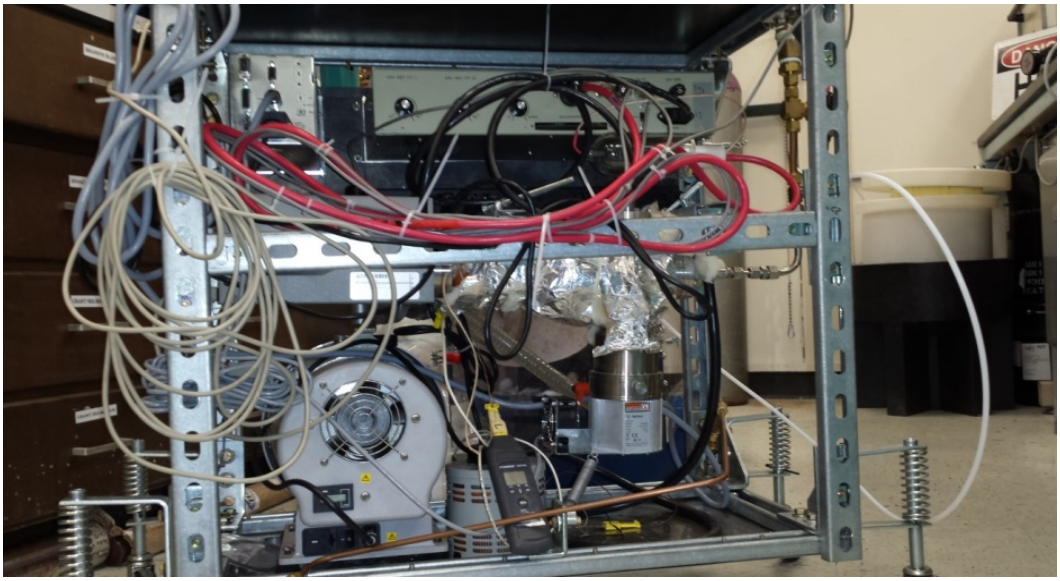

Figure 3-15: Mobile Mass spectrometer system used for hydrocarbon analysis

4 RESULTS

The results for all reported experiments are presented in the following sections. There are limited to the experiments in which GCMS or MS analysis was available. This is shown in Table 1.

Table 1 Gas irradiation experiments performed

Experiment	Description	Total Dose to Gas (Gy)
CO_2-H_2 Irradiation	A CO_2-H_2 mixture was irradiated by the NSCR immediately after shutdown	6.13E+3
Methane neutron Irradiation	Methane gas at 2.07 MPa was irradiated in the NSCR at 1 MW	9.7 E+5
Methane/Argon Irradiation	Methane/argon (50:50) gas at 2.07 MPa was irradiated in the NSCR at 1 MW	1.37E+6
Methane/Helium Irradiation	Methane/helium gas (36:64) at 1.034 MPa was irradiated in the NSCR at 1 MW	2.16E+6
Electron Beam Irradiation #1	Methane/helium gas mixtures (50:50) at 2.07 MPa was irradiated at the electron beam facility	2.71E+4

Table 1 (continued)

Electron Beam Irradiation #2	Methane/helium gas mixtures in varying concentrations at 2.07 MPa was irradiated at the electron beam facility	2.71E+4
Electron Beam Irradiation #3	Methane/helium gas mixtures in varying concentrations at 2.07 MPa and 5.515 MPa was irradiated at the electron beam facility	2.35E+04
Electron Beam Irradiation #4	Methane/helium/argon gas mixtures in varying concentrations at 2.07 MPa was irradiated at the electron beam facility	2.20E+5
La-140 irradiation	Methane/helium gas mixtures in varying concentrations at 6.894 MPa was irradiated using the La-140 source at the NSC.	2.40E+2
Methane/Helium Irradiations	Methane/helium (50:50) gas at 2.07 MPa was irradiated in the NSCR at 1 MW	1.12E+6

4.1 CO_2/H_2 Irradiation

The CO_2/H_2 experiment described in Section 3.1 was analyzed in the GCMS through direct injection. The direct injection of the hydrocarbons was done after the small vessel containing the gas sample was allowed to warm up, and the pressure within was higher than the pressure within the capillaries of the GCMS. A plot of the GC-MS spectrum for the irradiation is shown in Figure 4-1.

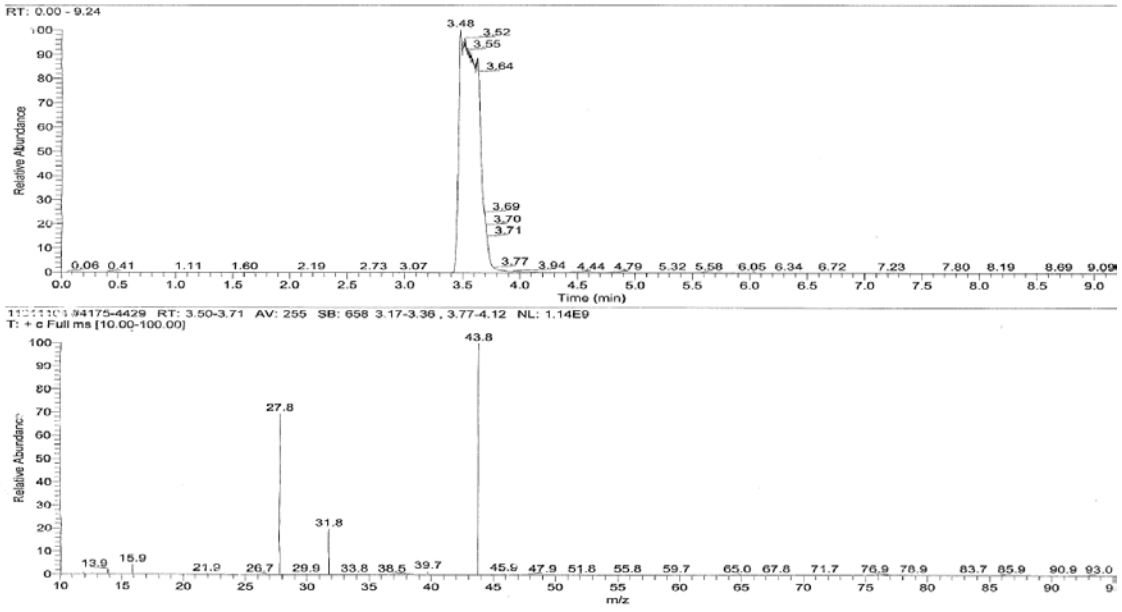

Figure 4-1: The GC-MS spectrum from the CO_2/H2 gas run

This separates out components of gas mixtures based off of their affinity for the inner surface of the column. The plot below the GC plot is the MS plot. This shows the

mass spectrum at a particular time in GC spectra. The time of the MS plot shown is between 3.5 and 3.71 minutes, which correspond to the large single peak. The MS spectrum shows the presence of oxygen, nitrogen and CO_2. Nitrogen and oxygen are contaminants that likely leaked into the small pressure vessel used to condense the gas; the peaks are at 13.9 and 27.9 for nitrogen, and 15.9 and 31.8 for oxygen. The hydrogen is not shown in the spectrum since the mass spectrometer is not able to detect anything at or below the mass of helium (MM=4) due to helium being the carrier gas. There was no observable indication of methane being formed from the irradiation of CO2 and H2 as the Beattie experiments have indicated.[29]

The vessel (Figure 3-1) was opened to search for any trace of the white polymeric powder described in the Beattie papers.[29] No powder was recovered. The inside walls of the vessel were completely cleaned and no a trace of powder or other solids was evident. It was concluded that this was not a fruitful research direction and the focus of the remaining tests were on methane conversion.

4.2 Irradiation of Methane at NSC

Methane gas was placed inside of the aluminum pressure vessel shown in Figure 3-4 and inserted into the reactor core at the NSC. The gas was extracted by using the NSC's argon transfer system. This allows for gas to be efficiently transferred from the irradiation vessel to an extraction vessel. The gas was analyzed from the extraction vessel. The gas had to be transferred to an extraction vessel because the irradiation vessel

was radioactive due to neutron activation and was not able to be removed from the reactor pool.

Three separate irradiations were performed in this manner; one using only methane, one with a mix of methane and argon, the last with a mix of methane and helium. The three experiments are described in more detail in the following pages. The gas filled vessel was placed into a dry tube (Figure 3-4) and set against the reactor core in position D3 according to the description in Section 3.2. Figure 4-2 below shows the NSC reactor and the reactor core running with dry tubes being irradiated.

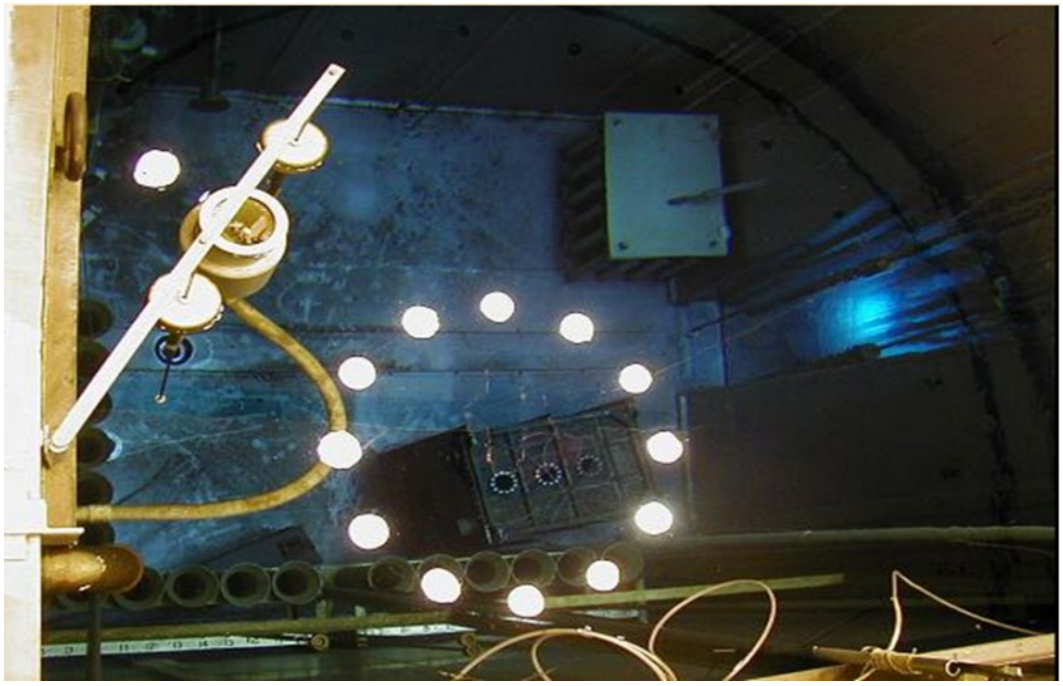

Figure 4-2: The reactor running at 1 MWth with dry tubes in irradiation slots

4.2.1 Methane Only Irradiation

The methane irradiation was completed in the small aluminum pressure vessel shown in Figure 3-4. The gas was extracted in a small pressure cylinder using the argon capture system. The gas was then injected directly from the extraction cylinders into the GC-MS instrument described in the CO2 experiments. The GC-MS spectrum of the methane irradiation is shown in Figure 4-3 below.

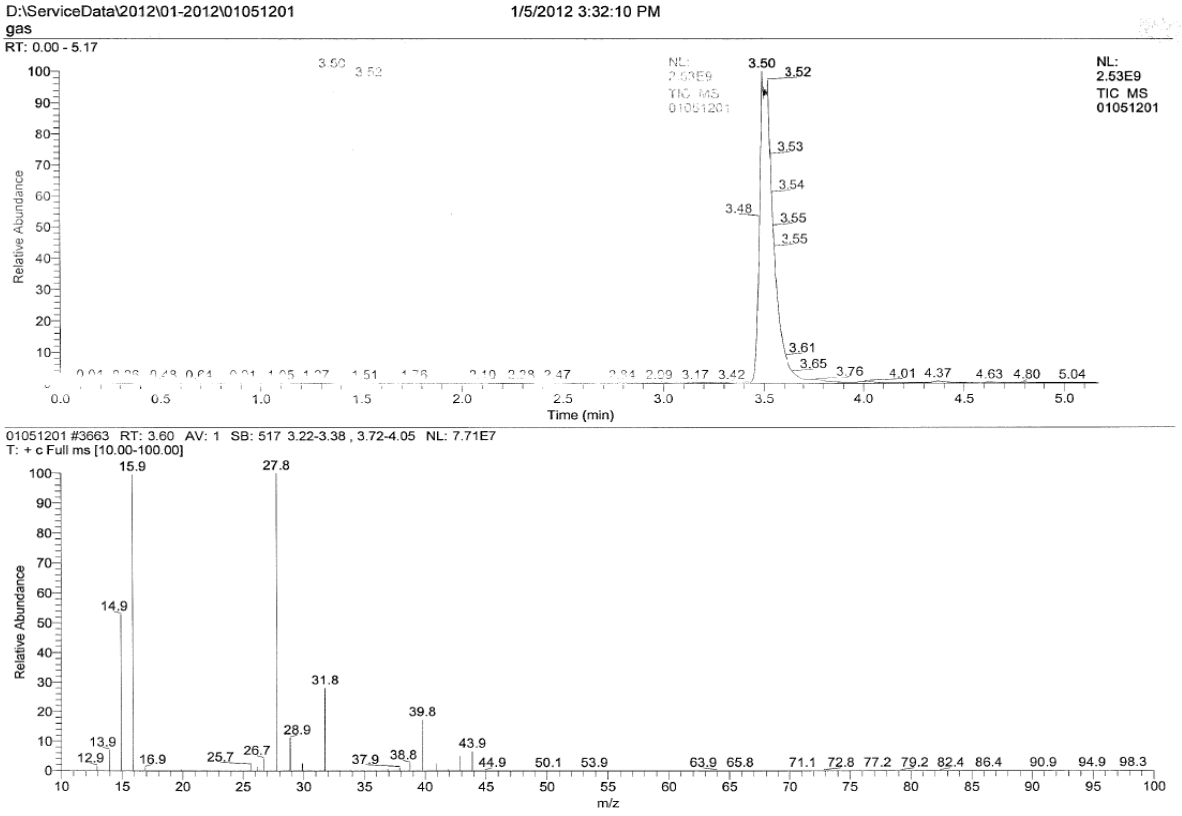

Figure 4-3: The GCMS spectrum for the methane reactor irradiations

The GC-MS spectrum above shows the presence of methane, ethane, and propane inside of the reaction mixture. The yields of ethane and propane are very small compared to methane. The peaks in the spectrum at 27.8 m/z and at 31.8 m/z show that contamination from air in the system was present. This is likely a result of imperfect injection methods into the GCMS. The GCMS spectrum shows a small tail from the main methane peak. This tail may be caused from heavier hydrocarbons which formed due to polymerization, were already present within the starting gas, or was due to column saturation. In other words, the basic observation is that higher mass hydrocarbons were formed at a low rate and the higher numbers had significant uncertainties.

4.2.2 Irradiation of Methane and Argon

The conversion of methane to higher hydrocarbons was very poor in the methane only irradiation. To increase the yields, a 50/50 mixture of argon and methane by mole fraction was irradiated. The argon was intended to act as an internal homogenous beta source by absorbing a neutron and then decaying. The gas was extracted using the argon capture system described above. The GC spectrum of the gas is shown in the Figure 4-4 below.

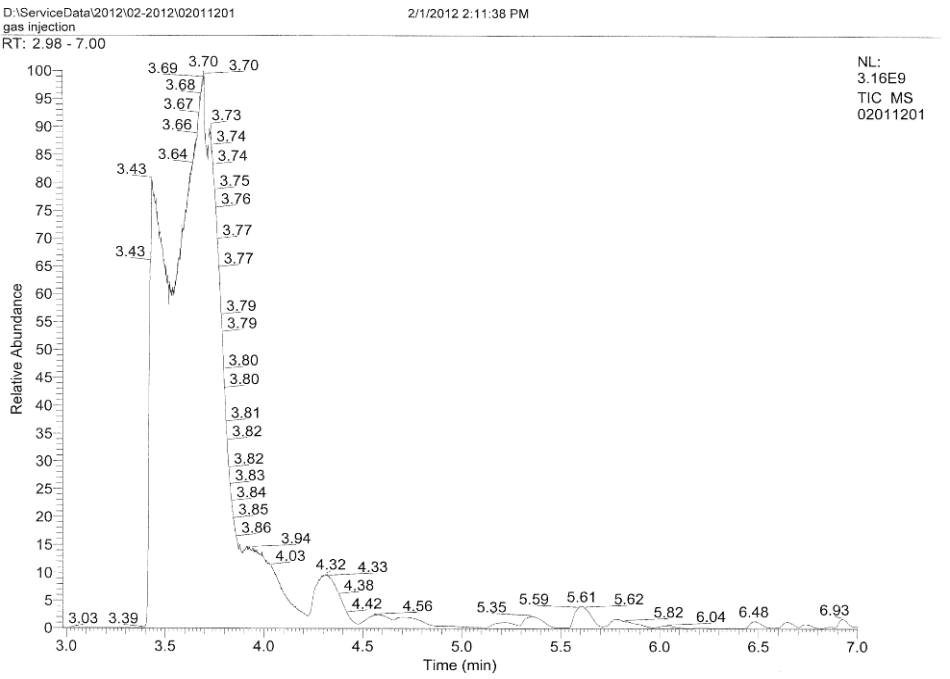

Figure 4-4: GC spectrum of the methane and argon run

According to the data in Figure 4-4, there were a great variety of heavy hydrocarbons in the product gas. Heavy hydrocarbons up to 98 amu in mass were detected. The methane in this spectrum is shown at 3.43 minutes. The argon is shown at 3.70 minutes. There looks to be a peak that is hidden in the argon spectrum at 3.73 minutes. This peak may be from ethylene. There is also an ethane peak at 3.94 minutes. After ethane, the peaks become very difficult to identify but they all correspond to hydrocarbons that have successively higher boiling points. It is not possible to identify each of the products because there are many conformational isomers that have different boiling points, and therefore different retention times. This spectrum is drastically different from

the previous methane only irradiation in that peaks of heavier hydrocarbons are present. After the test, it was estimated that the decay of the ^{41}Ar contributed about 92 Gy of beta dose to the gas mixture, only a minor component of the total dose at 3.37E6 Gy.

4.2.3 Irradiation of Methane and Helium

Methane and helium were irradiated in a similar fashion as the pure methane and the methane argon mixture. Heavy hydrocarbons up to 114 amu in mass were detected from the irradiation. The product spectrum was similar to that of the methane argon mixture. The GC-MS spectrum of the methane/helium run is shown in the Figure 4-5 below.

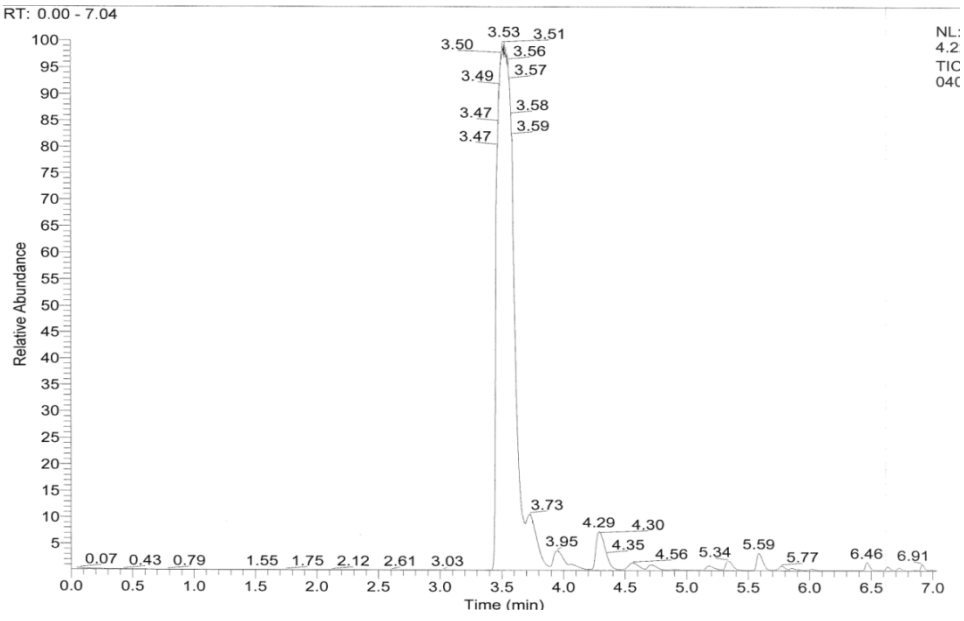

Figure 4-5: GC-MS spectrum from the helium methane run

The helium gas is not shown on this plot as it is not detectable. The methane peak is shown at 3.53 minutes, very similar to the previous irradiations. The peak at 3.73 may be an ethylene peak, which would then make the ethane peak at 3.95, which is similar to the methane/argon irradiation spectrum. There is also a peak from propane at 4.29. All of the peaks after propane are difficult to determine as many conformational isomers exist that all have different boiling points. This spectrum shows a very similar result to the argon/methane irradiation.

The second methane and helium run was analyzed using the qaudrupole mass spectrometer described in Section 3.x to calculate the hydrogen and ethane concentrations within the gas mixture. This was prepared by taking the difference of the measured m/z values of the irradiated gas and the starting gas. The error on each of the measurements is propagated to show the total error associated with each m/z difference calculation. The results are shown in Figure 4-6.

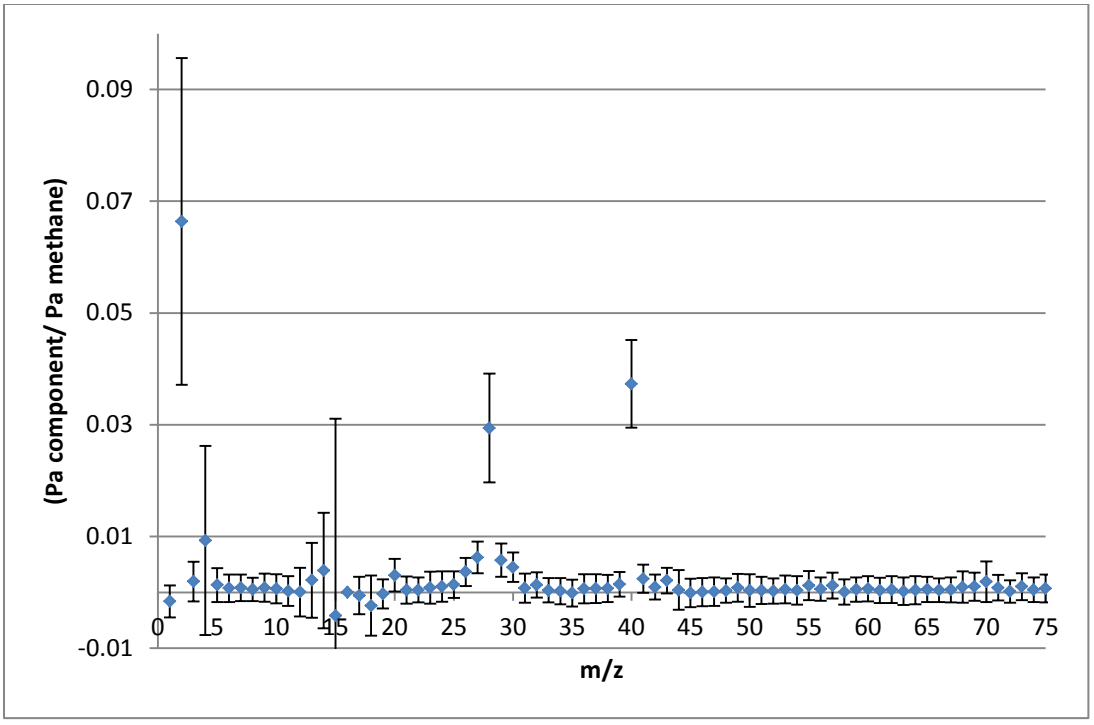

Figure 4-6: Products of NSCR irradiation of methane and helium

The NSCR irradiation experiments show the formation of product gas hydrogen (m/z=2) and ethane (m/z=28). The other products of the irradiations are evident by peaks in the spectrum below; these small peaks occur roughly every 14 m/z , which indicates another CH_2 unit added onto the chain. Unfortunately, most of the data points for these peaks have high error bars, making it difficult to say with confidence if there was any hydrocarbon conversion. This data is shown in Figure 4-7.

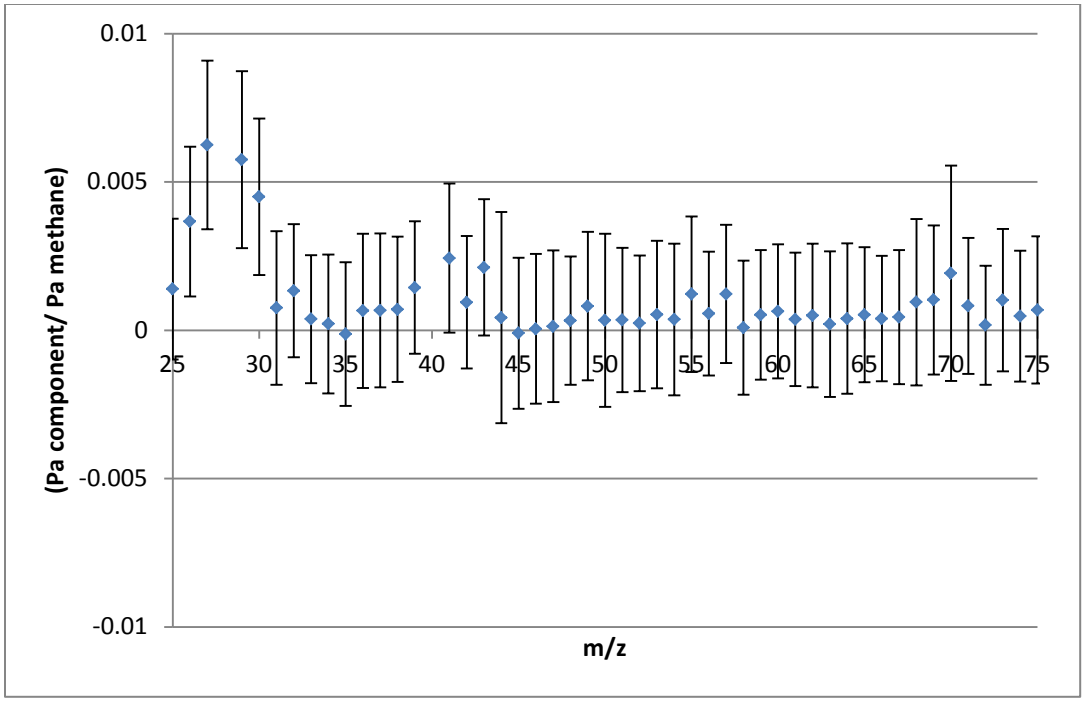

Figure 4-7: Products of NSCR irradiation of methane and helium

4.3 La-140 Experiments

The yields higher hydrocarbons from the LA-140 gamma irradiations at the NSC were undetectable with the GCMS. The analysis was done by inserting a needle directly to the valve on one of the tanks, then injecting gas in to the GMCS from the tank. The GC and MS spectra are shown in Figure 4-8.

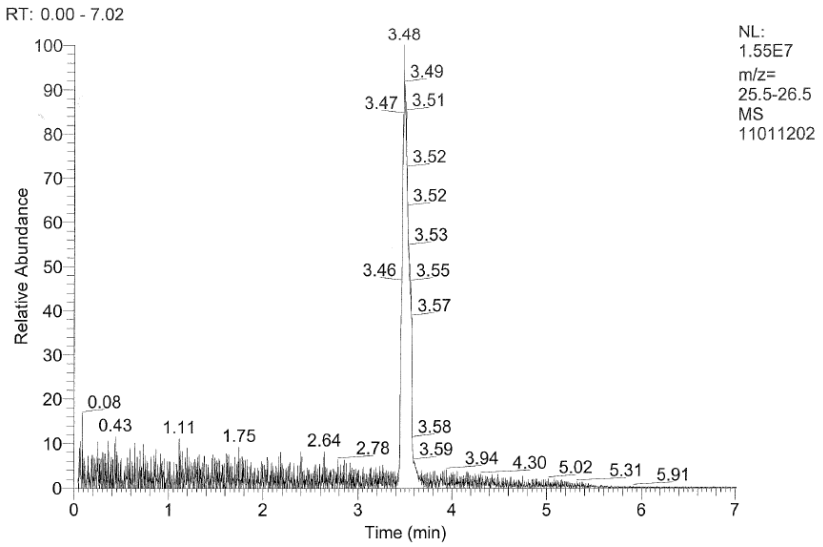

Figure 4-8: The GC spectrum of one of the gas tanks from the La-140 experiments

The GC spectrum shows a single peak, which corresponds to the ethane in the primary peak. The lack of a significant tail on the right of the peak shows no significant amount of heavier hydrocarbons were likely formed. The gas tanks also contained helium, but the GCMS instrument is unable to pick up helium since it is the carrier gas. There are no discernable peaks from other components that may have been produced by the irradiation.

The primary peak has a tail on the right; this peak represents components that are heavier than methane, but are unable to be separated by the CG column. This area corresponds to the time after the GCMS run is initiated between 3.74 and 3.95 minutes. The MS spectrum averaged over this time is shown in Figure 4-9.

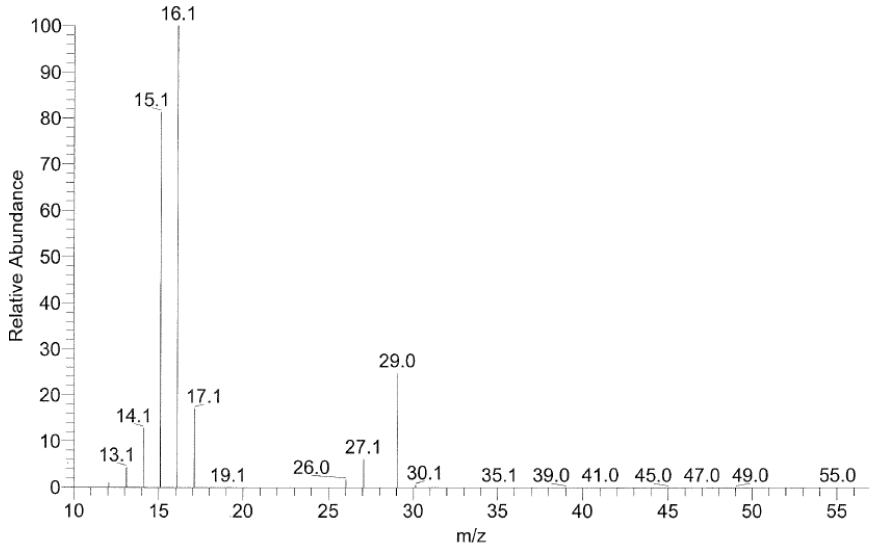

Figure 4-9: The MS spectrum for the GC plot between 3.74 and 3.95 minutes

The MS spectrum is shown for the time between 3.74 and 3.95 minutes. The MS spectrum is averaged over that time. This plot shows a peak at an m/z of 29.0, 27.1, and 26.0. These peaks correspond to ethane. There is a missing peak at 28, but this is likely the result of the N_2 and CO background subtraction.

4.4 Electron Beam Experiments

The electron beam experiments showed minimal yields of ethane and hydrogen, the yields of hydrogen and ethane from the experiments were so small that they cannot faithfully be discerned from the systematic error in the measurements. The measurements were made initially using the GCMS that was used for all of the other experi-

ments, and then moved on to the custom built mass spectrometer (Section 3.5.4) to measure hydrogen concentrations within gas samples. The target radiation dose was 50 kGy on the surface of the tank for the first two experiments. The MS spectrum for the first electron beam runs is shown in Figure 4-10 for the tail of the signal GC peak.

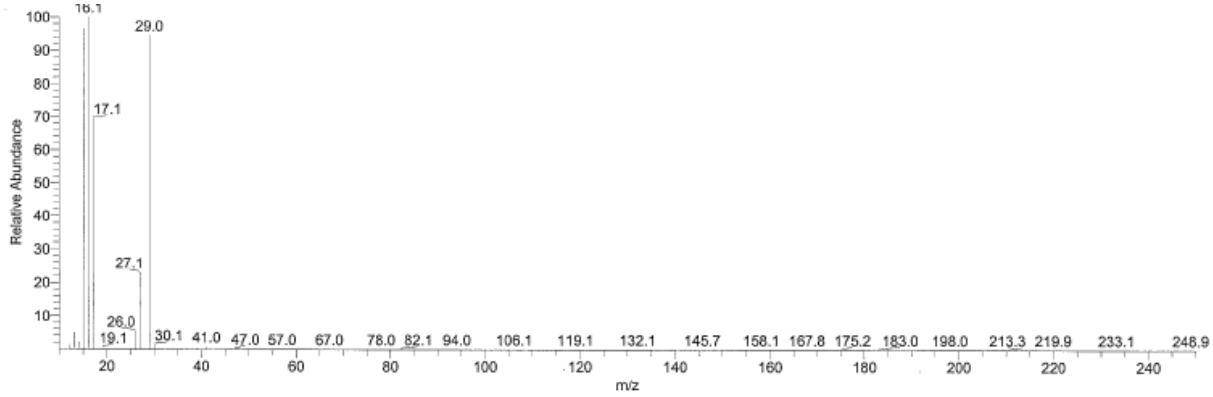

Figure 4-10: MS spectrum for methane in the initial electron beam run #1

The GCMS spectrum shows trace ethane and methane concentration throughout the entire GCMS run.

4.4.1 Electron Beam Run #2

This was the first electron beam irradiation in which the qaudrupole mass spectrometer (Section 3.5.4) was to be the primary analysis instrument. The gas mass numbers were scanned from 0 to 150 up to 20 times. The methane from the gas tank was

used as a background, and subtracted from the products gases signal. The results of the first electron beam experiments are shown in Table 2 below.

Table 2 Hydrogen and ethane measurements formed from irradiation in electron beam run #2

Tank	gas mix	pressure (psig)	hydrogen (Pa/Pa ME)	standard error	ethane	standard error
1	ME/He (30/270)	300	-0.018	6.58E-10	5.13E-09	0.004
2	ME/He (90/210)	300	-0.043	6.54E-09	1.61E-09	1.026
3	ME/He (210/90)	300	-0.029	1.68E-09	1.27E-09	0.002
4	Me (100)	100	N/A	N/A	N/A	N/A
5	ME/Ar (30/270)	300	0.941	1.44E-06	4.99E-08	8.518
6	ME/Ar (90/210)	300	-0.022	4.94E-09	1.1E-09	0.015
7	ME/Ar (210/90)	300	-0.029	3.55E-09	1.43E-09	0.013
8	Me (100)	300	7.312	1.04E-08	1.07E-09	2.732

The table above shows the concentrations of hydrogen and ethane measured during the run. This data is illustrated in Figure 4-11 below. These values are very low and near zero.

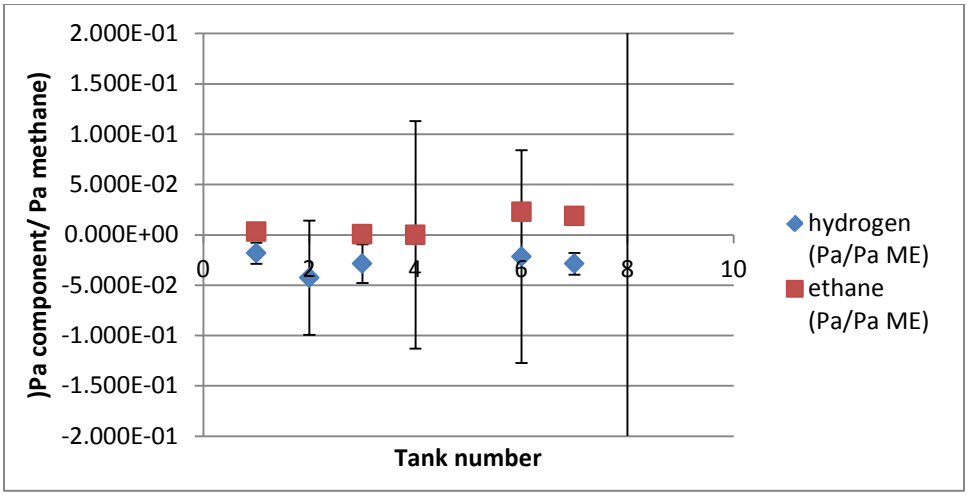

Figure 4-11 Conversion for electron beam run for ethane and hydrogen in Electron Beam run #2

4.4.2 Electron Beam Run #3

The first electron beam experiments were done using a mixture of methane and helium gas. This experiment was meant to test the effect of pressure on the radiolysis yields. Also, this experiment used higher concentrations of helium compared to methane gas. The results are shown in Table 3.

Table 3 Hydrogen and ethane measurements formed from irradiation in electron beam run #3

Tank	gas mix	pressure (psig)	hydrogen (Pa/Pa ME)	standard error	ethane	standard error
1	ME/He (30/270)	300	-0.046	H2	0.028	1.18E-09
2	ME/He (90/210)	300	0.074	1.07E-09	0.018	4.96E-10
3	ME/He (210/90)	300	1.247	9.25E-10	0.267	3.89E-10
4	Me (100)	100	-0.025	1.13E-10	-0.003	3.33E-10
5	ME/Ar (30/270)	800	0.941	2.39E-10	55.22	1E-09
6	ME/Ar (90/210)	800	0.116	5.51E-09	0.02	5.74E-10
7	ME/Ar (210/90)	800	0.107	4.67E-10	0.03	6.44E-10
8	Me (100)	800	0.049	5.87E-10	0.01	1.6E-10

The table above shows the concentrations of hydrogen and ethane measured during the run. This data is illustrated in Figure 4-12 below.

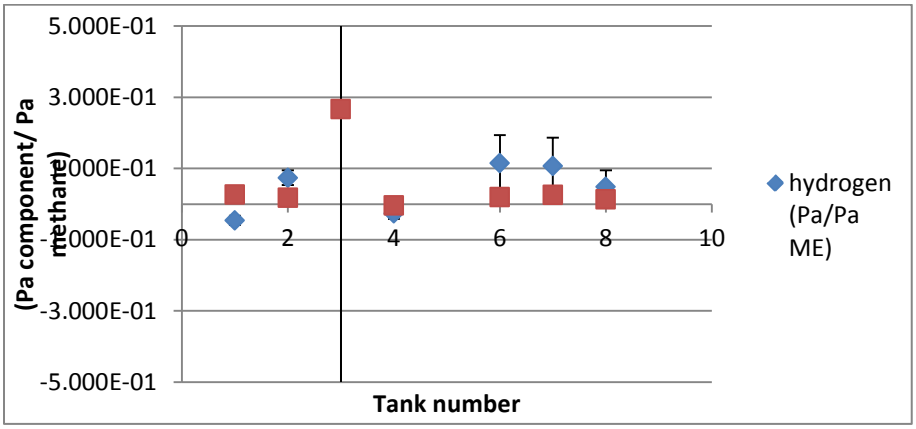

Figure 4-12 Conversion for electron beam run for ethane and hydrogen in Electron Beam run #3

4.4.3 Electron Beam Run #4

The next set of experiments used the mass spectrometer to measure the hydrogen and the ethane concentrations within each gas mixture. The mass spectrometer measured scanned for an m/z ratio between 1 and 150. The scan was done 20 times for each gas tank. The results for the gas tanks are shown in Table 4.

Table 4 Hydrogen and ethane measurements formed from irradiation in electron beam run #4

Tank	gas mix	pressure (psig)	Hydrogen (Pa/ Pa Me)	Standard error (Pa/ Pa Me)	Ethane (Pa/ Pa Me)	Standard error (Pa/ Pa Me)
1	ME/He (30/270)	300	0.276	0.419	-0.013	0.128
2	ME/He (90/210)	300	-0.372	0.140	-0.120	0.027
3	ME/He (210/90)	300	-0.047	0.033	-0.012	0.008
4	Me (100)	100	-0.058	0.023	-0.013	0.007
5	ME/Ar (30/270)	300	-0.402	0.192	-0.093	0.039
6	ME/Ar (90/210)	300	-0.020	0.030	-0.002	0.006
7	ME/Ar (210/90)	300	0.006	0.014	-0.001	0.004
8	Me (100)	300	-0.021	0.017	0.001	0.003

The table above shows the hydrogen and ethane concentrations for the long electron beam runs. Many of the average hydrogen and ethane concentrations, with initial concentrations subtracted, are often negative. This data is illustrated in Figure 4-13 below.

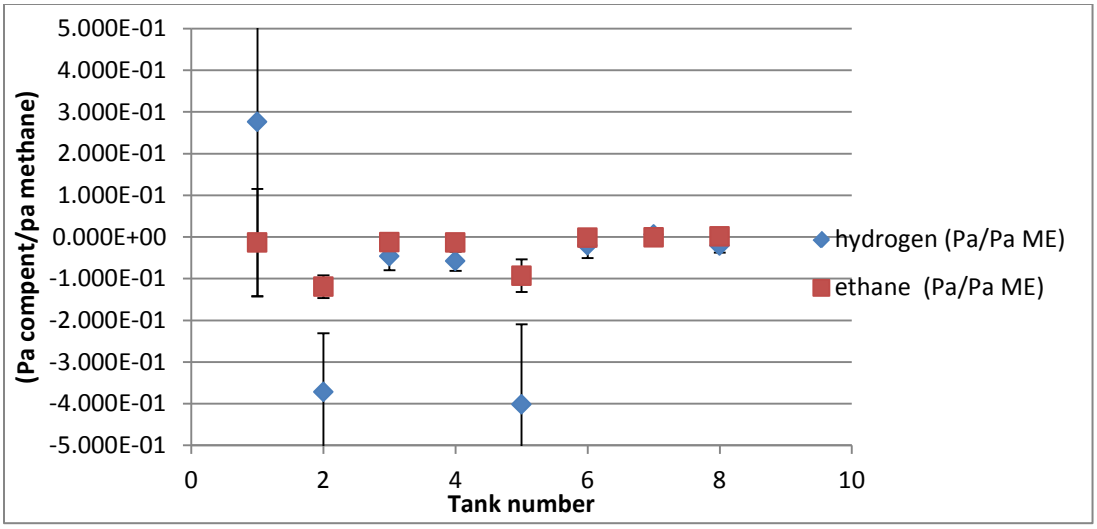

Figure 4-13 Conversion for electron beam run for ethane and hydrogen in Electron Beam run #4

4.5 Computational Verification of Results

The computational work for this experiment was performed using Monte Carlo transport code MCNPX. Each of the experiment configurations that were carried out in the reactor, the La-140 source, and the electron beam source were simulated with MCNPX to generate dose estimates. The dose estimates coming from the reactor did not include any burnup. Only the neutrons and fission photons were considered for the dose calculations for the reactor irradiations. Two dose calculations are of importance, first the total energy deposition from the all of the radiation. This is done using an F6 tally on MCNPX with neutron, gamma, and electron irradiation. The LET card is also used to compute the LET distribution for each of the radiations within the cells. This is used to

compare the different radiation sources for the number of ion pairs created along the radiations track length.

4.5.1 Methane Reactor Experiments

The methane experiments were simulated in MCNPX. The methane tank was placed in position A4, A3, or D3 of the NSCR. An F6 dose tally and an F4 flux tally were taken inside of the vessels. The F6 tally calculates energy deposition from particles per path length per particle, enabling the total energy deposition to be calculate with the appropriate source information (activity, particle flux) The F4 tally, which calculates normalized particle flux, was used to verify that the flux values within the irradiation areas were similar to measured levels from fission chambers under similar under the same operating conditions. This was used as a reference for the calculated power multiplier used for dose calculations. The F6 tally was used to estimate the total does from neutrons, electrons, and gammas. The flux tally only tracked neutron and proton fluxes. The proton fluxes are a result of knock-on collisions from the neutrons incident on the methane.

4.5.1.1 Methane Only

The simulated reaction vessel was placed into position A3 on the reactor in the simulation. A kcode simulation was run with 4000 particles for 500 cycles. The kcode simulation is used specifically for systems like reactors, in which particle generation can be self-sustaining, with no need for a source. This simulation runs several generations of particles, tracking all of the reaction that is happening within. This allows for a criticality factor, which is neutrons population in current generation divided by neutron population

in a previous generation, to be calculated. The keff value for the reactor was calculated to be 0.99149 ± 0.0004. The reaction vessel was split up into 4 cells in the simulation, so that it could occupy four lattice sites. An F4 and F6 tally was taken for each of the four cells, and averaged together. This reactor core assumes no burnup. The averaging takes into account for the spinning of irradiation cells in the reactor. This proton tracks were used to calculate the average LET of the protons moving through the gas. The MCNP experiment geometry is shown in Figure 4-14.

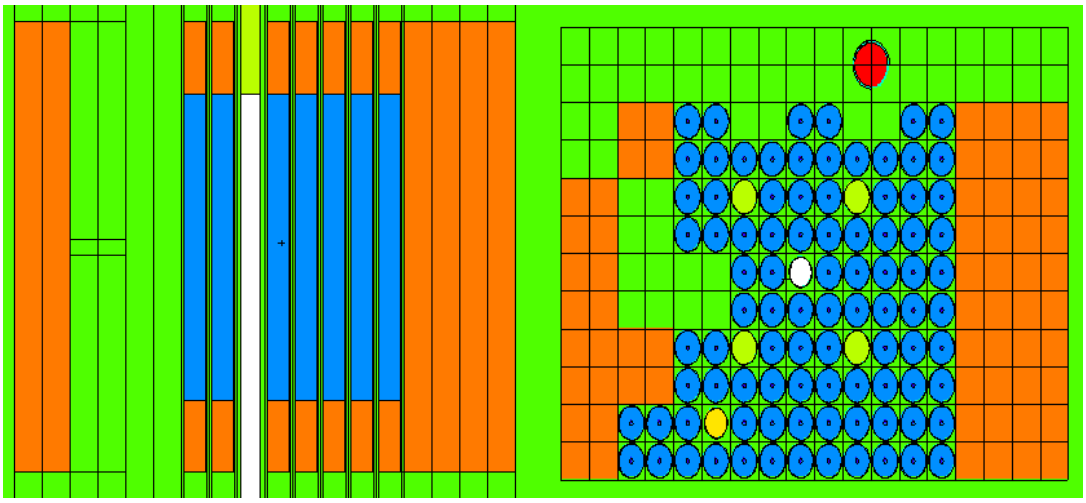

Figure 4-14 Experiment geometry as simulated by MCNP

The dose incident on the gas was calculated to be 31.7 Gy/s with a relative standard deviation Relative Standard Deviation (RSD) of 0.0091. The total dose over the 7 hour irradiation was calculated to be 789 kGy from neutron heating.

4.5.1.2 Methane/Argon

The simulated reaction vessel was placed into position A3 on the reactor in this simulation. A kcode simulation was run with 4000 particles for 500 cycles. The keff value for the reactor was calculated to be 0.99149 ± 0.0004. The reaction vessel was divided into 4 cells for the simulation so that it could occupy four lattice sites. This reactor core method assumes no burnup. An F4 and an F6 tally were taken for each of the four cells, and averaged together. This averaging enables the accounting for the spinning of irradiation cells in the reactor. This proton tracks were used to calculate the average LET of the protons moving through the gas. The MCNP experiment geometry is shown in Figure 4-15.

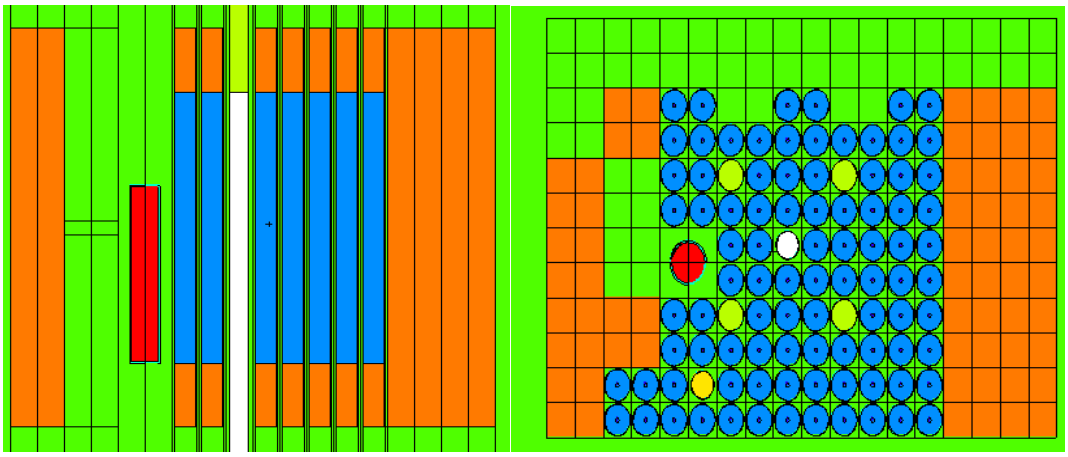

Figure 4-15: Experiment configuration for the methane-argon irradiation

The dose incident on the gas was calculated to be 31.7 Gy/s with a RSD of 0.0091. The total dose over the 7 hour irradiation was calculated to be 789 kGy from neutron and photon heating.

4.5.1.3 Methane/Helium

The simulated reaction vessel was also placed into position D3 on the reactor for simulation. A kcode simulation was run with 4000 particles for 500 cycles. The keff value for the reactor was calculated to be 0.99149 ± 0.0004. The reaction vessel was split up into 4 cells in the simulation, so that it could occupy four lattice sites. An F4 and F6 tally was taken for each of the four cells, and averaged together. This reactor is not modelled with any burnup. This position, unlike the other positions, does not spin the irradiation cells during irradiations, but it is surrounded by fuel on three sides of the irradiation vessel, which makes the flux fairly even throughout the irradiation zone. This proton tracks were used to calculate the average LET of the protons moving through the gas. The LET of the alpha particles were also calculated from collisions of neutrons and helium. The MCNP experiment geometry is shown in Figure 4-16.

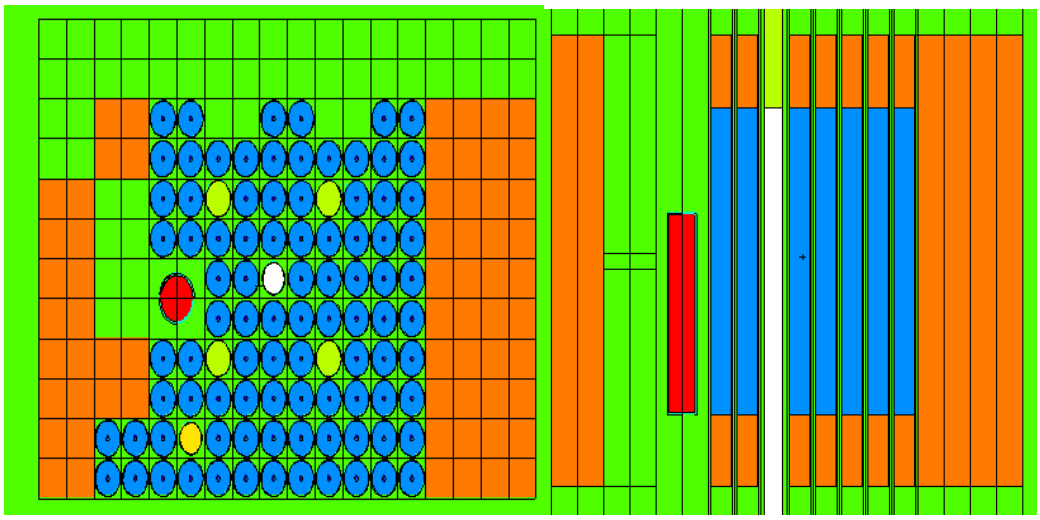

Figure 4-16 Experiment configuration for the helium methane configuration

The dose incident on the gas in the vessel was calculated to be 31.7 Gy/s with a RSD of 0.0091. The total dose over the 7 hour irradiation was calculated to be 789 kGy from neutron and photon heating.

The second helium-methane irradiation was done in the A4 position. A kcode simulation was run with 4000 particles for 500 cycles. The keff value for the reactor was calculated to be 0.99149 ± 0.0004. This reactor irradiation had very similar dose conditions to the first. The vessel was filled with to 164.7 psi methane, and 150 psi helium, to 300 psig total. This system is simulated in the MCNPX simulation as shown in Figure 4-17.

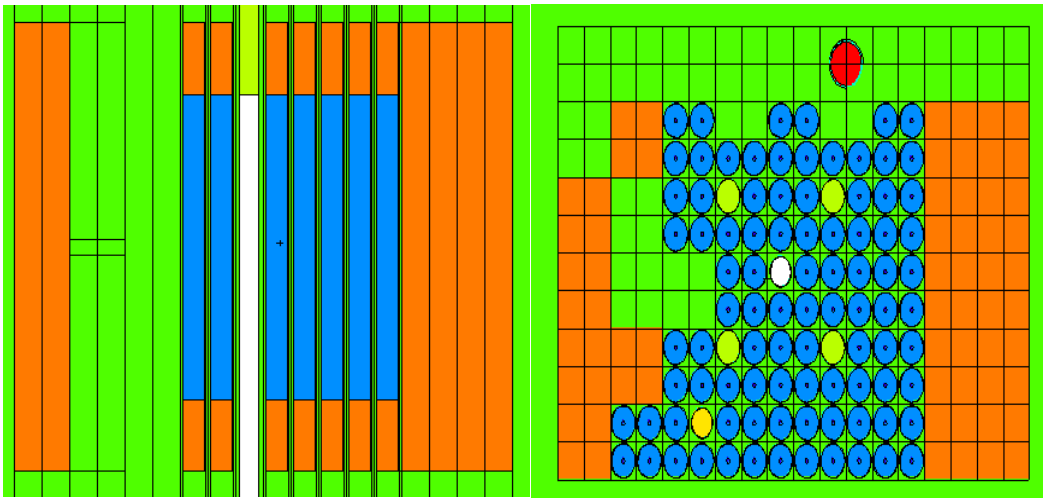

Figure 4-17 geometry of second methane-helium irradiation

The dose incident on the gas was calculated to be 31.7 Gy/s with a RSD of 0.0091. The total dose over the 7 hour irradiation was calculated to be 789 kGy from neutron and photon heating.

4.5.2 Electron Beam Experiments

An MCNP model was also created for the steel tanks in the electron beam facility. This simulation includes a simplified model of the tanks. A simplified model of the valves represented as rectangles and cylinders, and the stainless steel shields. The structural material was not includes in this simulation, it would not have a large effect on the dose to the tanks. The geometry is shown in Figure 4-18 as constructed by vised™, a graphics rendering software written in MCNPX.

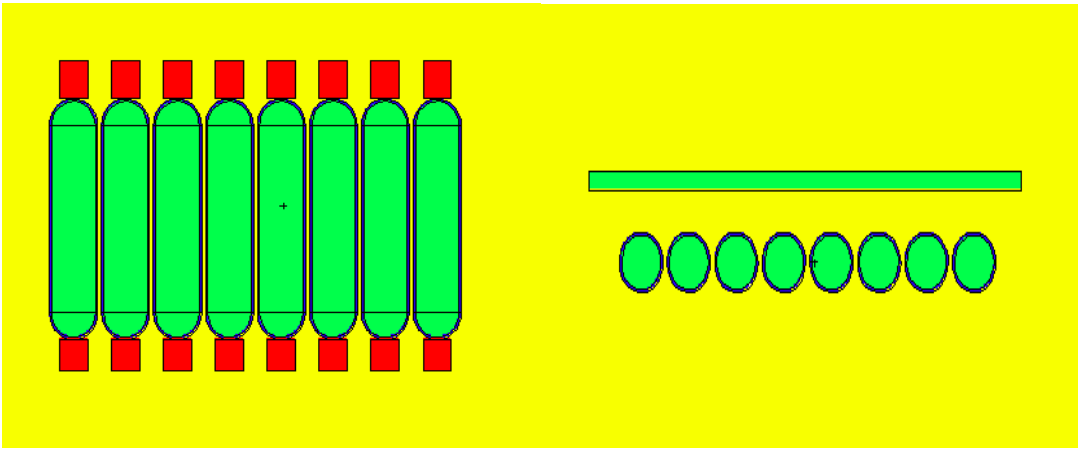

Figure 4-18 Electron beam irradiation tanks from Vised™

The source that was employed emulates the electron beam. It is a 10 MeV electron beam that is distributed homogenously as a line source. Two types of electron beam experiments were simulated for this system: One with the electron beam across all of the tanks as the tanks move past the source on the conveyor (experiments #1 and 2) and a second with the tanks held still (experiment #3).

The first set of experiments had the vessel sit on the conveyer belt, allowing it to pass under the beam. This has the effect of a homogenous irradiation across the entire vessel. The shields are meant to protect the valves from direct electron beam exposure, to prevent the non-metal bellows from radiation-induced failure.

The total dose to the gas within the tanks was found by applying an f6 dose tally in MCNP to the gas within each of the tanks. The tally was then multiplied by the total number of electrons emitted from the accelerator to calculate the dose.

4.5.2.1 Electron Beam Run #2

The vessel passed underneath the beam using a conveyer belt. The belt moves the vessel 1.2 feet/min when passing through irradiation area. The beam covers an area that is 1 cm wide and is 50 cm in length. The composition of each tank was 50/50 Me/He, at a pressure of 300 psig. The dose to the gas within the tanks is shown in Table 5.

Table 5 Electron beam run #2

Tank	Dose (MeV/g/particle)	Time (s)	particles (5 minutes)	Mass (g)	Energy (eV)	Gy (J/Kg)
1	3.05E-01	66.7	6.25E+17	1.39E-02	2.65E+21	3.05E+07
2	3.16E-01	66.7	6.25E+17	1.39E-02	2.75E+21	3.16E+07
3	3.19E-01	66.7	6.25E+17	1.39E-02	2.77E+21	3.19E+07
4	3.05E-01	66.7	6.25E+17	1.39E-02	2.65E+21	3.05E+07
5	3.04E-01	66.7	6.25E+17	1.39E-02	2.64E+21	3.04E+07
6	3.16E-01	66.7	6.25E+17	1.39E-02	2.74E+21	3.16E+07
7	3.05E-01	66.7	6.25E+17	1.39E-02	2.65E+21	3.05E+07
8	3.15E-01	66.7	6.25E+17	1.39E-02	2.74E+21	3.15E+07

4.5.2.2 Electron Beam Run #3

The dose and the LET for the second electron beam run were simulated using MCNP. The vessel passed underneath the beam using a conveyer belt. The belt moves the vessel 1.2 feet/min when passing through irradiation area. The beam covers an area that is 1 cm wide and is 50 cm in length. The composition of each tank was Me/He in

different ratios, at a pressure of 300 and 800 psig. The dose and LET are shown in Table 6 below for each of the tanks.

Table 6 Electron Beam run #3

Tank	Dose (MeV/g/particle)	time (s)	particles (5 minutes)	Mass (g)	Energy (eV)	Gy (J/Kg)
1	6.07E-02	66.7	6.25E+17	1.39E-02	5.27E+20	6.07E+06
2	6.66E-02	66.7	6.25E+17	1.39E-02	5.79E+20	6.66E+06
3	7.26E-02	66.7	6.25E+17	1.39E-02	6.31E+20	7.26E+06
4	6.89E-02	66.7	6.25E+17	1.39E-02	5.98E+20	6.89E+06
5	6.11E-02	66.7	6.25E+17	1.39E-02	5.31E+20	6.11E+06
6	6.09E-02	66.7	6.25E+17	1.39E-02	5.29E+20	6.09E+06
7	6.42E-02	66.7	6.25E+17	1.39E-02	5.58E+20	6.42E+06
8	6.58E-02	66.7	6.25E+17	1.39E-02	5.71E+20	6.58E+06

4.5.2.3 Electron Beam Run #4

This experiment was the setup in which the beam was held still is done experimentally by setting the tanks above the conveyer belt in a water-filled secondary tray (Section 3.3) such that the electron beam was incident on the same place of the system the entire irradiation. This method was used to deliver much higher doses than if the tanks were on the conveyer belt. The plot is shown in Table 7 below.

Table 7 MCNP calculations for the electron beam run #4

Tank	Dose (MeV/g/particle)	time (s)	particles	Mass (g)	Energy (eV)	Gy (J/Kg)
1	7.32E-02	300	2.81E+18	1.39E-02	2.86E+21	3.29E+07
2	7.13E-02	300	2.81E+18	1.39E-02	2.79E+21	3.21E+07
3	8.23E-02	300	2.81E+18	1.39E-02	3.22E+21	3.70E+07
4	8.44E-02	300	2.81E+18	1.39E-02	3.30E+21	3.80E+07
5	7.26E-02	300	2.81E+18	1.39E-02	2.84E+21	3.26E+07
6	7.30E-02	300	2.81E+18	1.39E-02	2.85E+21	3.29E+07
7	7.64E-02	300	2.81E+18	1.39E-02	2.98E+21	3.44E+07
8	8.00E-02	300	2.81E+18	1.39E-02	3.13E+21	3.60E+07

4.5.3 La-140

A homogenously distributed La-140 source was simulated in MCNPX. The source was simulated as La_2O_3 rods inside of an aluminum block. For the experiments, the source was activated to have an activity of 400 Ci, so this was the simulate strength for the MCNP estimates. The aluminum block containing the source sits underwater inside of a small cage. The vessel that was used for electron beam experiments had its steel shields removed and was submerged under water and centered against the source. The system was allowed to sit for 16 hours. The geometry for the source and the experiment can be seen in the Vised™ plot show in Figure 4-19.

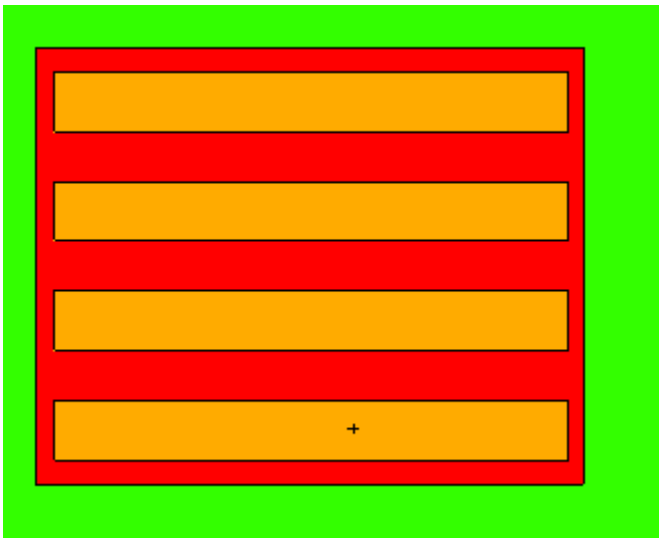

Figure 4-19 La-140 source in modelled in MCNPX

The pressure vessels were modelled with the source sitting directly on the La-140 source. This is shown in Figure 4-20.

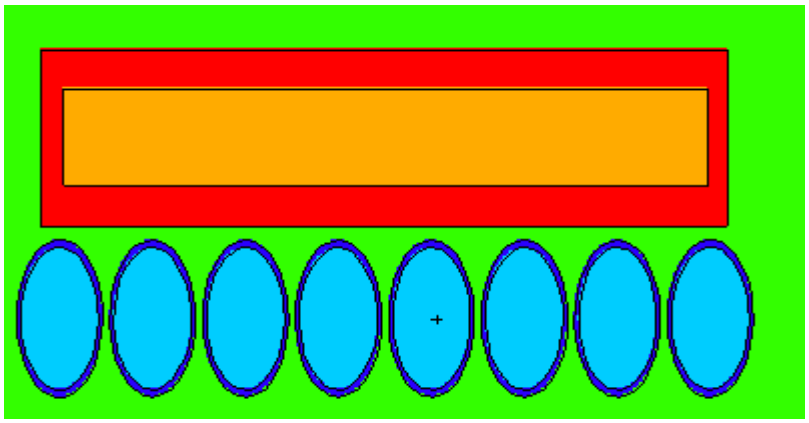

Figure 4-20 vessel sitting directly one top of the La-140 source

The La-140 source was specified by homogenously distributing La-140 throughout the La2O3 rods. The source was created by random sampling the starting position within the 4 rods. The dose to each of the tanks was correlated to the total activity of the La-140 Rods at 400 Ci. The total dose to the tanks was calculated by multiplication of the f6 tally result with the total number of decays that occurred during the experiment. The dose is calculated in Table 8 below for each of the tanks for the La-140 which was analyzed by GCMS.

Table 8 Dose to gas in tanks in La-140 experiments

Tank	Gas Mix (psi/psig)	Dose (Gy)
1	He/Me (0/1000)	113.365
2	He/Me (100/900)	170.2747
3	He/Me (200/800)	257.491
4	He/Me (300/700)	357.0598
5	He/Me (400/600)	386.6147
6	He/Me (500/500)	302.3365
7	He/Me (600/400)	210.0538
8	He/Me (700/300)	126.3742

5 DISCUSSION

5.1 Hydrogen and Ethane Measurements

The hydrogen generation in each of the vessel was measured with the mass spectrometer as a means to determine the amount of methane transformed during radiolysis. This is used as a metric for hydrocarbon conversion due to the difficulty of quantifying each of the products. Also, the formation of ethane is one of the primary products of methane irradiation. The concentrations of this molecule are higher than any of the other products of the radiolysis reaction except for hydrogen. It is also one of the common fragmentation products of heavier hydrocarbons cations created from ionization in the mass spectrometer. This is often used as a metric for the amounts of hydrocarbons created. The G-values for the last NSCR irradiation (Section 5.1) are given in the Table 9.

Table 9 Percent change and G-value of H_2 and selected hydrocarbons for the second methane/helium NSCR irradiation.

Gas	G-Value
H2	2.27±0.53
Methane	-3.83 ±2.36
Ethane	1.01±0.29
Propane	0.035±0.09
Butane	0.14±0.183

The G-values shown in Table 9 above are calculated using the sensitivity factors that are stored within the mass spectrometer for each of the gases.

5.2 CO_2-H_2 Experiments

The data from GCMS analysis of CO2-H2 experiments show no chemical change. This experiment was meant to emulate the Beattie experiment in which a mixture of CO_2 and tritium was added to a glass bulb and allowed to react. The Beattie experiment was modelled by MCNPX to simulate the tritium dose to the vessel. The dose calculated over the course of Beattie experiment with the highest yields was 2.77×10^8 Gy. The dose received during the CO_2-H_2 irradiation was calculated to be approximately 6.13×10^3 Gy. The dose was 5 orders of magnitude lower than in the Beattie experiments.

The dose rate in the NSCR radiation zone was over 2.26×10^3 Gy/hr at the time the vessel was placed at the reactor core. This was measured through the use a compensated ion chamber. Unfortunately, detector software crashed and all of the data was lost. An approximate dose calculation was done by correlating the dose to the detector and the decay power level of the reactor. The decay power equation is given in the equation below.

$$P_{decay} / P_o = 0.066 \left[t_s^{-0.2} - (t_s + \tau_s)^{-0.2} \right] \qquad 21$$

Where t_s is the time after the reactor is shutdown, and τ_s is the operating time of the reactor. The decay power was correlated to the dose rate measurements from the ion

chamber. The dose rate was then integrated over time from reactor shutdown to the end of the experiment, giving the total dose within the vessel. The dose is computed using a simple MCNP experiment to simulate the experiment in which Beattie observed the highest product yield. The dose in the Beattie experiment was computed to be 2.12 Gy/s. With Beattie's experiments running for up to 400 hours, the dose that was received by the gas was much higher than the dose received by the experiment in this thesis, even under the most generous assumptions in dose calculation. Overall, the CO_2-H_2 experiments done in this thesis did not show any results that were even comparable to the Beattie experiments; no methane was detected, no signs of any polymer formed.

5.3 Quenching Effects

The dominate energy transfer method for this gas was observed to be a static quenching mechanisms. This was the predominate method for energy loss, and lead to the extremely low yields of hydrogen gas reported.

One method for the quenching of molecules is through cluster formation in gas phase. Once a methane cation is created, other molecules will quickly cluster around the methane cation which is driven by Van Der Waals forces. There is rapid vibrational energy transfer between the C-H bonds of the excited cation and the surrounding molecules. This will lead to fast de-excitation of the molecules, quickly bringing their energy below the threshold for ion-molecule reactions. [35] This mechanism described above was likely the primary mechanism for the low yields of heavy hydrocarbon gases from product gases.

The high LET neutron irradiations are slightly different from the low LET neutron and gamma irradiations. The direct interaction of the neutron with methane in a high pressure gas causes an enormous amount of energy to be imparted onto the molecule. This can cause molecules to rapidly fragment. Ions with high energy can be created through scattering reaction of atoms and the neutrons. These high LET particles can move through the gas causing further ion-pair creation and fragmentation.

5.4 Energy Transfer

Since the polymers are in the presence of ionizing radiation, they may be broken down into smaller products. This side effect from active irradiation will reduce product yield and protect smaller hydrocarbons from ionizing radiation. Larger hydrocarbons are able to absorb energy and can be broken up by ionizing radiation. They are broken apart into smaller hydrocarbons, which will reduce the yield of heavy hydrocarbons. Since the ionization potential of the heavier hydrocarbons is smaller than lighter hydrocarbons, lighter hydrocarbons are able to transfer their energy to heavier hydrocarbons. This reduces the amount of lighter hydrocarbons that are able to initiate polymerization reactions.

Generally, long straight chain molecules have greater resilience to the radiation-induced breakdown than branched hydrocarbons.[25] These long straight chain hydrocarbons are able to transfer energy through intramolecular energy transfer (IVR) to quickly redistribute energy throughout the molecule.[25, 26] This has the effect of keeping energy delocalized within the molecules, lowering the chances that any one bond will have enough energy to dissociate. There is greater energy transfer through C-C

bonds of molecules than through the C-H bonds. This is due to the vibrations of the C-C atom all being attached and in close proximity to one another. There is little energy transfer between C-H bonds and C-C bonds in an alkane due to the difference in vibrational frequencies. When energy is absorbed by a C-H bond, the energy is localized between the C-H bonds attached to that carbon. There is some energy transfer to neighboring C-H bonds, but that is heavily dependent on the distance between the bonds.[25, 26]

For methane, there are only C-H bonds. So the only energy transfer technique is through vibrational energy distribution accelerated through clustering. The clustering brings molecules in close proximity to one another which allows for more efficient energy transfer from the excited ion to surrounding molecules. This brings the energy of the excited methane molecule to energy below that of the threshold for many dissociation reactions, lowering overall yields of heavier hydrocarbons.

5.5 Charge Transfer and Noble Gas Effects

Charge transfer is one of the primary ionization and excitation methods within radiolysis experiments. The requirement for charge transfer is simply having species of different ionization potentials. In many hydrocarbon radiolysis experiments, the presence of noble gas with higher ionization potentials serves two function which helps to increase yields. First, the higher ionization potentials of helium and argon compared to methane allow for charge transfer to occur.[11, 36] This can transmit enough excess energy to the methane molecules to allow for dissociation, generating reactive species.[37] The noble gas also acts as a non-interacting body that can shield the methane from static

quenching reactions. The noble gas has no vibrational or rotational energy levels, and electronic excited states that are higher energy than methane. Therefore, methane that is excited will not transfer energy to the noble gas. Also, the noble gas will reduce the collision frequency with quenching species, making fragmentation to more reactive species more likely.

5.6 Selected Methane Experiments

The three primary methane experiments of interest are the proton irradiation of the methane at atmospheric pressure by Sack[11], the flow experiments done Ponomarev[3], and the static irradiations by Sheridan-Libby[12]. These experiments were chosen because they encompass three types of methane irradiation experiments. The three experiments will be compared by the average LET of the irradiations calculated by MCNPX. These calculated vales is compared to selected

First, the Sack experiment used a high LET proton irradiation of methane at atmospheric pressures. The radiolysis produced high levels of ethane, ethylene, as well as heavier hydrocarbon with concentration decreasing as molecular mass increases.

The Ponomarev experiments used a high energy electron beam to irradiate light hydrocarbons at atmospheric pressures. This system flowed petroleum gas through an irradiation cell where it was irradiated by a 40 kW, 500 keV electron beam. The concentration of ions and radicals produced by this experiment was extremely high due to the power density within the gas stream. This allowed for the radicals and ions to be created in large amounts, and in close proximity to one another, which allowed from more effi-

cient combination of radical and ion species to form heavy hydrocarbons. This high power density, and lower pressure, allowed for high conversion of light gaseous alkanes into heavier, motor-grade liquid fuels.

The Sheridan-Libby experiments used a high intensity gamma source for the irradiation of solid methane. This experiment was very different from the others in that it used a gamma source (30 kCi Co-60) for the irradiation of mixture of solid methane and argon. These products of these irradiations were high molecular weight hydrocarbon waxes. The average molecular weight of the hydrocarbon wax is independent to dose between 0.001 to 1 MGy. This is an odd result since the density of the methane in a liquid form is much higher than in the experiments done in this thesis.

One of the possible explanations for the high molecular weight hydrocarbons is the high LET of the gamma radiation due to the high density of the methane and argon. This allows for a high concentration of ions and radicals to be created in close proximity to one another. This allows for combination of reaction radicals and ions. Also, the methane was only a small fraction of the liquid product, but the methane was still excited by direct radiation interaction and charge transfer from the argon. The methane also acts as a quenching gas since it has a lower ionization potential than argon, directing charge transfer from the argon to methane. The low concentrations of methane in argon shielded the methane from collisional de-excitation processes. The LET plots for the experiments are shown in Figure 5-1.

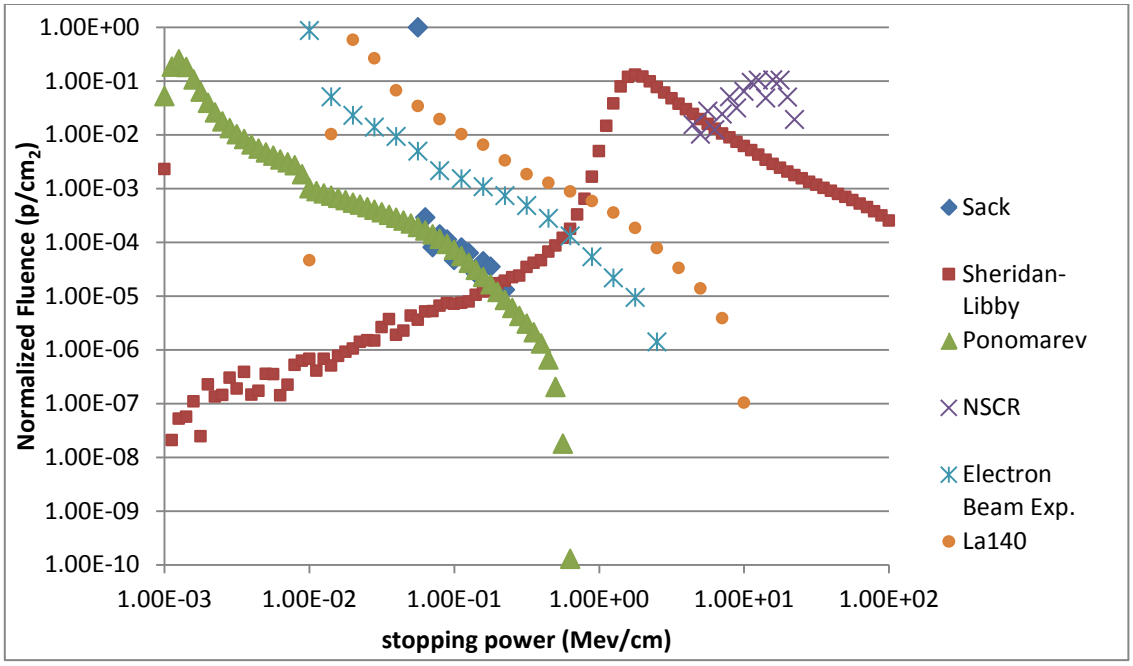

Figure 5-1: LET comparison of simulated Sheridan-Libby[9], Ponomarev[3], Sack.[11], electron beam runs, and NSRC runs.

The plot above shows the difference in linear energy transfer as a function of normalized particle flux. The Ponomarev experiment has a high intensity electron beam source used to polymerize methane. The electrons are a lower LET irradiation compared to the proton source, but the high intensity of the beam generated high concentrations of ion pairs and radicals.

The Sack experiment shows a similar trend in LET as the Ponomarev experiment, except for one spike between 56 and 63 keV. This peak is likely due to the high stopping power of the protons once they slow to lower energies.

The Sheridan-Libby experiments have a much higher LET compared to the Sack and the Ponomarev experiments due to the high concentrations of methane and argon in the mixtures. This allows for high concentrations of hydrocarbon radicals and ions to be created, allowing for hydrocarbon radicals and ions to combine into heavier hydrocarbons. Also, the low temperatures of the gas act to reduce the energy transfer rates from excited states to quenching species. This occurs for two reasons: First, the diffusion rate of quenching molecules is temperature dependent, greater temperatures correspond to higher diffusion rates. The higher diffusion rates allow for higher collision rates with the excited molecules and the quenching molecules, leading to greater de-excitation rates. The lower energy also decreases the intensity of radiative transfer through decreasing the population of vibrational overtones present in methane that are able to absorb energy.

The electron beam irradiations presented in this thesis had a higher LET than the Ponomarev experiments mostly due to the high pressure of the methane and noble gas. Unfortunately, gaseous product yields are low. This is likely due to the high concentrations of methane gas that acts as a quenching agent for the excited and ionized species. The gas will quickly de-excite the excited molecules, lowering the reaction yields.

5.7 Energy Efficiency

The energy requirement for the formation of long hydrocarbon chains is calculated by examining bond enthalpies for various hydrocarbons. This will give the total energy of the reaction by the difference in all bond energies between products and reactants. This data is supplied by Banksby *et al.* for a variety of light hydrocarbons [38].

$$\Delta H^{o}_{reaction} = \sum \Delta H^{o}_{products} - \sum \Delta H^{o}_{reactants} \quad (22)$$

Where $\Delta H^{o}_{reaction}$ is the formation energy for the reaction; the minimum energy input needed to make a product. The formation energy is often used in terms of KJ/mol, which can be translated to G-values often used in radiation chemistry. The energy of formation for light hydrocarbons is given in Table 10 below at a temperature of 298.1K.[39]

Table 10 Enthalpy of Formation for various hydrocarbons

Hydrocarbon	Energy of Formation (kJ/mol)	Enthalpy of Reaction from methane (kJ/mol)	eV/molecule	G-Value (molecules/100 eV)
Methane	-74	N/A	N/A	N/A
ethane	-84	119	1.23	81.08
propane	-103	198	2.05	48.73
butane	-125.79	297	3.08	32.49

The energy of formation is the lowest amount of energy that can be expended in order to make a molecule. This can be used as a metric to compare the energy efficiency of any chemical process. The energy of high yield radiolysis products is compared to the lowest energy requirement for product formation. The energy requirement for the production of selected hydrocarbon formed in radiolysis experiments vs. the theoretical energy requirements is given in Table 11 below.

Table 11 G-values (molecules/100 eV) comparison for various methane radiolysis experiments

Hydrocarbon	Sack	Sheirdan-Libby (0.15%)	Sheirdan-Libby (0.076%)	NSCR	Ponomarev (2009)	Theoretical
Methane	N/A	N/A	N/A	6.15E-01	N/A	N/A
Ethane	2.574104	2.4	1.3	3.44E-01	2.4092	81.08
Propane	0.41	0.049	0.64	1.11E-01	N/A	48.73
Butane	0.07	0.002	0.15	2.12E-01	N/A	32.48

The energy efficiency for many of these processes radiolysis experiments is very low compared to the theoretical energy requirements calculated by bond enthalpies. The electron beam radiolysis experiments yields were below the resolution of my mass spectrometer system. The error that was introduced into the measurements was due to systematic error from history effects. Over the lifetime of the spectrometer the internal surfaces started to foul with carbon deposits. These carbon deposits are likely sublimating within the detector head as it warms, causing deviation in normalized counts for each of the mass bins. The signal to noise ratio in the spectrometer began to decrease as all background counts in each of the bins increased. The reason for the drop in the signal is likely due to the decrease in mean free path of ions as they are traveling down the spectrometer tube caused by the increase in pressure from carbon dioxide and monoxide coming sublimating from the detector. This increase in pressure, and therefore molecular

density, will mean more ions will be attenuated prior to reaching the charge collector. This variation can be seen by analyzing the normalized pressure of various components with respect to the scan number in the mass spectrometer, this is shown in Figure 5-2for the methane/helium run in the NSCR.

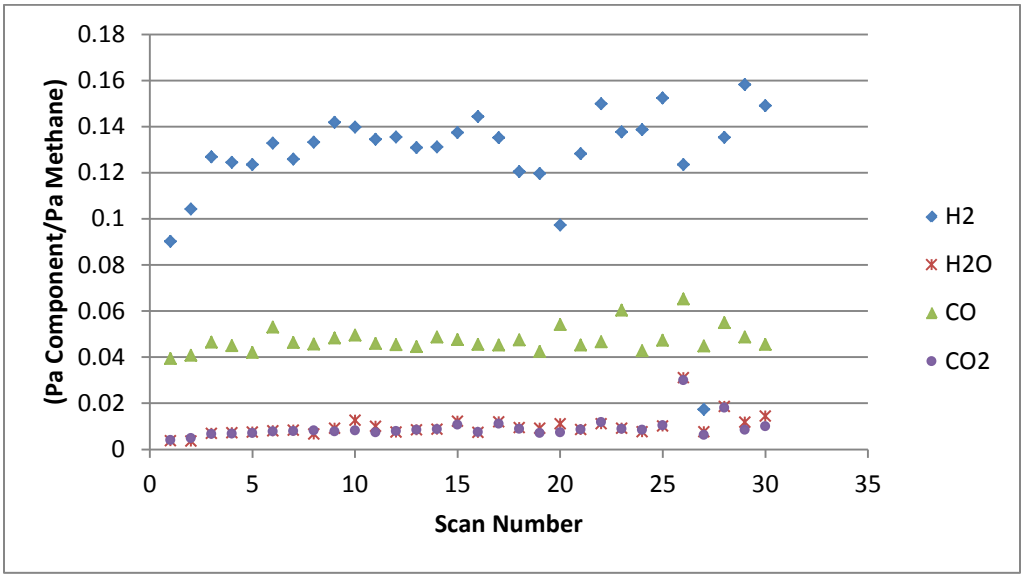

Figure 5-2: The variation in partial pressures of selected mass numbers with respect to scan numbers

This shows variation is the partial pressures with respect to scan numbers, which add bias to measurements. This can be seen too much greater effect in the other runs, such as the some of the electron beam irradiations. Figure -5-3 below shows the concentrations of various components with respect to scan number.

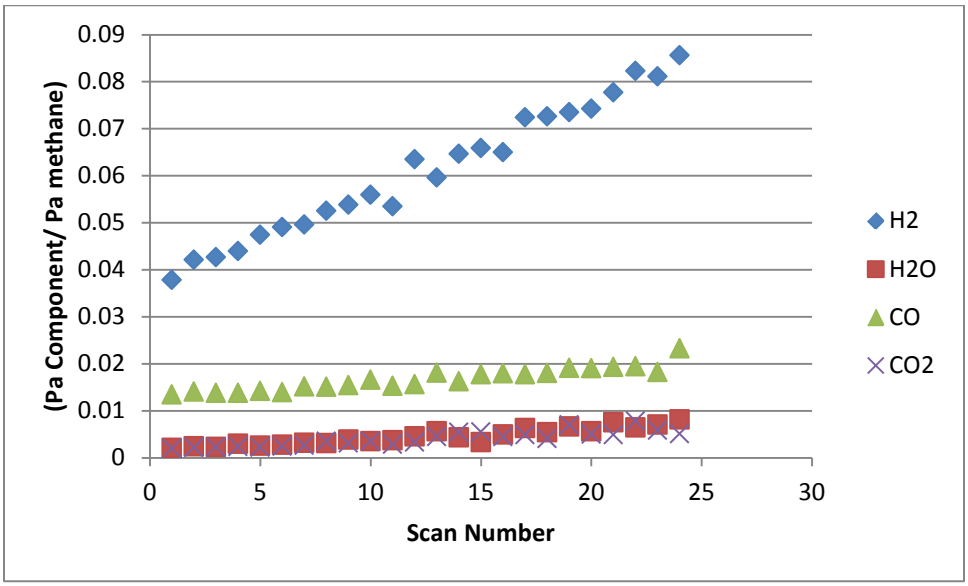

Figure -5-3: Variation is selected components with respect to scan number in electron beam experiment #4, tank 8

In Figure -5-3, it can be seen that all of the component rise over the course of the measurement, which adds significant error into the calculations. The cause of this drift was due to the mass spectrometer heating from long operation, and high hydrocarbon concentrations for prolonged period of time within my mass spectrometer. This is one of the major sources of error that will need to be addressed for future analysis with this mass spectrometer system is carried out.

6 SUMMARY

The principle finding of this thesis was that with high pressure methane gases, the chemical change was small for low LET radiations, and difficult to quaintly with a GCMS or a residual gas analyzer system. The yields for the La-140 and electron beam irradiation were very small, and contrasted sharply with literature values. This is likely due to the high pressure of the methane gas increasing the rate of collisional de-excitation, which lowered reaction yields.

The NSC Reactor irradiations show a measurable increase in the concentration of ethane and hydrogen, the La-140 and electron beam irradiations do not show measurable increases in hydrogen and ethane concentrations. The experiments that had shown measurable change in the hydrogen and ethane concentrations had the G-values of the individual reaction products calculated for the NSC reaction irradiations. The G-values for were calculated to be 2.61±0.62 and 1.16±0.34 for hydrogen and ethane production, respectively.

The tasks carried out in this thesis are given below.

1. Experimental systems were designed in order to carry out high pressure gas radiolysis experiments.
2. Instrumentation was developed in order to analyze evolved hydrogen gas concentrations as a result of energy absorbed during radiolysis.
3. Irradiations at the electron beam facility were done to calculate yields from low LET radiations

4. Irradiations were done at the NSC to compute dose from low and high LET radiations
5. The effects of noble gases at varying concentrations one chemical conversion were analyzed for low LET

6.1 Future Experimental Work

The future of this work is to continue the investigation of addition reactions with sources other than radiation sources. Also, batch systems are to be abandoned in favor of flow systems that lower the competing destruction reaction rates. The most suitable energy source would be high intensity tunable laser sources. This would for more precise control of fragmentation through the targeting of certain bonds (e.g. C-H or C-C). The high intensity laser source would lead to higher conversions of heavier hydrocarbons through the creation of high density of radical species which can then undergo recombination reactions.

Experiments at low temperature with liquefied gas would also be of interest following the work of Sheridan-Libby. The high conversions of methane to high molecular weight hydrocarbon should be studied further with various radiation sources. The lower temperature is expected to hamper vibrational energy transfer through decreased Doppler broadening. This may be the reason for such high molecular weight compounds at high molecular densities.

REFERENCES

[1] G. Henrici-Olivé and S. Olivé, "The Fischer-Tropsch synthesis: molecular weight distribution of primary products and reaction mechanism," *Angewandte Chemie International Edition in English*, vol. 15, 1976, pp. 136-141.

[2] S. Yurchak, "Development of mobil's fixed-bed methanol-to-gasoline (MTG) process," in *Studies in Surface Science and Catalysis*. vol. 36, D.M. Bibby, C.D. Chang, R.F. Howe, and S. Yurchak, Eds.: Elsevier, 1988, pp. 251-272.

[3] A. V. Ponomarev, "Electron-beam radiolysis of gaseous alkanes under circulation conditions: Gas-to-liquid transformation," *Radiation Physics and Chemistry*, vol. 78, 2009, pp. 48-56.

[4] A. C. Vosloo, "Fischer–Tropsch: a futuristic view," *Fuel Processing Technology*, vol. 71, 2001, pp. 149-155.

[5] R. L. Clough, "High-energy radiation and polymers: A review of commercial processes and emerging applications," *Nuclear Instruments & Methods in Physics Research Section B-Beam Interactions with Materials and Atoms*, vol. 185, 2001, pp. 8-33.

[6] EIA, (3/21/2014). *AEO2014 early release overview*. Available: http://www.eia.gov/forecasts/aeo/er/early_elecgen.cfm

[7] D. J. Wilhelm, D. R. Simbeck, A. D. Karp, and R. L. Dickenson, "Syngas production for gas-to-liquids applications: Technologies, issues and outlook," *Fuel Processing Technology*, vol. 71, 2001, pp. 139-148.

[8] C. A. Jones, J. J. Leonard, and J. A. Sofranko, "Fuels for the future: Remote gas conversion," *Energy & Fuels*, vol. 1, 1987, pp. 12-16.

[9] M. Sheridan, E. Sheridan, W. F. Greer, and Libby, "Polymer production in the .gamma.-radiolysis of methane, ethane, and ethylene solutions in liquid argon," *Journal of the American Chemical Society*, vol. 94, 1972, pp. 2614-2618.

[10] A. Chapiro, "Radiation induced polymerization," *Radiation Physics and Chemistry (1977)*, vol. 14, 1979, pp. 101-116.

[11] N. J. Sack, R. Schuster, A. Hofmann, A. Khedim, and R. Koppmann, "Current-density effects and the importance of charge-transfer processes in the radiolysis of methane - Astrophysical Implications," *Astrophysical Journal*, vol. 360, 1990, pp. 305-312.

[12] M. E. Sheridan, E. Greer, and W. F. Libby, "Polymer production in the .gamma.-radiolysis of methane, ethane, and ethylene solutions in liquid argon," *Journal of the American Chemical Society*, vol. 94, 1972, pp. 2614-2618.

[13] A. Mozumder, "Chapter 4 - Ionization and excitation phenomena," in *Fundamentals of Radiation Chemistry*, A. Mozumder, San Diego: Academic Press, 1999, pp. 71-120.

[14] A. Mozumder, "Chapter 6 - The solvated electron," in *Fundamentals of Radiation Chemistry*, A. Mozumder, San Diego: Academic Press, 1999, pp. 145-197.

[15] B. P. Straughan and S. Walker, "Dissociation energies of diatomic molecules," in *Spectroscopy*, B. P. Straughan and S. Walker, Netherlands: Springer, 1976, pp. 103-119.

[16] K. H. Gericke. (2/17/2014), Braunschweig University of Technology, *Dissociation and Predissociation*. Available: http://www.pci.tu-bs.de/aggericke/PC4e/Kap_III/Praediss.htm

[17] W. M. Stacey, "Neutron nuclear reactions," in *Nuclear Reactor Physics*, Hoboken, New Jersey: Wiley-VCH Verlag GmbH & Co. KGaA, 2007, pp. 1-32.

[18] A. Mozumder, "Chapter 2 - Interaction of radiation with matter: Energy transfer from fast charged particles," in *Fundamentals of Radiation Chemistry*, A. Mozumder, San Diego: Academic Press, 1999, pp. 5-39.

[19] A. Mozumder, "Chapter 3 - Structure of charged particle tracks in condensed media," in *Fundamentals of Radiation Chemistry*, A. Mozumder, San Diego: Academic Press, 1999, pp. 41-69.

[20] G. F. Knoll, "Radiation interactions", in *Radiation Detection and Measurement,* 3 ed, Hoboken, New Jersey: John Wiley & Sons, 1999, pp. 49-53.

[21] *Review of the Universe, (3/14/2014), Quantum Field Theory, Compton Scattering,*. Available: http://universe-review.ca/R15-12-QFT10.htm

[22] W. M. Stacey, "Neutron thermalization," in *Nuclear Reactor Physics*, Hoboken, New Jersey: Wiley-VCH Verlag GmbH & Co. KGaA, 2007, pp. 453-481.

[23] H. Bethe, "Zur Theorie des Durchgangs schneller Korpuskularstrahlen durch Materie," *Annalen der Physik,* vol. 397, pp. 325-400, 1930.

[24] H.-Y. Li, J.-S. Liu, C. Wang, G.-Q. Ni, R.-X. Li, and Z.-Z. Xu, "Coulomb expansion of deuterated methane clusters irradiated by an ultrashort intense laser pulse," *Chinese Physics B*, vol. 17, 2008, p. 1237.

[25] R. H. Partridge, "Excitation energy transfer in alkanes. I. exciton model," *The Journal of Chemical Physics,* vol. 52, 1970, pp. 2485-2490.

[26] R. H. Partridge, "Excitation energy transfer in alkanes. III. radiation chemistry of alkane polymers," *The Journal of Chemical Physics*, vol. 52, 1970, pp. 2501-2510.

[27] M. A. Eliason and J. O. Hirschfelder, "General collision theory treatment for the rate of bimolecular, gas phase reactions," *The Journal of Chemical Physics,* vol. 30, 1959, pp. 1426-1436.

[28] R. A. A. Robert J. Silbey, M. G. Bawendi, "Kinetic theory of gases," *Physical Chemistry,* 4th ed, Hoboken, New Jersey: John Wiley & Sons, 2004, pp. 614-640

[29] W. H. Beattie, "The radiolysis of mixtures of carbon dioxide and hydrogen," *International Journal of Chemical Kinetics,* vol. 4, 1972, pp. 463-477.

[30] S. P. Holloway, J. B. Olomo, T. D. Mac Mahon, and B. W. Hooton, "Decay scheme data for 239U, 154Eu and 140Ba/140La," in *Nuclear Data for Science and Technology*, K. H. Böckhoff., ed Netherlands: Springer, 1983, pp. 287-290.

[31] H. Skoog, S. Crouch, J. Holler,"Gas chromotography", *Principles or Instrumental Analysis*, 6 ed, Belmont, California: Brooks/Cole, 2007, pp. 788-810.

[32] N. W. Kyaw Thet. (3/21/2014). *Gas Chromatography*. Available: http://chemwiki.ucdavis.edu/Analytical_Chemistry/Instrumental_Analysis/Chromatography/Gas_Chromatography

[33] O. Khan. *(3/14/2014) Mass Analyzers (Mass Spectrometry)*. Available: http://chemwiki.ucdavis.edu/Analytical_Chemistry/Instrumental_Analysis/Mass_Spectrometry/Mass_Spectrometers_(Instrumentation)/Mass_Analyzers_(Mass_Spectrometry)

[34] G. L. Glish and R. W. Vachet, "The basics of mass spectrometry in the twenty-first century," *Nat Rev Drug Discov,* vol. 2, 2003, pp. 140-150.

[35] J. L. Magee and K. Funabashi, "The clustering of ions in irradiated gases," *Radiation Research,* vol. 10, 1959, pp. 622-635, 1959.

[36] S. Jo, D. H. Lee, S. Kang, and Y.-H. Song, "Methane activation using noble gases in a dielectric barrier discharge reactor," *Physics of Plasmas,* vol. 20, 2013.

[37] P. Tosi, D. Cappelletti, O. Dmitriev, S. Giordani, D. Bassi, D. R. Latimer, *et al.*, "Dissociative charge-transfer of argon ions with methane molecules from ultralow to superthermal collision energies," *Journal of Physical Chemistry,* vol. 99, 1995, pp. 15538-15543.

[38] S. J. Blanksby and G. B. Ellison, "Bond dissociation energies of organic molecules," *Accounts of Chemical Research,* vol. 36, 2003, pp. 255-263.

[39] C. M. Thacker, H. O. Folkins, and E. L. Miller, "Free energies of formation of gaseous hydrocarbons and related substances," *Industrial & Engineering Chemistry,* vol. 33, 1941, pp. 584-590.

APPENDIX

7.1 VBA Code

The code below is a VBA script that is used to read ASCII files from the folders on my computer. The program reads and imports all data onto excel sheets, performs some data rejection techniques, then acquires corrected averages and standard deviations. The code is copied below.

```
Sub readfromfile()


'Dimension Variables
Dim folder As String
Dim filename As String
Dim stringline As String
Dim stringarray
Dim pressure(1000) As Double
Dim IIMax, IIMax2, JJMax As Integer
Dim II, JJ, KK As Integer
Dim A As Integer
Dim foundFile As String
Dim listbox1 As Range
Dim strDatarray(1000) As String


Const forreading = 1, forwriting = 2, forappending = 8
Const TristateUseDefault = -2, TristateTrue = -1, tristate-
false = 0

A = 22
Set mydoc = ActiveWorkbook.ActiveSheet

folder = mydoc.Cells(1, 2)

Application.ScreenUpdating = False 'The program should run
faster if the picture is not updated

'============================================================
==============================
'**Get the list for the names of the files**
```

```
'============================================================
==============================

Set fs = CreateObject("Scripting.FileSystemObject") '}
Set f = fs.GetFolder(folder) '                       }See
help menu
Set fc = f.Files '                                   }
II = 0
For Each f1 In fc
    If Right(f1.Name, 3) = "txt" Then 'Only files with
"TXT" on the end will be used
        strDatarray(II) = f1.Name 'Collect the names in a
array
        II = II + 1 'Name will be saved next time in the
next position
    End If
Next
IIMax = II

'============================================================
==============================
'** Read files **
'****If the presure value is negative, then the values are
thrown out
'============================================================
==============================
JJ = 0
Do While JJ < IIMax
filename = strDatarray(JJ)
    mydoc.Cells(3, 2 + 2 * JJ) = 1 + JJ 'this is for the
modidied data
    mydoc.Cells(4, 2 + 2 * JJ) = filename 'this is for the
modidied data
    Set outread = Cre-
ateObject("Scripting.FileSystemObject").opentextfile(folder
& "\" & filename, forreading, False)
    II = 0
        Do While Not outread.atendofstream
            stringline = outread.Readline
                '***Teilen String zu Worter***
                stringarray = Split(stringline, ",") '
split line by a comma
                If II >= A Then ' set line number for read-
ing
                If JJ = 0 Then
```

```
                        mydoc.Cells(5 + II - A, 2 * JJ + 1)
= stringarray(0) ' read MtoZ only once
                End If
                mydoc.Cells(5 + II - A, 2 * JJ + 2) =
stringarray(1) ' insert raw data
                    If (stringarray(1) < 0) Then
                           mydoc.Cells(5 + II - A, 2 * JJ +
3) = "" 'insert blank
                    Else
                            mydoc.Cells(5 + II - A, 2 * JJ
+ 3) = stringarray(1) ' replace with value from adjacent
cell
                    End If
                End If
                IIMax2 = II
                II = II + 1
        Loop
        JJMax = JJ
    JJ = JJ + 1
Loop

mydoc.Cells(2, 1) = IIMax2 - A
mydoc.Cells(3, 1) = JJMax

'============================================================
==================================
'Normalization of the data by m/z=16 for odd columns
'============================================================
==================================
'Modification 1/27/14- normalization was modified to take
into account the continuous nature
'of fluctuations

JJ = 0
' dy = 0
II = 0

Do While JJ <= JJMax
 '   II = 15
    ' dy = Cells(5 + II, 2 * JJ + 4) - Cells(5 + II, 2 * JJ
+ 2)
    ' dynamic normalization
    Do While II <= IIMax2 - A
   ' fraction = ((II - 15) / (IIMax2 - A - 1))
```

```
        If (Cells(5 + II, 2 * JJ + 3) = Cells(5 + II, 2 *
JJ + 2)) Then
        Cells(5 + II, 2 * JJ + 3) = Cells(5 + II, 2 * JJ +
3) / (Cells(5 + 15, 2 * JJ + 2))
        End If
        II = II + 1
   Loop
    II = 0
'    II = 0 ' Do the lower half of the normalization

 '   Do While II < 15
  '      fraction = ((IIMax2 - A - 16 + II) / (IIMax2 - A -
1))
   '     Cells(5 + II, 2 * JJ + 3) = Cells(5 + II, 2 * JJ +
3) / (Cells(5 + 15, 2 * JJ + 2) + dy * fraction)
   '     II = II + 1
   ' Loop
    JJ = JJ + 1
Loop
JJ = 0


'=============================================================
====================================
'*****averageing and statistics******
' The data will be combed through, outliers will be re-
placed with blank spaces
'=============================================================
====================================

Dim Avg As Double
Dim STD As Double
Dim CI As Double
Dim upCI As Double
Dim lowCI As Double
Dim T As Double

T = 0
JJ = 0
II = 0
Avg = 0
STD = 0
CI = 0
upCI = 0
lowCI = 0
```

```
Do While II <= IIMax2 - A
    Do While JJ <= JJMax
        Avg = Avg + Cells(II + 5, 2 * JJ + 3).Value
        JJ = JJ + 1
    Loop
    Avg = Avg / JJ
    JJ = 0
    Do While JJ <= JJMax
        STD = STD + (Cells(II + 5, 2 * JJ + 3).Value - Avg)
^ 2
        JJ = JJ + 1
    Loop
    STD = Sqr(STD / JJMax)

    If (II = 15) Then
        Cells(II + 5, 2 * JJMax + 5) = II + 1 'MtoZ
        Cells(II + 5, 2 * JJMax + 6) = Avg 'Mean Values
        Cells(II + 5, 2 * JJMax + 7) = STD ' Standard Devi-
ation
        Cells(II + 5, 2 * JJMax + 8) = STD / Avg 'RSD
        Cells(II + 5, 2 * JJMax + 9) = Avg 'Lower bound of
95% CI for t test
        Cells(II + 5, 2 * JJMax + 10) = Avg 'Upper bound of
95% CI for t test
    Else
        Cells(II + 5, 2 * JJMax + 5) = II + 1 'MtoZ
        Cells(II + 5, 2 * JJMax + 6) = Avg 'Mean Values
        Cells(II + 5, 2 * JJMax + 7) = STD ' Standard Devi-
ation
        Cells(II + 5, 2 * JJMax + 8) = STD / Avg 'RSD
        Cells(II + 5, 2 * JJMax + 9) = Avg - WorksheetFunc-
tion.Confidence_T(0.05, STD, JJ) 'Lower bound of 95% CI for
t test
        Cells(II + 5, 2 * JJMax + 10) = Avg + Worksheet-
Function.Confidence_T(0.05, STD, JJ) 'Upper bound of 95% CI
for t test
    End If
    STD = 0
    Avg = 0
    JJ = 0
    II = II + 1
Loop
II = 0
JJ = 0
```

```
Cells(II + 3, 2 * JJMax + 7) = "Cells with only zero data
rejection"
Cells(II + 4, 2 * JJMax + 5) = "MtoZ"
Cells(II + 4, 2 * JJMax + 6) = "Mean"
Cells(II + 4, 2 * JJMax + 7) = "STDEV.S"
Cells(II + 4, 2 * JJMax + 8) = "RSD"
Cells(II + 4, 2 * JJMax + 9) = "LowerCI"
Cells(II + 4, 2 * JJMax + 10) = "UpperCI"

'=========================================================
========
' This is a series of conditional statistical procedures
for the rejectio of outliers from the main data det
'=========================================================
========
Dim MatA(1000, 1000) As Double
Dim Sig As Double
Dim Uppa As Double
Dim Lowa As Double

Sig = 3 'The rejection criterian

Do While JJ <= JJMax
    Do While II <= IIMax2 - A
    If (II <> 15) Then
        MatA(II, JJ) = Cells(II + 5, 2 * JJ + 3).Value
        Lowa = (-1 * Sig * Cells(II + 5, 2 * JJMax + 7) +
Cells(II + 5, 2 * JJMax + 6))
        Uppa = (1 * Sig * Cells(II + 5, 2 * JJMax + 7) +
Cells(II + 5, 2 * JJMax + 6))
            If (MatA(II, JJ) < Lowa) Then
                Cells(II + 5, 2 * JJ + 3) = ""
            End If
            If (MatA(II, JJ) > Uppa) Then
                Cells(II + 5, 2 * JJ + 3) = ""
            End If
            If (MatA(II, JJ) < 0) Then
                Cells(II + 5, 2 * JJ + 3) = ""
            End If
    End If
        II = II + 1
    Loop
    II = 0
    JJ = JJ + 1
Loop
```

```
JJ = 0

'=========================================================
=====================================
'This is the data after stastical rejection has been ap-
plied
'=========================================================
=====================================

Cells(II + 3, 2 * JJMax + 14) = "Cells with  data rejec-
tion"
Cells(II + 4, 2 * JJMax + 12) = "MtoZ"
Cells(II + 4, 2 * JJMax + 13) = "Mean"
Cells(II + 4, 2 * JJMax + 14) = "STDEV.S"
Cells(II + 4, 2 * JJMax + 15) = "RSD"
Cells(II + 4, 2 * JJMax + 16) = "LowerCI"
Cells(II + 4, 2 * JJMax + 17) = "UpperCI"
Cells(II + 4, 2 * JJMax + 18) = "deltaRSD"

'================================================
'Initialization
'================================================

T = 0
JJ = 0
II = 0
Avg = 0
STD = 0
CI = 0
upCI = 0
lowCI = 0

'=========================================================
=
'Second averages and STDEV
'=========================================================
=

Do While II <= IIMax2 - A

    Do While JJ <= JJMax
        Avg = Avg + Cells(II + 5, 2 * JJ + 3).Value
        JJ = JJ + 1
    Loop
    Avg = Avg / JJ
```

```
    JJ = 0
    Do While JJ <= JJMax
        STD = STD + (Cells(II + 5, 2 * JJ + 3).Value - Avg)
^ 2
        JJ = JJ + 1
    Loop
    STD = Sqr(STD / JJMax)

    If (II = 15) Then
        Cells(II + 5, 2 * JJMax + 12) = II + 1 'MtoZ
        Cells(II + 5, 2 * JJMax + 13) = Avg 'Mean Values
        Cells(II + 5, 2 * JJMax + 14) = STD ' Standard De-
viation
        Cells(II + 5, 2 * JJMax + 15) = STD / Avg 'RSD
        Cells(II + 5, 2 * JJMax + 16) = Avg 'Lower bound of
95% CI for t test
        Cells(II + 5, 2 * JJMax + 17) = Avg 'Upper bound of
95% CI for t test
    Else
        Cells(II + 5, 2 * JJMax + 12) = II + 1 'MtoZ
        Cells(II + 5, 2 * JJMax + 13) = Avg 'Mean Values
        Cells(II + 5, 2 * JJMax + 14) = STD ' Standard De-
viation
        Cells(II + 5, 2 * JJMax + 15) = STD / Avg 'RSD
        Cells(II + 5, 2 * JJMax + 16) = Avg - Worksheet-
Function.Confidence_T(0.05, STD, JJ) 'Lower bound of 95% CI
for t test
        Cells(II + 5, 2 * JJMax + 17) = Avg + Worksheet-
Function.Confidence_T(0.05, STD, JJ) 'Upper bound of 95% CI
for t test
    End If
    STD = 0
    Avg = 0
    JJ = 0
    Cells(II + 5, 2 * JJMax + 18) = Cells(II + 5, 2 * JJMax
+ 8) - Cells(II + 5, 2 * JJMax + 15)
    II = II + 1
Loop
II = 0
JJ = 0

'=========================================================
========
' Error propagation is going to be done to the corrected
values
```

```
'=========================================================
========

End Sub
```

7.2 MCNP Decks

A number of MCNP simulations were done to get dose and LET values to estimate the dose received by the different vessels undergoing irradiation. Each of these decks was written for MCNPX, and is given in the follow sections

6.1.1 Electron Beam run #2

```
Ebeam experiments
c -cell cards
c -gas
001 21 5.24E-04 -001 imp:e=1 imp:p=1
002 22 5.24E-04 -002 imp:e=1 imp:p=1
003 23 5.24E-04 -003 imp:e=1 imp:p=1
004 24 5.24E-04 -004 imp:e=1 imp:p=1
005 25 1.36E-03 -005 imp:e=1 imp:p=1
006 26 1.36E-03 -006 imp:e=1 imp:p=1
007 27 1.36E-03 -007 imp:e=1 imp:p=1
008 28 1.36E-03 -008 imp:e=1 imp:p=1
c -the main tanks-rcc
101 1 -7.6 001 -101 imp:e=1 imp:p=1
102 1 -7.6 002 -102 imp:e=1 imp:p=1
103 1 -7.6 003 -103 imp:e=1 imp:p=1
104 1 -7.6 004 -104 imp:e=1 imp:p=1
105 1 -7.6 005 -105 imp:e=1 imp:p=1
106 1 -7.6 006 -106 imp:e=1 imp:p=1
107 1 -7.6 007 -107 imp:e=1 imp:p=1
108 1 -7.6 008 -108 imp:e=1 imp:p=1
c --gas caps -so
011 21 5.24E-04 001 -011 imp:e=1 imp:p=1
012 22 5.24E-04 002 -012 imp:e=1 imp:p=1
013 23 5.24E-04 003 -013 imp:e=1 imp:p=1
014 24 1.91E-04 004 -014 imp:e=1 imp:p=1
```

```
015 25 5.24E-04 005 -015 imp:e=1 imp:p=1
016 26 5.24E-04 006 -016 imp:e=1 imp:p=1
017 27 5.24E-04 007 -017 imp:e=1 imp:p=1
018 28 5.24E-04 008 -018 imp:e=1 imp:p=1
021 21 5.24E-04 001 -021 imp:e=1 imp:p=1
022 22 5.24E-04 002 -022 imp:e=1 imp:p=1
023 23 5.24E-04 003 -023 imp:e=1 imp:p=1
024 24 1.91E-04 004 -024 imp:e=1 imp:p=1
025 25 5.24E-04 005 -025 imp:e=1 imp:p=1
026 26 5.24E-04 006 -026 imp:e=1 imp:p=1
027 27 5.24E-04 007 -027 imp:e=1 imp:p=1
028 28 5.24E-04 008 -028 imp:e=1 imp:p=1
c -tank caps -so
111 1 -7.6 011 101 -111 imp:e=1 imp:p=1
112 1 -7.6 012 102 -112 imp:e=1 imp:p=1
113 1 -7.6 013 103 -113 imp:e=1 imp:p=1
114 1 -7.6 014 104 -114 imp:e=1 imp:p=1
115 1 -7.6 015 105 -115 imp:e=1 imp:p=1
116 1 -7.6 016 106 -116 imp:e=1 imp:p=1
117 1 -7.6 017 107 -117 imp:e=1 imp:p=1
118 1 -7.6 018 108 -118 imp:e=1 imp:p=1
121 1 -7.6 021 101 -121 imp:e=1 imp:p=1
122 1 -7.6 022 102 -122 imp:e=1 imp:p=1
123 1 -7.6 023 103 -123 imp:e=1 imp:p=1
124 1 -7.6 024 104 -124 imp:e=1 imp:p=1
125 1 -7.6 025 105 -125 imp:e=1 imp:p=1
126 1 -7.6 026 106 -126 imp:e=1 imp:p=1
127 1 -7.6 027 107 -127 imp:e=1 imp:p=1
128 1 -7.6 028 108 -128 imp:e=1 imp:p=1
c -valves
131 4 -7.5 -131 imp:e=1 imp:p=1
132 4 -7.5 -132 imp:e=1 imp:p=1
133 4 -7.5 -133 imp:e=1 imp:p=1
134 4 -7.5 -134 imp:e=1 imp:p=1
135 4 -7.5 -135 imp:e=1 imp:p=1
136 4 -7.5 -136 imp:e=1 imp:p=1
137 4 -7.5 -137 imp:e=1 imp:p=1
138 4 -7.5 -138 imp:e=1 imp:p=1
141 4 -7.5 -141 imp:e=1 imp:p=1
142 4 -7.5 -142 imp:e=1 imp:p=1
143 4 -7.5 -143 imp:e=1 imp:p=1
144 4 -7.5 -144 imp:e=1 imp:p=1
145 4 -7.5 -145 imp:e=1 imp:p=1
146 4 -7.5 -146 imp:e=1 imp:p=1
147 4 -7.5 -147 imp:e=1 imp:p=1
```

```
148 4 -7.5 -148 imp:e=1 imp:p=1
c - valve caps
151 4 -7.5 -151 imp:e=1 imp:p=1
152 4 -7.5 -152 imp:e=1 imp:p=1
153 4 -7.5 -153 imp:e=1 imp:p=1
154 4 -7.5 -154 imp:e=1 imp:p=1
155 4 -7.5 -155 imp:e=1 imp:p=1
156 4 -7.5 -156 imp:e=1 imp:p=1
157 4 -7.5 -157 imp:e=1 imp:p=1
158 4 -7.5 -158 imp:e=1 imp:p=1
161 4 -7.5 -161 imp:e=1 imp:p=1
162 4 -7.5 -162 imp:e=1 imp:p=1
163 4 -7.5 -163 imp:e=1 imp:p=1
164 4 -7.5 -164 imp:e=1 imp:p=1
165 4 -7.5 -165 imp:e=1 imp:p=1
166 4 -7.5 -166 imp:e=1 imp:p=1
167 4 -7.5 -167 imp:e=1 imp:p=1
168 4 -7.5 -168 imp:e=1 imp:p=1
c -water
c 201
c 202
c 203
c 204
c 205
c 206
c 207
c 208
c -sheilds
301 1 -7.5 -301 imp:e=1 imp:p=1
302 1 -7.5 -302 imp:e=1 imp:p=1
c -source
c 401 3 -.00125 -401 imp:e=1 imp:p=1
c --The universe
998 3 -0.00125 -999 #001 #002 #003 #004 #005 #006 #007 #008
&
                    #101 #102 #103 #104 #105 #106 #107 #108
&
                    #011 #012 #013 #014 #015 #016 #017 #018
&
                    #021 #022 #023 #024 #025 #026 #027 #028
&
                    #111 #112 #113 #114 #115 #116 #117 #118
&
                    #121 #122 #123 #124 #125 #126 #127 #128
&
```

```
                    #131 #132 #133 #134 #135 #136 #137 #138
&
                    #141 #142 #143 #144 #145 #146 #147 #148
&
                    #151 #152 #153 #154 #155 #156 #157 #158
&
                    #161 #162 #163 #164 #165 #166 #167 #168
&
                    #301 #302 imp:e=1 imp:p=1
999 0 999 imp:e=0 imp:p=0

c -surface cards
c -gas-main cylinders
001 rcc 0    0 0 0 0 17.626  2.3
002 rcc 5.5  0 0 0 0 17.626  2.3
003 rcc 11   0 0 0 0 17.626  2.3
004 rcc 16.5 0 0 0 0 17.626  2.3
005 rcc 22   0 0 0 0 17.626  2.3
006 rcc 27.5 0 0 0 0 17.626  2.3
007 rcc 33   0 0 0 0 17.626 2.3
008 rcc 38.5 0 0 0 0 17.626  2.3
c -gas caps
011 s 0     0 0 2.3
012 s 5.5   0 0 2.3
013 s 11    0 0 2.3
014 s 16.5  0 0 2.3
015 s 22    0 0 2.3
016 s 27.5  0 0 2.3
017 s 33    0 0 2.3
018 s 38.5  0 0 2.3
021 s 0     0 17.626 2.3
022 s 5.5   0 17.626 2.3
023 s 11    0 17.626 2.3
024 s 16.5  0 17.626 2.3
025 s 22    0 17.626 2.3
026 s 27.5  0 17.626 2.3
027 s 33    0 17.626 2.3
028 s 38.5  0 17.626 2.3
c -steel tanks
101 rcc 0     0 0 0 0 17.626 2.54
102 rcc 5.5   0 0 0 0 17.626 2.54
103 rcc 11    0 0 0 0 17.626 2.54
104 rcc 16.5  0 0 0 0 17.626 2.54
105 rcc 22    0 0 0 0 17.626 2.54
106 rcc 27.5  0 0 0 0 17.626 2.54
```

```
107 rcc 33    0 0 0 0 17.626 2.54
108 rcc 38.5  0 0 0 0 17.626 2.54
c --tank caps
111 s 0     0 0 2.54
112 s 5.5   0 0 2.54
113 s 11    0 0 2.54
114 s 16.5  0 0 2.54
115 s 22    0 0 2.54
116 s 27.5  0 0 2.54
117 s 33    0 0 2.54
118 s 38.5  0 0 2.54
121 s 0     0 17.626 2.54
122 s 5.5   0 17.626 2.54
123 s 11    0 17.626 2.54
124 s 16.5  0 17.626 2.54
125 s 22    0 17.626 2.54
126 s 27.5  0 17.626 2.54
127 s 33    0 17.626 2.54
128 s 38.5  0 17.626 2.54
c -valves
131 rpp -1.5  1.5   -1.5 1.5 -5.46 -2.54
132 rpp  4    7     -1.5 1.5 -5.46 -2.54
133 rpp  9.5  12.5  -1.5 1.5 -5.46 -2.54
134 rpp  15   18    -1.5 1.5 -5.46 -2.54
135 rpp  20.5 23.5  -1.5 1.5 -5.46 -2.54
136 rpp  26.0 29.0  -1.5 1.5 -5.46 -2.54
137 rpp  31.5 34.5  -1.5 1.5 -5.46 -2.54
138 rpp  37.0 40.0  -1.5 1.5 -5.46 -2.54
141 rpp -1.5  1.5   -1.5 1.5 20.1676 23.7076
142 rpp  4    7     -1.5 1.5 20.1676 23.7076
143 rpp  9.5  12.5  -1.5 1.5 20.1676 23.7076
144 rpp  15   18    -1.5 1.5 20.1676 23.7076
145 rpp  20.5 23.5  -1.5 1.5 20.1676 23.7076
146 rpp  26.0 29.0  -1.5 1.5 20.1676 23.7076
147 rpp  31.5 34.5  -1.5 1.5 20.1676 23.7076
148 rpp  37.0 40.0  -1.5 1.5 20.1676 23.7076
c -valve caps
151 rcc 0     1.5  -4   0 2 0 0.75
152 rcc 5.5   1.5  -4   0 2 0 0.75
153 rcc 11    1.5  -4   0 2 0 0.75
154 rcc 16.5  1.5  -4   0 2 0 0.75
155 rcc 22    1.5  -4   0 2 0 0.75
156 rcc 27.5  1.5  -4   0 2 0 0.75
157 rcc 33    1.5  -4   0 2 0 0.75
158 rcc 38.5  1.5  -4   0 2 0 0.75
```

```
161 rcc 0     1.5  21.5 0 2 0 0.75
162 rcc 5.5   1.5  21.5 0 2 0 0.75
163 rcc 11    1.5  21.5 0 2 0 0.75
164 rcc 16.5  1.5  21.5 0 2 0 0.75
165 rcc 22    1.5  21.5 0 2 0 0.75
166 rcc 27.5  1.5  21.5 0 2 0 0.75
167 rcc 33    1.5  21.5 0 2 0 0.75
168 rcc 38.5  1.5  21.5 0 2 0 0.75
c -supports
c 201
c 202
c 203
c 204
c 205
c 206
c 207
c 208
c -sheilds
301 rpp  -6.0 44.0 6 7.5 -7 0
302 rpp  -6.0 44.0 6 7.5 16.5 23.5
c - source
c 401 s 22 95 20 10
c -the universe
999 rpp -20 60 -20 120 -30 60

c -data cards
c
mode e p
nps 5E5
c sdef pos=22 95 20 erg=10.0 dir 0.95 vec 0 -1 0
SDEF PAR= p ERG=10 x=d1 y=10 z=d2 DIR=1 VEC=0 -1 0
SI1 -6 44
SP1   0  1
c SI2  7.813  9.813
SI2  -8 27
SP2   0  1
f4:e 001 002 003 004 005 006 007 008
fc4 Proton flux LET
e4 1e-2 19ilog 10
ft4 LET
f6:p,e 001 002 003 004 005 006 007 008 &
       101 102 103 104 105 106 107 108 &
       011 012 013 014 015 016 017 018 &
       021 022 023 024 025 026 027 028
m1    24000.70c 1.7385E-2 $ SS-304
```

```
      26000.70c 5.9206E-2
      28000.70c 7.6995E-3
      25055.70c 1.7320E-3
m21   6000.70c 4.94286E-05
      1001.70c 0.000197715 $methane
      2004.70c 0.000474315 $helium
m22   6000.70c 9.93565E-05
      1001.70c 0.000397426 $methane
      2004.70c 0.000424387 $helium
m23   6000.70c 0.000149284
      1001.70c 0.000597138 $methane
      2004.70c 0.000374459 $helium
m24   6000.70c 0.000199212
      1001.70c 0.000796849 $methane
      2004.70c 0.000324531 $helium
m25   6000.70c 4.94286E-05
      1001.70c 0.000197715 $methane
      2004.70c 0.001306447 $helium
m26   6000.70c 9.93565E-05
      1001.70c 0.000397426 $methane
      2004.70c 0.001256519 $helium
m27   6000.70c 0.000149284
      1001.70c 0.000597138 $methane
      2004.70c 0.001206591 $helium
m28   6000.70c 0.000199212
      1001.70c 0.000796849 $methane
      2004.70c 0.001156663 $helium
m3    7014.70c 1 $N2
m4    26000.70c 0.000076 $Brass
      29000.70c 0.050887
      30000.70c 0.024199
      50000.70c 0.000109
      82000.70c 0.000126
mt21 poly.10t
mt22 poly.10t
mt23 poly.10t
mt24 poly.10t
mt25 poly.10t
mt26 poly.10t
mt27 poly.10t
mt28 poly.10t
```

6.1.2 Electron Beam run #3

```
Ebeam experiments
c -cell cards
c -gas
001 21 5.24E-04 -001 imp:e=1 imp:p=1
002 22 5.24E-04 -002 imp:e=1 imp:p=1
003 23 5.24E-04 -003 imp:e=1 imp:p=1
004 24 1.91E-04 -004 imp:e=1 imp:p=1
005 25 5.24E-04 -005 imp:e=1 imp:p=1
006 26 5.24E-04 -006 imp:e=1 imp:p=1
007 27 5.24E-04 -007 imp:e=1 imp:p=1
008 28 5.24E-04 -008 imp:e=1 imp:p=1
c -the main tanks-rcc
101 1 -7.6 001 -101 imp:e=1 imp:p=1
102 1 -7.6 002 -102 imp:e=1 imp:p=1
103 1 -7.6 003 -103 imp:e=1 imp:p=1
104 1 -7.6 004 -104 imp:e=1 imp:p=1
105 1 -7.6 005 -105 imp:e=1 imp:p=1
106 1 -7.6 006 -106 imp:e=1 imp:p=1
107 1 -7.6 007 -107 imp:e=1 imp:p=1
108 1 -7.6 008 -108 imp:e=1 imp:p=1
c --gas caps -so
011 21 5.24E-04 001 -011 imp:e=1 imp:p=1
012 22 5.24E-04 002 -012 imp:e=1 imp:p=1
013 23 5.24E-04 003 -013 imp:e=1 imp:p=1
014 24 1.91E-04 004 -014 imp:e=1 imp:p=1
015 25 5.24E-04 005 -015 imp:e=1 imp:p=1
016 26 5.24E-04 006 -016 imp:e=1 imp:p=1
017 27 5.24E-04 007 -017 imp:e=1 imp:p=1
018 28 5.24E-04 008 -018 imp:e=1 imp:p=1
021 21 5.24E-04 001 -021 imp:e=1 imp:p=1
022 22 5.24E-04 002 -022 imp:e=1 imp:p=1
023 23 5.24E-04 003 -023 imp:e=1 imp:p=1
024 24 1.91E-04 004 -024 imp:e=1 imp:p=1
025 25 5.24E-04 005 -025 imp:e=1 imp:p=1
026 26 5.24E-04 006 -026 imp:e=1 imp:p=1
027 27 5.24E-04 007 -027 imp:e=1 imp:p=1
028 28 5.24E-04 008 -028 imp:e=1 imp:p=1
c -tank caps -so
111 1 -7.6 011 101 -111 imp:e=1 imp:p=1
112 1 -7.6 012 102 -112 imp:e=1 imp:p=1
113 1 -7.6 013 103 -113 imp:e=1 imp:p=1
114 1 -7.6 014 104 -114 imp:e=1 imp:p=1
```

```
115 1 -7.6 015 105 -115 imp:e=1 imp:p=1
116 1 -7.6 016 106 -116 imp:e=1 imp:p=1
117 1 -7.6 017 107 -117 imp:e=1 imp:p=1
118 1 -7.6 018 108 -118 imp:e=1 imp:p=1
121 1 -7.6 021 101 -121 imp:e=1 imp:p=1
122 1 -7.6 022 102 -122 imp:e=1 imp:p=1
123 1 -7.6 023 103 -123 imp:e=1 imp:p=1
124 1 -7.6 024 104 -124 imp:e=1 imp:p=1
125 1 -7.6 025 105 -125 imp:e=1 imp:p=1
126 1 -7.6 026 106 -126 imp:e=1 imp:p=1
127 1 -7.6 027 107 -127 imp:e=1 imp:p=1
128 1 -7.6 028 108 -128 imp:e=1 imp:p=1
c -valves
131 4 -7.5 -131 imp:e=1 imp:p=1
132 4 -7.5 -132 imp:e=1 imp:p=1
133 4 -7.5 -133 imp:e=1 imp:p=1
134 4 -7.5 -134 imp:e=1 imp:p=1
135 4 -7.5 -135 imp:e=1 imp:p=1
136 4 -7.5 -136 imp:e=1 imp:p=1
137 4 -7.5 -137 imp:e=1 imp:p=1
138 4 -7.5 -138 imp:e=1 imp:p=1
141 4 -7.5 -141 imp:e=1 imp:p=1
142 4 -7.5 -142 imp:e=1 imp:p=1
143 4 -7.5 -143 imp:e=1 imp:p=1
144 4 -7.5 -144 imp:e=1 imp:p=1
145 4 -7.5 -145 imp:e=1 imp:p=1
146 4 -7.5 -146 imp:e=1 imp:p=1
147 4 -7.5 -147 imp:e=1 imp:p=1
148 4 -7.5 -148 imp:e=1 imp:p=1
c - valve caps
151 4 -7.5 -151 imp:e=1 imp:p=1
152 4 -7.5 -152 imp:e=1 imp:p=1
153 4 -7.5 -153 imp:e=1 imp:p=1
154 4 -7.5 -154 imp:e=1 imp:p=1
155 4 -7.5 -155 imp:e=1 imp:p=1
156 4 -7.5 -156 imp:e=1 imp:p=1
157 4 -7.5 -157 imp:e=1 imp:p=1
158 4 -7.5 -158 imp:e=1 imp:p=1
161 4 -7.5 -161 imp:e=1 imp:p=1
162 4 -7.5 -162 imp:e=1 imp:p=1
163 4 -7.5 -163 imp:e=1 imp:p=1
164 4 -7.5 -164 imp:e=1 imp:p=1
165 4 -7.5 -165 imp:e=1 imp:p=1
166 4 -7.5 -166 imp:e=1 imp:p=1
167 4 -7.5 -167 imp:e=1 imp:p=1
```

```
168 4 -7.5 -168 imp:e=1 imp:p=1
c -water
c 201
c 202
c 203
c 204
c 205
c 206
c 207
c 208
c -sheilds
301 1 -7.5 -301 imp:e=1 imp:p=1
302 1 -7.5 -302 imp:e=1 imp:p=1
c -source
c 401 3 -.00125 -401 imp:e=1 imp:p=1
c --The universe
998 3 -0.00125 -999 #001 #002 #003 #004 #005 #006 #007 #008
&
                    #101 #102 #103 #104 #105 #106 #107 #108
&
                    #011 #012 #013 #014 #015 #016 #017 #018
&
                    #021 #022 #023 #024 #025 #026 #027 #028
&
                    #111 #112 #113 #114 #115 #116 #117 #118
&
                    #121 #122 #123 #124 #125 #126 #127 #128
&
                    #131 #132 #133 #134 #135 #136 #137 #138
&
                    #141 #142 #143 #144 #145 #146 #147 #148
&
                    #151 #152 #153 #154 #155 #156 #157 #158
&
                    #161 #162 #163 #164 #165 #166 #167 #168
&
                    #301 #302 imp:e=1 imp:p=1
999 0 999 imp:e=0 imp:p=0

c -surface cards
c -gas-main cylinders
001 rcc 0    0 0 0 0 17.626  2.3
002 rcc 5.5  0 0 0 0 17.626  2.3
003 rcc 11   0 0 0 0 17.626  2.3
004 rcc 16.5 0 0 0 0 17.626  2.3
```

```
005 rcc 22   0 0 0 0 17.626  2.3
006 rcc 27.5 0 0 0 0 17.626  2.3
007 rcc 33   0 0 0 0 17.626 2.3
008 rcc 38.5 0 0 0 0 17.626  2.3
c -gas caps
011 s 0     0 0 2.3
012 s 5.5   0 0 2.3
013 s 11    0 0 2.3
014 s 16.5  0 0 2.3
015 s 22    0 0 2.3
016 s 27.5  0 0 2.3
017 s 33    0 0 2.3
018 s 38.5  0 0 2.3
021 s 0     0 17.626 2.3
022 s 5.5   0 17.626 2.3
023 s 11    0 17.626 2.3
024 s 16.5  0 17.626 2.3
025 s 22    0 17.626 2.3
026 s 27.5  0 17.626 2.3
027 s 33    0 17.626 2.3
028 s 38.5  0 17.626 2.3
c -steel tanks
101 rcc 0     0 0 0 0 17.626 2.54
102 rcc 5.5   0 0 0 0 17.626 2.54
103 rcc 11    0 0 0 0 17.626 2.54
104 rcc 16.5  0 0 0 0 17.626 2.54
105 rcc 22    0 0 0 0 17.626 2.54
106 rcc 27.5  0 0 0 0 17.626 2.54
107 rcc 33    0 0 0 0 17.626 2.54
108 rcc 38.5  0 0 0 0 17.626 2.54
c --tank caps
111 s 0     0 0 2.54
112 s 5.5   0 0 2.54
113 s 11    0 0 2.54
114 s 16.5  0 0 2.54
115 s 22    0 0 2.54
116 s 27.5  0 0 2.54
117 s 33    0 0 2.54
118 s 38.5  0 0 2.54
121 s 0     0 17.626 2.54
122 s 5.5   0 17.626 2.54
123 s 11    0 17.626 2.54
124 s 16.5  0 17.626 2.54
125 s 22    0 17.626 2.54
126 s 27.5  0 17.626 2.54
```

```
127 s 33    0 17.626 2.54
128 s 38.5  0 17.626 2.54
c -valves
131 rpp -1.5  1.5   -1.5 1.5 -5.46 -2.54
132 rpp  4    7     -1.5 1.5 -5.46 -2.54
133 rpp  9.5  12.5  -1.5 1.5 -5.46 -2.54
134 rpp  15   18    -1.5 1.5 -5.46 -2.54
135 rpp  20.5 23.5  -1.5 1.5 -5.46 -2.54
136 rpp  26.0 29.0  -1.5 1.5 -5.46 -2.54
137 rpp  31.5 34.5  -1.5 1.5 -5.46 -2.54
138 rpp  37.0 40.0  -1.5 1.5 -5.46 -2.54
141 rpp -1.5  1.5   -1.5 1.5 20.1676 23.7076
142 rpp  4    7     -1.5 1.5 20.1676 23.7076
143 rpp  9.5  12.5  -1.5 1.5 20.1676 23.7076
144 rpp  15   18    -1.5 1.5 20.1676 23.7076
145 rpp  20.5 23.5  -1.5 1.5 20.1676 23.7076
146 rpp  26.0 29.0  -1.5 1.5 20.1676 23.7076
147 rpp  31.5 34.5  -1.5 1.5 20.1676 23.7076
148 rpp  37.0 40.0  -1.5 1.5 20.1676 23.7076
c -valve caps
151 rcc 0     1.5  -4   0 2 0 0.75
152 rcc 5.5   1.5  -4   0 2 0 0.75
153 rcc 11    1.5  -4   0 2 0 0.75
154 rcc 16.5  1.5  -4   0 2 0 0.75
155 rcc 22    1.5  -4   0 2 0 0.75
156 rcc 27.5  1.5  -4   0 2 0 0.75
157 rcc 33    1.5  -4   0 2 0 0.75
158 rcc 38.5  1.5  -4   0 2 0 0.75
161 rcc 0     1.5  21.5 0 2 0 0.75
162 rcc 5.5   1.5  21.5 0 2 0 0.75
163 rcc 11    1.5  21.5 0 2 0 0.75
164 rcc 16.5  1.5  21.5 0 2 0 0.75
165 rcc 22    1.5  21.5 0 2 0 0.75
166 rcc 27.5  1.5  21.5 0 2 0 0.75
167 rcc 33    1.5  21.5 0 2 0 0.75
168 rcc 38.5  1.5  21.5 0 2 0 0.75
c -supports
c 201
c 202
c 203
c 204
c 205
c 206
c 207
c 208
```

```
c -sheilds
301 rpp  -6.0 44.0 6 7.5 -7 0
302 rpp  -6.0 44.0 6 7.5 16.5 23.5
c - source
c 401 s 22 95 20 10
c -the universe
999 rpp -20 60 -20 120 -30 60

c -data cards
c
mode e p
nps 5E5
c sdef pos=22 95 20 erg=10.0 dir 0.95 vec 0 -1 0
SDEF PAR= p ERG=10 x=d1 y=10 z=d2 DIR=1 VEC=0 -1 0
SI1 -6 44
SP1   0  1
c SI2  7.813  9.813
SI2  7.813  9.813
SP2   0  1
f4:e 001 002 003 004 005 006 007 008
fc4 Proton flux LET
e4 1e-2 19ilog 10
ft4 LET
f6:p,e 001 002 003 004 005 006 007 008 &
       101 102 103 104 105 106 107 108 &
       011 012 013 014 015 016 017 018 &
       021 022 023 024 025 026 027 028
m1    24000.70c 1.7385E-2 $ SS-304
      26000.70c 5.9206E-2
      28000.70c 7.6995E-3
      25055.70c 1.7320E-3
m21   6000.70c 7.43926E-05
      1001.70c 0.00029757 $methane
      18000.70c 0.000449351 $helium
m22   6000.70c 0.000174248
      1001.70c 0.000696994 $methane
      18000.70c 0.000349495 $helium
m23   6000.70c 0.00037396
      1001.70c 0.00149584 $methane
      18000.70c 0.000149784 $helium
m24   6000.70c 0.000190891
      1001.70c 0.000763564 $methane
m25   6000.70c 7.43926E-05
      1001.70c 0.00029757 $methane
      18000.70c 0.000449351 $helium
```

```
m26   6000.70c 0.000174248
      1001.70c 0.000696994 $methane
      18000.70c 0.000349495 $helium
m27   6000.70c 0.00037396
      1001.70c 0.00149584 $methane
      18000.70c 0.000149784 $helium
m28   6000.70c 0.000523744
      1001.70c 0.002094975 $methane
m3    7014.70c 1 $N2
m4    26000.70c 0.000076 $Brass
      29000.70c 0.050887
      30000.70c 0.024199
      50000.70c 0.000109
      82000.70c 0.000126
mt21 poly.10t
mt22 poly.10t
mt23 poly.10t
mt24 poly.10t
mt25 poly.10t
mt26 poly.10t
mt27 poly.10t
mt28 poly.10t
```

6.1.3 La-140 Irradiation

```
c Ebeam experiments
c -cell cards
C LA SOURCE
c OUTER STUFF
701 10 1.69E-03 -1101 +1201 -1202 imp:e=1 imp:p=1
702 10 1.69E-03 -1102 +1201 -1202 imp:e=1 imp:p=1
703 10 1.69E-03 -1103 +1201 -1202 imp:e=1 imp:p=1
704 10 1.69E-03 -1104 +1201 -1202 imp:e=1 imp:p=1
705 20 1.69E-03-2.70 +1200 -1203 +1301 -1303 +1401 -1402 &
   #7011.69E-03 #702 #703 #704   imp:e=1 imp:p=1
c -gas 1.69E-03
001 21 1.36E-035.24E-04 -001 imp:e=1 imp:p=1
002 22 5.24E-04 -002 imp:e=1 imp:p=1
003 23 5.24E-04 -003 imp:e=1 imp:p=1
004 24 5.24E-04 -004 imp:e=1 imp:p=1
005 25 1.36E-03 -005 imp:e=1 imp:p=1
006 26 1.36E-03 -006 imp:e=1 imp:p=1
007 27 1.36E-03 -007 imp:e=1 imp:p=1
```

```
008 28 1.36E-03 -008 imp:e=1 imp:p=1
c -the main tanks-rcc
101 1 -7.6 001 -101 imp:e=1 imp:p=1
102 1 -7.6 002 -102 imp:e=1 imp:p=1
103 1 -7.6 003 -103 imp:e=1 imp:p=1
104 1 -7.6 004 -104 imp:e=1 imp:p=1
105 1 -7.6 005 -105 imp:e=1 imp:p=1
106 1 -7.6 006 -106 imp:e=1 imp:p=1
107 1 -7.6 007 -107 imp:e=1 imp:p=1
108 1 -7.6 008 -108 imp:e=1 imp:p=1
c --gas caps -so
011 2 -0.0139 001 -011 imp:e=1 imp:p=1
012 2 -0.0139 002 -012 imp:e=1 imp:p=1
013 2 -0.0139 003 -013 imp:e=1 imp:p=1
014 2 -0.0139 004 -014 imp:e=1 imp:p=1
015 2 -0.0139 005 -015 imp:e=1 imp:p=1
016 2 -0.0139 006 -016 imp:e=1 imp:p=1
017 2 -0.0139 007 -017 imp:e=1 imp:p=1
018 2 -0.0139 008 -018 imp:e=1 imp:p=1
021 2 -0.0139 001 -021 imp:e=1 imp:p=1
022 2 -0.0139 002 -022 imp:e=1 imp:p=1
023 2 -0.0139 003 -023 imp:e=1 imp:p=1
024 2 -0.0139 004 -024 imp:e=1 imp:p=1
025 2 -0.0139 005 -025 imp:e=1 imp:p=1
026 2 -0.0139 006 -026 imp:e=1 imp:p=1
027 2 -0.0139 007 -027 imp:e=1 imp:p=1
028 2 -0.0139 008 -028 imp:e=1 imp:p=1
c -tank caps -so
111 1 -7.6 011 101 -111 imp:e=1 imp:p=1
112 1 -7.6 012 102 -112 imp:e=1 imp:p=1
113 1 -7.6 013 103 -113 imp:e=1 imp:p=1
114 1 -7.6 014 104 -114 imp:e=1 imp:p=1
115 1 -7.6 015 105 -115 imp:e=1 imp:p=1
116 1 -7.6 016 106 -116 imp:e=1 imp:p=1
117 1 -7.6 017 107 -117 imp:e=1 imp:p=1
118 1 -7.6 018 108 -118 imp:e=1 imp:p=1
121 1 -7.6 021 101 -121 imp:e=1 imp:p=1
122 1 -7.6 022 102 -122 imp:e=1 imp:p=1
123 1 -7.6 023 103 -123 imp:e=1 imp:p=1
124 1 -7.6 024 104 -124 imp:e=1 imp:p=1
125 1 -7.6 025 105 -125 imp:e=1 imp:p=1
126 1 -7.6 026 106 -126 imp:e=1 imp:p=1
127 1 -7.6 027 107 -127 imp:e=1 imp:p=1
128 1 -7.6 028 108 -128 imp:e=1 imp:p=1
c -valves
```

```
131 4 -7.5 -131 imp:e=1 imp:p=1
132 4 -7.5 -132 imp:e=1 imp:p=1
133 4 -7.5 -133 imp:e=1 imp:p=1
134 4 -7.5 -134 imp:e=1 imp:p=1
135 4 -7.5 -135 imp:e=1 imp:p=1
136 4 -7.5 -136 imp:e=1 imp:p=1
137 4 -7.5 -137 imp:e=1 imp:p=1
138 4 -7.5 -138 imp:e=1 imp:p=1
141 4 -7.5 -141 imp:e=1 imp:p=1
142 4 -7.5 -142 imp:e=1 imp:p=1
143 4 -7.5 -143 imp:e=1 imp:p=1
144 4 -7.5 -144 imp:e=1 imp:p=1
145 4 -7.5 -145 imp:e=1 imp:p=1
146 4 -7.5 -146 imp:e=1 imp:p=1
147 4 -7.5 -147 imp:e=1 imp:p=1
148 4 -7.5 -148 imp:e=1 imp:p=1
c - valve caps
151 4 -7.5 -151 imp:e=1 imp:p=1
152 4 -7.5 -152 imp:e=1 imp:p=1
153 4 -7.5 -153 imp:e=1 imp:p=1
154 4 -7.5 -154 imp:e=1 imp:p=1
155 4 -7.5 -155 imp:e=1 imp:p=1
156 4 -7.5 -156 imp:e=1 imp:p=1
157 4 -7.5 -157 imp:e=1 imp:p=1
158 4 -7.5 -158 imp:e=1 imp:p=1
161 4 -7.5 -161 imp:e=1 imp:p=1
162 4 -7.5 -162 imp:e=1 imp:p=1
163 4 -7.5 -163 imp:e=1 imp:p=1
164 4 -7.5 -164 imp:e=1 imp:p=1
165 4 -7.5 -165 imp:e=1 imp:p=1
166 4 -7.5 -166 imp:e=1 imp:p=1
167 4 -7.5 -167 imp:e=1 imp:p=1
168 4 -7.5 -168 imp:e=1 imp:p=1
c -supports
c 201
c 202
c 203
c 204
c 205
c 206
c 207
c 208
c -sheilds
c 301 2 -7.5 -301 imp:e=1 imp:p=1
c 302 2 -7.5 -302 imp:e=1 imp:p=1
```

```
c -source
c 401 3 -.00125 -401 imp:e=1 imp:p=1
c --The universe
998 3 0.10004 -999 #001 #002 #003 #004 #005 #006 #007 #008
&
                    #101 #102 #103 #104 #105 #106 #107 #108
&
                    #011 #012 #013 #014 #015 #016 #017 #018
&
                    #021 #022 #023 #024 #025 #026 #027 #028
&
                    #111 #112 #113 #114 #115 #116 #117 #118
&
                    #121 #122 #123 #124 #125 #126 #127 #128
&
                    #131 #132 #133 #134 #135 #136 #137 #138
&
                    #141 #142 #143 #144 #145 #146 #147 #148
&
                    #151 #152 #153 #154 #155 #156 #157 #158
&
                    #161 #162 #163 #164 #165 #166 #167 #168
&
                    #701 #702 #703 #704 #705 imp:e=1
imp:p=1
999 0 999 imp:e=0 imp:p=0

c -surface cards
C -------LA surface cards----------
1101 c/x 5.8575 0.1775 1.5875
1102 c/x 5.8575 5.8925 1.5875
1103 c/x 5.8575 11.6075 1.5875
1104 c/x 5.8575 17.3225 1.5875
$ x z r
1200 px -1.07
1201 px 0.2
1202 px 38.3
1203 px 39.57
1301 py 3.0
1302 py 5.8575
1303 py 8.715
1401 pz -2.68
1402 pz 20.18
c -gas-main cylinders
001 rcc 0    0 0 0 0 17.626  2.3
```

```
002 rcc 5.5  0 0 0 0 17.626  2.3
003 rcc 11   0 0 0 0 17.626  2.3
004 rcc 16.5 0 0 0 0 17.626  2.3
005 rcc 22   0 0 0 0 17.626  2.3
006 rcc 27.5 0 0 0 0 17.626  2.3
007 rcc 33   0 0 0 0 17.626 2.3
008 rcc 38.5 0 0 0 0 17.626  2.3
c -gas caps
011 s 0     0 0 2.3
012 s 5.5   0 0 2.3
013 s 11    0 0 2.3
014 s 16.5  0 0 2.3
015 s 22    0 0 2.3
016 s 27.5  0 0 2.3
017 s 33    0 0 2.3
018 s 38.5  0 0 2.3
021 s 0     0 17.626 2.3
022 s 5.5   0 17.626 2.3
023 s 11    0 17.626 2.3
024 s 16.5  0 17.626 2.3
025 s 22    0 17.626 2.3
026 s 27.5  0 17.626 2.3
027 s 33    0 17.626 2.3
028 s 38.5  0 17.626 2.3
c -steel tanks
101 rcc 0     0 0 0 0 17.626 2.54
102 rcc 5.5   0 0 0 0 17.626 2.54
103 rcc 11    0 0 0 0 17.626 2.54
104 rcc 16.5  0 0 0 0 17.626 2.54
105 rcc 22    0 0 0 0 17.626 2.54
106 rcc 27.5  0 0 0 0 17.626 2.54
107 rcc 33    0 0 0 0 17.626 2.54
108 rcc 38.5  0 0 0 0 17.626 2.54
c --tank caps
111 s 0     0 0 2.54
112 s 5.5   0 0 2.54
113 s 11    0 0 2.54
114 s 16.5  0 0 2.54
115 s 22    0 0 2.54
116 s 27.5  0 0 2.54
117 s 33    0 0 2.54
118 s 38.5  0 0 2.54
121 s 0     0 17.626 2.54
122 s 5.5   0 17.626 2.54
123 s 11    0 17.626 2.54
```

```
124 s 16.5  0 17.626 2.54
125 s 22    0 17.626 2.54
126 s 27.5  0 17.626 2.54
127 s 33    0 17.626 2.54
128 s 38.5  0 17.626 2.54
c -valves
131 rpp -1.5  1.5   -1.5 1.5 -5.46 -2.54
132 rpp  4    7     -1.5 1.5 -5.46 -2.54
133 rpp  9.5  12.5  -1.5 1.5 -5.46 -2.54
134 rpp  15   18    -1.5 1.5 -5.46 -2.54
135 rpp  20.5 23.5  -1.5 1.5 -5.46 -2.54
136 rpp  26.0 29.0  -1.5 1.5 -5.46 -2.54
137 rpp  31.5 34.5  -1.5 1.5 -5.46 -2.54
138 rpp  37.0 40.0  -1.5 1.5 -5.46 -2.54
141 rpp -1.5  1.5   -1.5 1.5 20.1676 23.7076
142 rpp  4    7     -1.5 1.5 20.1676 23.7076
143 rpp  9.5  12.5  -1.5 1.5 20.1676 23.7076
144 rpp  15   18    -1.5 1.5 20.1676 23.7076
145 rpp  20.5 23.5  -1.5 1.5 20.1676 23.7076
146 rpp  26.0 29.0  -1.5 1.5 20.1676 23.7076
147 rpp  31.5 34.5  -1.5 1.5 20.1676 23.7076
148 rpp  37.0 40.0  -1.5 1.5 20.1676 23.7076
c -valve caps
151 rcc 0     1.5  -4   0 2 0 0.75
152 rcc 5.5   1.5  -4   0 2 0 0.75
153 rcc 11    1.5  -4   0 2 0 0.75
154 rcc 16.5  1.5  -4   0 2 0 0.75
155 rcc 22    1.5  -4   0 2 0 0.75
156 rcc 27.5  1.5  -4   0 2 0 0.75
157 rcc 33    1.5  -4   0 2 0 0.75
158 rcc 38.5  1.5  -4   0 2 0 0.75
161 rcc 0     1.5  21.5 0 2 0 0.75
162 rcc 5.5   1.5  21.5 0 2 0 0.75
163 rcc 11    1.5  21.5 0 2 0 0.75
164 rcc 16.5  1.5  21.5 0 2 0 0.75
165 rcc 22    1.5  21.5 0 2 0 0.75
166 rcc 27.5  1.5  21.5 0 2 0 0.75
167 rcc 33    1.5  21.5 0 2 0 0.75
168 rcc 38.5  1.5  21.5 0 2 0 0.75
c -supports
c 201
c 202
c 203
c 204
c 205
```

```
c 206
c 207
c 208
c -sheilds
c 301 rpp  -6.0 44.0 6 7.5 -7 0
c 302 rpp  -6.0 44.0 6 7.5 16.5 23.5
c - source
c 401 s 22 95 20 10
c -the universe
999 rpp -20 60 -20 120 -30 60

c -data cards
c
mode e p
nps 1e6
sdef CEL=D1 RAD=D2 pos=20 5 9 eff=0.0001
si1 L 701 702 703 704
sp1 D 1 1 1 1
si2 0 22
sp2 -21 1
f4:e 001 002 003 004 005 006 007 008
fc4 Proton flux LET
e4 1e-2 19ilog 10
ft4 LET
f6:p,e 001 002 003 004 005 006 007 008 &
       101 102 103 104 105 106 107 108 &
       011 012 013 014 015 016 017 018 &
       021 022 023 024 025 026 027 028
m1    24000.70c 1.7385E-2 $ SS-304
      26000.70c 5.9206E-2
      28000.70c 7.6995E-3
      25055.70c 1.7320E-3
m21   6000.70c 0.001688728
      1001.70c 0.006754913 $methane
m22   6000.70c 0.000190891
      1001.70c 0.000763564 $methane
      2004.70c 0.001497837 $helium
m23   6000.70c 0.000357317
      1001.70c 0.001429269 $methane
      2004.70c 0.001331411 $helium
m24   6000.70c 0.000523744
      1001.70c 0.002094975 $methane
      2004.70c 0.001164984 $helium
m25   6000.70c 0.00069017
      1001.70c 0.00276068 $methane
```

```
      2004.70c 0.000998558 $helium
m26   6000.70c 0.000856596
      1001.70c 0.003426386 $methane
      2004.70c 0.000832132 $helium
m27   6000.70c 0.001023023
      1001.70c 0.004092091 $methane
      2004.70c 0.000665705 $helium
m28   6000.70c 0.001189449
      1001.70c 0.004757796 $methane
      2004.70c 0.000499279 $helium
m3    8016.70c 1 $H20
      1000.70c 2
m4    29000.70c 3
      30000.70c 1
m10   57140.70c 0.4 $ La-140
      08016.70c 0.6 $ Oxygen
m20   13027.70c 1.0 $ Aluminium - density = 2.70g/cc
```

6.1.4 NSCR Methane Only

```
NSC TRIGA Reactor
c
c -- Cell Cards --
c
c -- Fuel Pin --
100   1 0.042909 -100 +111 -112        u=1 imp:n=1
101   2 0.087011 +100 -101 +111 -112   u=1 imp:n=1
102   3 0.086023 +101 -102 +110 -113   u=1 imp:n=1
103   7 0.081299 -101 +110 -111        u=1 imp:n=1
104   7 0.081299 -101 +112 -113        u=1 imp:n=1
105   4 0.100040 +102                  u=1 imp:n=1
106   4 0.100040 -102 -110             u=1 imp:n=1
107   4 0.100040 -102 +113             u=1 imp:n=1
c
c -- Water Hole --
201  4 0.100040 -103                   u=2 imp:n=1
c
c -- Graphite Hole --
300  7 0.081299 300 -301 -103          u=3 imp:n=1
302  4 0.10004  -300:+301             u=3 imp:n=1
c
c -- Shim Safety -- vary these for k
40   1 0.042909 -100 +42 -41           u=4 imp:n=1
```

```
41   2 0.087011 +100 -101 +42 -41      u=4 imp:n=1
42   3 0.086023 +101 -102 +42 -40     u=4 imp:n=1
43   4 0.100040 +102                   u=4 imp:n=1
44   4 0.100040 -102 -42              u=4 imp:n=1
45   4 0.100040 -102 +40               u=4 imp:n=1
46   5 0.127794 -101 -40 +41           u=4 imp:n=1 $borated
graphite
c
c -- Regulating Rod -- in at some %?
50   6 0.135143 -50 -52 +53            u=5 imp:n=1 $B4C
powder
51   3 0.086023 +50 -51 +53 -52        u=5 imp:n=1
52   4 0.100040 +51:+52:-53            u=5 imp:n=1
c -- Transient Rod -- OUT
60   0          -50 +62 -63            u=6 imp:n=1
61   5 0.127794 -50 +63 -64            u=6 imp:n=1
62   3 0.086023 +50 -51 +62 -64        u=6 imp:n=1
63   4 0.100040 +51:-62:+64            u=6 imp:n=1
c
c -- Irradiation area in water hole --
70 4 0.10004 -70 -71                            u=7 imp:n=1
71 4 0.10004 -70 +72                            u=7 imp:n=1
72 4 0.10004 +70                                u=7 imp:n=1
73 4 0.10004 -70 +71 -72                        u=7 imp:n=1
c
90 8 -0.013884 -91            u=9  imp:n=1
91 3 0.127794 91 -90          u=9  imp:n=1
910 4 0.10004 90              u=9  imp:n=1
92 8 -0.013884 -93            u=10 imp:n=1
93 3 0.127794 93 -92          u=10 imp:n=1
932 4 0.10004 92              u=10  imp:n=1
94 8 -0.013884 -95            u=11 imp:n=1
95 3 0.127794 95 -94          u=11 imp:n=1
945 4 0.10004 94              u=11  imp:n=1
96 8 -0.013884 -97            u=12 imp:n=1
97 3 0.127794 97 -96          u=12 imp:n=1
967 4 0.10004 96              u=12  imp:n=1
c
c         - Fuel Assembly  Lattice -
600   0  -702 +701 -704 +703 lat=1 u=15 fill=0:17 0:11 0:0
      3 3 1 1 1 1 1 1 1 1 1 1 1 3 3 3 3
      3 3 1 1 1 5 1 1 1 1 1 1 1 3 3 3 3
      3 3 3 3 1 1 1 1 1 1 1 1 1 3 3 3 3
      3 3 3 3 1 1 4 1 1 1 4 1 1 1 3 3 3 3
      3 3 7 7 2 2 1 1 1 1 1 1 1 1 3 3 3 3
```

```
      3 3 7 7 2 2 1 1 6 1 1 1 1 1 3 3 3 3
      3 3 2 2 1 1 1 1 1 1 1 1 1 1 3 3 3 3
      3 3 2 2 1 1 4 1 1 1 4 1 1 1 3 3 3 3
      2 2 3 3 1 1 1 1 1 1 1 1 1 1 3 3 3 3
      2 2 3 3 1 1 2 2 1 1 2 2 1 1 3 3 3 3
      2 2 2 2 2 2 2 2 2 2 12 9 2 2 2 2 2 2
      2 2 2 2 2 2 2 2 2 2 2 11 10 2 2 2 2 2 2   imp:n=1 vol=1
601   0       +600 -601 +602 -603 +604 -605 fill=15
imp:n=1 vol=1 $Window
c
c         - Universe -
998   0    +800                imp:n=0 $ void space outside
water cyl
997   4    0.100040  -800 #601 imp:n=1 $ water cyl

c -- Surface Cards --
c
c -- Fuel Pin Surfaces --
100   c/z 1.9431 1.9431 0.2280
101   c/z 1.9431 1.9431 1.7411
102   c/z 1.9431 1.9431 1.7920
110   pz -8.89
111   pz 0.00
112   pz 38.10
113   pz 46.99
c -- water/graphite holes --
103   c/z 1.9431 1.9431 5.0
c -graphite
300 pz -8.89
301 pz  46.99
c -- Core --
600   px  0.00
601   px  69.9516
602   py  0.00
603   py  46.6344
604   pz  -50
605   pz   80
c -- Pin Cell Surfaces --
701   px 0.0
702   px 3.8862
703   py 0.0
704   py 3.8862
c -- Surrounding Water Region --
800   rpp -10 80 -10 120 -55 85
c -- Shim Safety Surfaces
```

```
c reusing 100,101,102
40    pz  55.06
41    pz  19.05
42    pz  -19.05
c -- Transient Rod Surfaces and Regulating rod surfaces --
50    c/z 1.9431 1.9431 1.5164 $ inner radius
51    c/z 1.9431 1.9431 1.5876 $ outer radius
c -- regulating rod --
52    pz  57.15
53    pz  19.05
c -- transient --
62  pz -31.75
63  pz 38.1
64  pz 76.2
c -- irradiation area --
70 rpp 0 +3.8862 0 3.8862 -8.89 46.99
71 pz 18.05
72 pz 20.05
c --irradiation tank
90 rcc 0 3.8862 0 0 0 25 2.5
91 rcc 0 3.8862 0.25 0 0 24.5 2.25
92 rcc 0 0 0 0 0 25 2.5
93 rcc 0 0 0.25 0 0 24.5 2.25
94 rcc 3.8862 0 0 0 0 25 2.5
95 rcc 3.8862 0 0.25 0 0 24.5 2.25
96 rcc 3.8862 3.8862 0 0 0 25 2.5
97 rcc 3.8862 3.8862 0.25 0 0 24.5 2.25

c -- Data Cards --
c
mode n p h
kcode 4000 1.0 50 1000
ksrc  37.4758 25.8172 19.05
f4:h 90 92 94 96
fc4 Proton flux LET in MeV/cm
e4 1e-3 99ilog 100
ft4 LET
PHYS:N 100 0 0 -1 -1 0 0.999
f6:n,p 90 92 94 96
m1    40000.66c 4.2909E-2 $ Zirconium
m2    92234.70c 8.2300E-6 $ U-ZrH
      92235.70c 1.082197E-3
      92236.70c 1.2100E-5
      92238.70c 4.3213E-3
      40000.66c 3.2280E-2
```

```
      72000.50c 1.9368E-6
      68166.70c 7.7170E-5
      68167.70c 5.2990E-5
      6000.70c 1.7870E-2
      1001.70c 4.9158E-2
m3    24000.50c 1.7385E-2 $ SS-304
      26000.50c 5.9206E-2
      28000.50c 7.6995E-3
      25055.70c 1.7320E-3
m4    1001.70c 6.6691E-2
      8016.70c 3.3346E-2 $ Light water
m5    6000.70c 1.0082E-1 $ Borated Graphite 0.127794
      5010.70c 2.1824E-2
      5011.70c 5.1500E-3
m6    6000.70c 2.7247E-2 $ B4C Powder 0.135143
      5010.70c 2.0598E-2
      5011.70c 8.7298E-2
m7    6000.70c 8.1299E-2 $ Graphite
m8    6000.70c 0.200000
      1001.70c 0.800000 $methane
mt2   h/zr.10t
      zr/h.10t
mt4   lwtr.10t
mt5   grph.10t
mt7   grph.10t
mt8   poly.10t
```

6.1.5 NSCR Methane/Argon

```
NSC TRIGA Reactor
c
c -- Cell Cards --
c
c -- Fuel Pin --
100   1 0.042909 -100 +111 -112        u=1 imp:n=1
101   2 0.087011 +100 -101 +111 -112   u=1 imp:n=1
102   3 0.086023 +101 -102 +110 -113   u=1 imp:n=1
103   7 0.081299 -101 +110 -111        u=1 imp:n=1
104   7 0.081299 -101 +112 -113        u=1 imp:n=1
105   4 0.100040 +102                  u=1 imp:n=1
106   4 0.100040 -102 -110             u=1 imp:n=1
107   4 0.100040 -102 +113             u=1 imp:n=1
c
c -- Water Hole --
201  4 0.100040 -103                   u=2 imp:n=1
```

```
c
c -- Graphite Hole --
300  7 0.081299 300 -301 -103          u=3 imp:n=1
302  4 0.10004  -300:+301              u=3 imp:n=1
c
c -- Shim Safety -- vary these for k
40   1 0.042909 -100 +42 -41           u=4 imp:n=1
41   2 0.087011 +100 -101 +42 -41      u=4 imp:n=1
42   3 0.086023 +101 -102 +42 -40     u=4 imp:n=1
43   4 0.100040 +102                   u=4 imp:n=1
44   4 0.100040 -102 -42              u=4 imp:n=1
45   4 0.100040 -102 +40               u=4 imp:n=1
46   5 0.127794 -101 -40 +41           u=4 imp:n=1 $borated
graphite
c
c -- Regulating Rod -- in at some %?
50   6 0.135143 -50 -52 +53            u=5 imp:n=1 $B4C
powder
51   3 0.086023 +50 -51 +53 -52        u=5 imp:n=1
52   4 0.100040 +51:+52:-53            u=5 imp:n=1
c -- Transient Rod -- OUT
60   0          -50 +62 -63            u=6 imp:n=1
61   5 0.127794 -50 +63 -64            u=6 imp:n=1
62   3 0.086023 +50 -51 +62 -64        u=6 imp:n=1
63   4 0.100040 +51:-62:+64            u=6 imp:n=1
c
c -- Irradiation area in water hole --
70 4 0.10004 -70 -71                           u=7 imp:n=1
71 4 0.10004 -70 +72                           u=7 imp:n=1
72 4 0.10004 +70                               u=7 imp:n=1
73 4 0.10004 -70 +71 -72                       u=7 imp:n=1
c
90 8 -0.06 -91                u=9  imp:n=1
91 3 0.127794 91 -90          u=9  imp:n=1
910 4 0.10004 90              u=9  imp:n=1
92 8 -0.06 -93                u=10 imp:n=1
93 3 0.127794 93 -92          u=10 imp:n=1
932 4 0.10004 92              u=10  imp:n=1
94 8 -0.06 -95                u=11 imp:n=1
95 3 0.127794 95 -94          u=11 imp:n=1
945 4 0.10004 94              u=11  imp:n=1
96 8 -0.06 -97                u=12 imp:n=1
97 3 0.127794 97 -96          u=12 imp:n=1
967 4 0.10004 96              u=12  imp:n=1
c
```

```
c         - Fuel Assembly  Lattice -
600   0  -702 +701 -704 +703 lat=1 u=15 fill=0:17 0:11 0:0
      3 3 1 1 1 1 1 1 1 1 1 1 1 3 3 3 3
      3 3 1 1 1 5 1 1 1 1 1 1 1 3 3 3 3
      3 3 3 3 1 1 1 1 1 1 1 1 1 3 3 3 3
      3 3 3 3 1 1 4 1 1 1 4 1 1 1 3 3 3 3
      3 3 7 7 12 9 1 1 1 1 1 1 1 1 3 3 3 3
      3 3 7 7 11 10 1 1 6 1 1 1 1 1 3 3 3 3
      3 3 2 2 1 1 1 1 1 1 1 1 1 1 3 3 3 3
      3 3 2 2 1 1 4 1 1 1 4 1 1 1 3 3 3 3
      2 2 3 3 1 1 1 1 1 1 1 1 1 1 3 3 3 3
      2 2 3 3 1 1 2 2 1 1 2 2 1 1 3 3 3 3
      2 2 2 2 2 2 2 2 2 2 2 2 2 2 2 2 2 2
      2 2 2 2 2 2 2 2 2 2 2 2 2 2 2 2 2 2    imp:n=1 vol=1
601   0       +600 -601 +602 -603 +604 -605 fill=15
imp:n=1 vol=1 $Window
c
c         - Universe -
998   0    +800                imp:n=0 $ void space outside
water cyl
997   4    0.100040  -800 #601 imp:n=1 $ water cyl

c -- Surface Cards --
c
c -- Fuel Pin Surfaces --
100   c/z 1.9431 1.9431 0.2280
101   c/z 1.9431 1.9431 1.7411
102   c/z 1.9431 1.9431 1.7920
110   pz -8.89
111   pz 0.00
112   pz 38.10
113   pz 46.99
c -- water/graphite holes --
103   c/z 1.9431 1.9431 5.0
c -graphite
300 pz -8.89
301 pz  46.99
c -- Core --
600   px  0.00
601   px  69.9516
602   py  0.00
603   py  46.6344
604   pz  -50
605   pz   80
c -- Pin Cell Surfaces --
```

```
701   px 0.0
702   px 3.8862
703   py 0.0
704   py 3.8862
c -- Surrounding Water Region --
800   rpp -10 80 -10 120 -55 85
c -- Shim Safety Surfaces
c reusing 100,101,102
40    pz  55.06
41    pz  19.05
42    pz  -19.05
c -- Transient Rod Surfaces and Regulating rod surfaces --
50    c/z 1.9431 1.9431 1.5164 $ inner radius
51    c/z 1.9431 1.9431 1.5876 $ outer radius
c -- regulating rod --
52    pz  57.15
53    pz  19.05
c -- transient --
62  pz -31.75
63  pz 38.1
64  pz 76.2
c -- irradiation area --
70 rpp 0 +3.8862 0 3.8862 -8.89 46.99
71 pz 18.05
72 pz 20.05
c --irradiation tank
90 rcc 0 3.8862 0 0 0 25 2.5
91 rcc 0 3.8862 0.25 0 0 24.5 2.25
92 rcc 0 0 0 0 0 25 2.5
93 rcc 0 0 0.25 0 0 24.5 2.25
94 rcc 3.8862 0 0 0 0 25 2.5
95 rcc 3.8862 0 0.25 0 0 24.5 2.25
96 rcc 3.8862 3.8862 0 0 0 25 2.5
97 rcc 3.8862 3.8862 0.25 0 0 24.5 2.25

c -- Data Cards --
c
mode n p h
kcode 4000 1.0 50 1000
ksrc  37.4758 25.8172 19.05
f4:h 90 92 94 96
fc4 Proton flux LET in MeV/cm
e4 1e-3 99ilog 100
ft4 LET
PHYS:N 100 0 0 -1 -1 0 0.999
```

```
f6:n,p 90 92 94 96
m1    40000.66c 4.2909E-2 $ Zirconium
m2    92234.70c 8.2300E-6 $ U-ZrH
      92235.70c 1.082197E-3
      92236.70c 1.2100E-5
      92238.70c 4.3213E-3
      40000.66c 3.2280E-2
      72000.50c 1.9368E-6
      68166.70c 7.7170E-5
      68167.70c 5.2990E-5
      6000.70c 1.7870E-2
      1001.70c 4.9158E-2
m3    24000.50c 1.7385E-2 $ SS-304
      26000.50c 5.9206E-2
      28000.50c 7.6995E-3
      25055.70c 1.7320E-3
m4    1001.70c 6.6691E-2
      8016.70c 3.3346E-2 $ Light water
m5    6000.70c 1.0082E-1 $ Borated Graphite 0.127794
      5010.70c 2.1824E-2
      5011.70c 5.1500E-3
m6    6000.70c 2.7247E-2 $ B4C Powder 0.135143
      5010.70c 2.0598E-2
      5011.70c 8.7298E-2
m7    6000.70c 8.1299E-2 $ Graphite
m8    6000.70c 2.5e-4
      1001.70c 1e-3 $methane
      18000.59c 2.73e-4 $Argon
mt2   h/zr.10t
      zr/h.10t
mt4   lwtr.10t
mt5   grph.10t
mt7   grph.10t
mt8   poly.10t
```

6.1.6 NSCR Methane/Helium

```
NSC TRIGA Reactor
c
c -- Cell Cards --
c
c -- Fuel Pin --
100   1 0.042909 -100 +111 -112        u=1 imp:n=1
101   2 0.087011 +100 -101 +111 -112   u=1 imp:n=1
102   3 0.086023 +101 -102 +110 -113   u=1 imp:n=1
```

```
103   7 0.081299 -101 +110 -111        u=1 imp:n=1
104   7 0.081299 -101 +112 -113        u=1 imp:n=1
105   4 0.100040 +102                  u=1 imp:n=1
106   4 0.100040 -102 -110             u=1 imp:n=1
107   4 0.100040 -102 +113             u=1 imp:n=1
c
c -- Water Hole --
201  4 0.100040 -103                   u=2 imp:n=1
c
c -- Graphite Hole --
300  7 0.081299 300 -301 -103          u=3 imp:n=1
302  4 0.10004  -300:+301              u=3 imp:n=1
c
c -- Shim Safety -- vary these for k
40   1 0.042909 -100 +42 -41           u=4 imp:n=1
41   2 0.087011 +100 -101 +42 -41      u=4 imp:n=1
42   3 0.086023 +101 -102 +42 -40     u=4 imp:n=1
43   4 0.100040 +102                   u=4 imp:n=1
44   4 0.100040 -102 -42              u=4 imp:n=1
45   4 0.100040 -102 +40               u=4 imp:n=1
46   5 0.127794 -101 -40 +41           u=4 imp:n=1 $borated
graphite
c
c -- Regulating Rod -- in at some %?
50   6 0.135143 -50 -52 +53            u=5 imp:n=1 $B4C
powder
51   3 0.086023 +50 -51 +53 -52        u=5 imp:n=1
52   4 0.100040 +51:+52:-53            u=5 imp:n=1
c -- Transient Rod -- OUT
60   0          -50 +62 -63            u=6 imp:n=1
61   5 0.127794 -50 +63 -64            u=6 imp:n=1
62   3 0.086023 +50 -51 +62 -64        u=6 imp:n=1
63   4 0.100040 +51:-62:+64            u=6 imp:n=1
c
c -- Irradiation area in water hole --
70 4 0.10004 -70 -71                            u=7 imp:n=1
71 4 0.10004 -70 +72                            u=7 imp:n=1
72 4 0.10004 +70                                u=7 imp:n=1
73 4 0.10004 -70 +71 -72                        u=7 imp:n=1
c
90 8 -0.06 -91                u=9  imp:n=1
91 3 0.127794 91 -90          u=9  imp:n=1
910 4 0.10004 90              u=9  imp:n=1
92 8 -0.06 -93                u=10 imp:n=1
93 3 0.127794 93 -92          u=10 imp:n=1
```

```
932 4 0.10004 92              u=10  imp:n=1
94 8 -0.06 -95                u=11 imp:n=1
95 3 0.127794 95 -94          u=11 imp:n=1
945 4 0.10004 94              u=11  imp:n=1
96 8 -0.06 -97                u=12 imp:n=1
97 3 0.127794 97 -96          u=12 imp:n=1
967 4 0.10004 96              u=12  imp:n=1
c
c         - Fuel Assembly  Lattice -
600   0  -702 +701 -704 +703 lat=1 u=15 fill=0:17 0:11 0:0
      3 3 1 1 1 1 1 1 1 1 1 1 1 3 3 3 3
      3 3 1 1 1 5 1 1 1 1 1 1 1 3 3 3 3
      3 3 3 3 1 1 1 1 1 1 1 1 1 3 3 3 3
      3 3 3 3 1 1 4 1 1 1 4 1 1 1 3 3 3 3
      3 3 7 7 12 9 1 1 1 1 1 1 1 1 3 3 3 3
      3 3 7 7 11 10 1 1 6 1 1 1 1 1 3 3 3 3
      3 3 2 2 1 1 1 1 1 1 1 1 1 1 3 3 3 3
      3 3 2 2 1 1 4 1 1 1 4 1 1 1 3 3 3 3
      2 2 3 3 1 1 1 1 1 1 1 1 1 1 3 3 3 3
      2 2 3 3 1 1 2 2 1 1 2 2 1 1 3 3 3 3
      2 2 2 2 2 2 2 2 2 2 2 2 2 2 2 2 2 2
      2 2 2 2 2 2 2 2 2 2 2 2 2 2 2 2 2 2    imp:n=1 vol=1
601   0       +600 -601 +602 -603 +604 -605 fill=15
imp:n=1 vol=1 $Window
c
c         - Universe -
998   0    +800                imp:n=0 $ void space outside
water cyl
997   4    0.100040  -800 #601 imp:n=1 $ water cyl

c -- Surface Cards --
c
c -- Fuel Pin Surfaces --
100   c/z 1.9431 1.9431 0.2280
101   c/z 1.9431 1.9431 1.7411
102   c/z 1.9431 1.9431 1.7920
110   pz -8.89
111   pz 0.00
112   pz 38.10
113   pz 46.99
c -- water/graphite holes --
103   c/z 1.9431 1.9431 5.0
c -graphite
300 pz -8.89
301 pz  46.99
```

```
c -- Core --
600   px  0.00
601   px  69.9516
602   py  0.00
603   py  46.6344
604   pz  -50
605   pz   80
c -- Pin Cell Surfaces --
701   px 0.0
702   px 3.8862
703   py 0.0
704   py 3.8862
c -- Surrounding Water Region --
800   rpp -10 80 -10 120 -55 85
c -- Shim Safety Surfaces
c reusing 100,101,102
40    pz  55.06
41    pz  19.05
42    pz  -19.05
c -- Transient Rod Surfaces and Regulating rod surfaces --
50    c/z 1.9431 1.9431 1.5164 $ inner radius
51    c/z 1.9431 1.9431 1.5876 $ outer radius
c -- regulating rod --
52    pz  57.15
53    pz  19.05
c -- transient --
62  pz -31.75
63  pz 38.1
64  pz 76.2
c -- irradiation area --
70 rpp 0 +3.8862 0 3.8862 -8.89 46.99
71 pz 18.05
72 pz 20.05
c --irradiation tank
90 rcc 0 3.8862 0 0 0 25 2.5
91 rcc 0 3.8862 0.25 0 0 24.5 2.25
92 rcc 0 0 0 0 0 25 2.5
93 rcc 0 0 0.25 0 0 24.5 2.25
94 rcc 3.8862 0 0 0 0 25 2.5
95 rcc 3.8862 0 0.25 0 0 24.5 2.25
96 rcc 3.8862 3.8862 0 0 0 25 2.5
97 rcc 3.8862 3.8862 0.25 0 0 24.5 2.25

c -- Data Cards --
c
```

```
mode n p h
kcode 4000 1.0 50 1000
ksrc  37.4758 25.8172 19.05
f4:h 90 92 94 96
fc4 Proton flux LET in MeV/cm
e4 1e-3 99ilog 100
ft4 LET
PHYS:N 100 0 0 -1 -1 0 0.999
f6:n,p 90 92 94 96
m1    40000.66c 4.2909E-2 $ Zirconium
m2    92234.70c 8.2300E-6 $ U-ZrH
      92235.70c 1.082197E-3
      92236.70c 1.2100E-5
      92238.70c 4.3213E-3
      40000.66c 3.2280E-2
      72000.50c 1.9368E-6
      68166.70c 7.7170E-5
      68167.70c 5.2990E-5
      6000.70c 1.7870E-2
      1001.70c 4.9158E-2
m3    24000.50c 1.7385E-2 $ SS-304
      26000.50c 5.9206E-2
      28000.50c 7.6995E-3
      25055.70c 1.7320E-3
m4    1001.70c 6.6691E-2
      8016.70c 3.3346E-2 $ Light water
m5    6000.70c 1.0082E-1 $ Borated Graphite 0.127794
      5010.70c 2.1824E-2
      5011.70c 5.1500E-3
m6    6000.70c 2.7247E-2 $ B4C Powder 0.135143
      5010.70c 2.0598E-2
      5011.70c 8.7298E-2
m7    6000.70c 8.1299E-2 $ Graphite
m8    6000.70c 1.5e-4
      1001.70c 6e-4 $methane
      2004.66c  1.31e-4 $helium
mt2   h/zr.10t
      zr/h.10t
mt4   lwtr.10t
mt5   grph.10t
mt7   grph.10t
mt8   poly.10t
```

6.1.7 NSCR Methane/Helium 2

```
NSC TRIGA Reactor
c
c -- Cell Cards --
c
c -- Fuel Pin --
100   1 0.042909 -100 +111 -112        u=1 imp:n=1
101   2 0.087011 +100 -101 +111 -112   u=1 imp:n=1
102   3 0.086023 +101 -102 +110 -113   u=1 imp:n=1
103   7 0.081299 -101 +110 -111        u=1 imp:n=1
104   7 0.081299 -101 +112 -113        u=1 imp:n=1
105   4 0.100040 +102                  u=1 imp:n=1
106   4 0.100040 -102 -110             u=1 imp:n=1
107   4 0.100040 -102 +113             u=1 imp:n=1
c
c -- Water Hole --
201  4 0.100040 -103                   u=2 imp:n=1
c
c -- Graphite Hole --
300  7 0.081299 300 -301 -103          u=3 imp:n=1
302  4 0.10004  -300:+301              u=3 imp:n=1
c
c -- Shim Safety -- vary these for k
40   1 0.042909 -100 +42 -41           u=4 imp:n=1
41   2 0.087011 +100 -101 +42 -41      u=4 imp:n=1
42   3 0.086023 +101 -102 +42 -40     u=4 imp:n=1
43   4 0.100040 +102                   u=4 imp:n=1
44   4 0.100040 -102 -42              u=4 imp:n=1
45   4 0.100040 -102 +40               u=4 imp:n=1
46   5 0.127794 -101 -40 +41           u=4 imp:n=1 $borated
graphite
c
c -- Regulating Rod -- in at some %?
50   6 0.135143 -50 -52 +53            u=5 imp:n=1 $B4C
powder
51   3 0.086023 +50 -51 +53 -52        u=5 imp:n=1
52   4 0.100040 +51:+52:-53            u=5 imp:n=1
c -- Transient Rod -- OUT
60   0          -50 +62 -63            u=6 imp:n=1
61   5 0.127794 -50 +63 -64            u=6 imp:n=1
62   3 0.086023 +50 -51 +62 -64        u=6 imp:n=1
63   4 0.100040 +51:-62:+64            u=6 imp:n=1
c
```

```
c -- Irradiation area in water hole --
70 4 0.10004 -70 -71                              u=7 imp:n=1
71 4 0.10004 -70 +72                              u=7 imp:n=1
72 4 0.10004 +70                                  u=7 imp:n=1
73 4 0.10004 -70 +71 -72                          u=7 imp:n=1
c
90 8 -0.06 -91                u=9  imp:n=1
91 3 0.127794 91 -90          u=9  imp:n=1
910 4 0.10004 90              u=9  imp:n=1
92 8 -0.06 -93                u=10 imp:n=1
93 3 0.127794 93 -92          u=10 imp:n=1
932 4 0.10004 92              u=10  imp:n=1
94 8 -0.06 -95                u=11 imp:n=1
95 3 0.127794 95 -94          u=11 imp:n=1
945 4 0.10004 94              u=11  imp:n=1
96 8 -0.06 -97                u=12 imp:n=1
97 3 0.127794 97 -96          u=12 imp:n=1
967 4 0.10004 96              u=12  imp:n=1
c
c         - Fuel Assembly  Lattice -
600   0  -702 +701 -704 +703 lat=1 u=15 fill=0:17 0:11 0:0
      3 3 1 1 1 1 1 1 1 1 1 1 1 3 3 3 3
      3 3 1 1 1 5 1 1 1 1 1 1 1 3 3 3 3
      3 3 3 3 1 1 1 1 1 1 1 1 1 3 3 3 3
      3 3 3 3 1 1 4 1 1 1 4 1 1 1 3 3 3 3
      3 3 7 7 2 2 1 1 1 1 1 1 1 3 3 3 3
      3 3 7 7 2 2 1 1 6 1 1 1 1 1 3 3 3 3
      3 3 2 2 1 1 1 1 1 1 1 1 1 1 3 3 3 3
      3 3 2 2 1 1 4 1 1 1 4 1 1 1 3 3 3 3
      2 2 3 3 1 1 1 1 1 1 1 1 1 1 3 3 3 3
      2 2 3 3 1 1 2 2 1 1 2 2 1 1 3 3 3 3
      2 2 2 2 2 2 2 2 2 2 12 9 2 2 2 2 2 2
      2 2 2 2 2 2 2 2 2 2 11 10 2 2 2 2 2 2    imp:n=1
vol=1
601   0       +600 -601 +602 -603 +604 -605 fill=15
imp:n=1 vol=1 $Window
c
c         - Universe -
998   0    +800                imp:n=0 $ void space outside
water cyl
997   4    0.100040  -800 #601 imp:n=1 $ water cyl

c -- Surface Cards --
c
c -- Fuel Pin Surfaces --
```

```
100   c/z 1.9431 1.9431 0.2280
101   c/z 1.9431 1.9431 1.7411
102   c/z 1.9431 1.9431 1.7920
110   pz -8.89
111   pz 0.00
112   pz 38.10
113   pz 46.99
c -- water/graphite holes --
103   c/z 1.9431 1.9431 5.0
c -graphite
300 pz -8.89
301 pz  46.99
c -- Core --
600   px  0.00
601   px  69.9516
602   py  0.00
603   py  46.6344
604   pz  -50
605   pz   80
c -- Pin Cell Surfaces --
701   px 0.0
702   px 3.8862
703   py 0.0
704   py 3.8862
c -- Surrounding Water Region --
800   rpp -10 80 -10 120 -55 85
c -- Shim Safety Surfaces
c reusing 100,101,102
40    pz  55.06
41    pz  19.05
42    pz  -19.05
c -- Transient Rod Surfaces and Regulating rod surfaces --
50    c/z 1.9431 1.9431 1.5164 $ inner radius
51    c/z 1.9431 1.9431 1.5876 $ outer radius
c -- regulating rod --
52    pz  57.15
53    pz  19.05
c -- transient --
62  pz -31.75
63  pz 38.1
64  pz 76.2
c -- irradiation area --
70 rpp 0 +3.8862 0 3.8862 -8.89 46.99
71 pz 18.05
72 pz 20.05
```

```
c --irradiation tank
90 rcc 0 3.8862 0 0 0 25 2.5
91 rcc 0 3.8862 0.25 0 0 24.5 2.25
92 rcc 0 0 0 0 0 25 2.5
93 rcc 0 0 0.25 0 0 24.5 2.25
94 rcc 3.8862 0 0 0 0 25 2.5
95 rcc 3.8862 0 0.25 0 0 24.5 2.25
96 rcc 3.8862 3.8862 0 0 0 25 2.5
97 rcc 3.8862 3.8862 0.25 0 0 24.5 2.25

c -- Data Cards --
c
mode n h p
kcode 4000 1.0 50 1000
ksrc  37.4758 25.8172 19.05
f4:h 90 92 94 96
fc4 Proton flux LET in MeV/cm
e4 1e-3 99ilog 100
ft4 LET
PHYS:N 20 0 0 -101 -1 0 1.001
f6:p,n 90 92 94 96
m1    40000.66c 4.2909E-2 $ Zirconium
m2    92234.70c 8.2300E-6 $ U-ZrH
      92235.70c 1.082197E-3
      92236.70c 1.2100E-5
      92238.70c 4.3213E-3
      40000.66c 3.2280E-2
      72000.50c 1.9368E-6
      68166.70c 7.7170E-5
      68167.70c 5.2990E-5
      6000.70c 1.7870E-2
      1001.70c 4.9158E-2
m3    24000.50c 1.7385E-2 $ SS-304
      26000.50c 5.9206E-2
      28000.50c 7.6995E-3
      25055.70c 1.7320E-3
m4    1001.70c 6.6691E-2
      8016.70c 3.3346E-2 $ Light water
m5    6000.70c 1.0082E-1 $ Borated Graphite 0.127794
      5010.70c 2.1824E-2
      5011.70c 5.1500E-3
m6    6000.70c 2.7247E-2 $ B4C Powder 0.135143
      5010.70c 2.0598E-2
      5011.70c 8.7298E-2
m7    6000.70c 8.1299E-2 $ Graphite
```

```
m8    6000.70c 1.5e-4
      1001.70c 6e-4 $methane
      2004.66c  1.31e-4 $helium
mt2   h/zr.10t
      zr/h.10t
mt4   lwtr.10t
mt5   grph.10t
mt7   grph.10t
mt8   poly.10t
```

6.1.8 Ponomarev

```
The is the Ponomarev experiment
c
c -cell cards
100 1 -.0006 -100  imp:e=1 imp:p=1 imp:h=1
101 2 -4.5 -101 100 imp:e=1 imp:p=1 imp:h=1
102 3 -.00127 -102 #101 #100 imp:e=1 imp:p=1 imp:h=1
103 0 102 imp:e=0 imp:p=0 imp:h=0

c -surface cards
100 rcc 0 0 2.5e-3 0 0 11.995 4.9
101 rcc 0 0 0 0 0 12 5
102 so 30

c -data cards
mode e p
nps 1e6
sdef erg=.5 pos= 0 0 -0.005 dir 1 vec 0 0 1 par= e
f4:e 100
fc4 Proton flux LET in MeV/cm
e4 1e-3 99ilog 100
ft4 LET
f6:e,p 100 101
c -material cards
m1    6000.70c  3.16155E-05
      1001.70c  0.000126462
m2    5000.70c  0.004977
      8000.70c  0.045289
      8000.70c  0.045289
      13000.70c 0.000580
      14000.70c 0.018037
      19000.70c 0.000114
m3    7014.70c 1 $N2
```

6.1.9 Beattie

```
Beattie experiments
c
c -cell cards
001 1 -.00014 -001 imp:p=1 imp:e=1 $tritium CO2 mix
002 2 -2.230 001 -002 imp:p=1 imp:e=1 $borosilicate
003 0 002 imp:p=0 imp:e=0 $void space

c -surface cards
001 so 6.19
002 so 6.3

c -data cards
mode e p
nps 1e6
sdef erg=d1 cell=1 rad=d2 par= e erg= .0062
si1 L 0.0054 $ Discrete Co-60 Energies, in MeV
sp1 D 1.0 $ Equiprobable
si2 H 0 6.20 $ Radial Bin Distribution from 0.0 cm to 6.2
cm
sp2 -21 2 $ Power law sampling to 2nd power, for spherical
sources
f6:e,p 001
c -material cards
m1    6000.70c -1.279e-5
      1003.70c -9.153e-5
      8016.70c -1.705e-5
m2    5000.70c  0.004977
      8000.70c  0.045289
      8000.70c  0.045289
      13000.70c 0.000580
      14000.70c 0.018037
      19000.70c 0.000114
mt1   poly.10t
```

6.1.10 Sack

```
This is the Sack experiment
c
c -cell cards
100 1 -.0006 -100  imp:e=1 imp:p=1 imp:h=1
101 2 -4.5 -101 100 imp:e=1 imp:p=1 imp:h=1
102 3 -.00127 -102 #101 #100 imp:e=1 imp:p=1 imp:h=1
103 0 102 imp:e=0 imp:p=0 imp:h=0
```

```
c -surface cards
100 rcc 0 0 2.5e-3 0 0 11.995 4.9
101 rcc 0 0 0 0 0 12 5
102 so 30

c -data cards
mode e p h
nps 1e7
sdef erg=6.5 pos= 0 0 -0.005 dir 1 vec 0 0 1 par= h
f4:h 100
fc4 Proton flux LET in MeV/cm
e4 4e-2 99ilog 0.1
ft4 LET
f6:e,p,h 100 101
PHYS:H 100 0 -1 J 0 J 1 3J 0.917
c -material cards
m1    6000.70c  3.16155E-05
      1001.70c  0.000126462
m2    5000.70c  0.004977
      8000.70c  0.045289
      8000.70c  0.045289
      13000.70c 0.000580
      14000.70c 0.018037
      19000.70c 0.000114
m3    7014.70c 1 $N2
```

6.1.11 Sheridan-Libby

```
Sheridan-Libby
c
c -cell cards
100 1 .021077 -100 imp:p=1 imp:e=1
101 2 -2.3 100 -101 imp:p=1 imp:e=1
102 3 -7.2 -103 imp:p=1 imp:e=1
103 4 -.00125 -104 #100 #101 #102 imp:p=1 imp:e=1
104 0 104 imp:p=0 imp:e=0

c -surface cards
100 rcc 0 0 0 0 0 10 6.5
101 rcc 0 0 0.2 0 0 9.6 6.3
103 rcc 0 15 0 0 0 5 2
104 so 30

c -data cards
```

```
mode p e
nps 1e6
sdef erg=d1 pos= 0 15 2.5 par= p
si1 L 1.173 1.33 $ Discrete Co-60 Energies, in MeV
sp1 D 1.0 1.0 $ Equiprobable
f6:e,p 100
f4:e 100
fc4 Proton flux LET in MeV/cm
e4 1e-3 99ilog 100
ft4 LET
m1    6000.70c  3.16155E-05
      18040.70c 0.021045385
      1001.70c  0.000126462
m2    5000.70c  0.004977
      8000.70c  0.045289
      8000.70c  0.045289
      13000.70c 0.000580
      14000.70c 0.018037
      19000.70c 0.000114
m3    28000.70c 1
m4    7000.70c  1
```